GEOMEMBRANE - SAND INTERFACE FRICTION

A THESIS SUBMITTED TO
THE GRADUATE SCHOOL OF NATURAL AND APPLIED SCIENCES OF
THE MIDDLE EAST TECHNICAL UNIVERSITY

BY

MİZYAL İZGİN

IN PARTIAL FULFILLMENT OF THE REQUIREMENTS FOR THE DEGREE OF
MASTER OF SCIENCE
IN
THE DEPARTMENT OF CIVIL ENGINEERING

JULY 1997

Approval of the Graduate School of Natural and Applied Sciences.

Prof. Dr. Tayfur ÖZTÜRK
Director

I certify that this thesis satisfies all the requirements as a thesis for the degree of Master of Science.

Prof. Dr. Fuat ERBATUR
Head of Department

This is to certify that we have read this thesis and that in our opinion it is fully adequate, in scope and quality, as a thesis for the degree of Master of Science.

Prof. Dr. Yıldız WASTI
Supervisor

Examining Committee Members:

Prof. Dr. Yener ÖZKAN
Prof. Dr. Altay BİRAND
Prof. Dr. Yıldız WASTI
Assist. Prof. Dr. Erdal ÇOKCA
Osman ÇANDIR (MSc in CE)

ABSTRACT

GEOMEMBRANE - SAND INTERFACE FRICTION

İzgin, Mizyal

M.S., Department of Civil Engineering

Supervisor: Prof. Dr. Yıldız Wasti

July 1997, 171 pages

In geotechnical applications such as the lining of canals or waste containments where geosynthetics are placed on inclined surfaces, the correct assessment of the interface shear properties between the geosynthetics and soils or between different kinds of geosyhtetics becomes an important issue. Inclined board or tilting table tests are believed to create test conditions that are close to real conditions, particuarly where normal stressese are very low.

In the present experimental study, the interface friction angle between geomembrane and granular soil was measured using a specially constructed inclined board test apparatus. Two granular soils of comparable gradation but of quite contrasting particle roundness and geomembranes with smooth and rough (textured) surfaces were used in the experiments in the normal stress range of approximately 5 to 50 kPa. Direct shear box tests were also carried out for comparison.

It has been found that the rough geomembranes performaed better thn the smooth geomembranes on both types of soils. In additon, the tests conducted on crushed stone revealed higher interface friction angles than Ottawa Sand with rounded particles.

Key Words : Inclined Board test, Tilting Board Test, Direct Shear Box Tests, Geomembrane, Friction Angle

ÖZ

GEOMEMBRAN VE KUM ARASINDAKİ YÜZEY SÜRTÜNMESİ

İzgin, Mizyal
Yüksek Lisans, İnşaat Mühendisliği Bölümü
Tez Yöneticisi: Prof. Dr. Yıldız Wasti
Temmuz 1997, 171 sayfa

Geosentetiklerin eğik düzlemlere yerleştirildiği, kanal kaplaması ya da çöp atık sahaları gibi geoteknik uygulamalarda, geosentetiklerle zemin türleri veya geosentetiklerin birbirleri arasındaki yüzey kesme özellikleri önemli bir konudur. Eğik düzlem ya da kalkan masa deneylerinin, özellikle dikey yüklerin çok düşük olduğu durumlarda gerçek koşullara yakın deney koşulları sağladığına inanılmaktadır.

Mevcut deneysel çalışmada, geomembran ve kum arasındaki yüzey sürtünme açısı özel olarak geliştirilen bir eğik düzlem test cihazı yardımıyla ölçülmüştür. Deneylerde, dane boyu ve dağılımı açısından yakın olmakla birlikte, dane yuvarlaklığı oldukça farklı iki çeşit kum ile düz ve pürüzlü membranlar kullanılmış ve dikey gerilme aralığı yaklaşık 5-50 kPa olarak tutulmuştur. Karşılaştırma için direkt kesme deneyleri de kullanılmıştır.

Her iki zemin tipinde de, pürüzlü membranın düz membrana göre açık bir şekilde daha yüksek sürtünme açıları verdiği gözlenmiştir. Ayrıca kırma taş üzerinde yapılan deneylerde de, yuvarlak daneli Ottawa kumundan daha yüksek sürtünme açıları elde edilmiştir.

Anahtar Kelimeler :Eğik Düzlem Deneyi, Kalkan Masa Deneyi, Direkt Kesme Deneyi, Geomembran, Sürtünme Açısı

To My Beloved Grand Daddy Cemal ERTAN

Robert College, 1943-BS (EE)

Purdue Uni., USA, 1945-MS (EE)

ACKNOWLEDGMENTS

I would like to express my sincere gratitude to Prof. Dr. Yıldız Wasti for her guidance, valuable suggestions and patience throughout the research.

Very special thanks are extended to the geotechnical teaching staff of METU for their suggestions and helpful ideas, and, to the staff of the Soil Mechanics Laboratory especially to Mr. Ali Bal for their help during testing.

To my family I offer sincere thanks for their endless patience all through the study. Special thanks are also due to the NÜVE family, especially to Mr. Yaşar Delibaş for their valuable help during the design stage of the apparatus

I am indebted to research assistant Onur Sonuvar for his continuous help and support in every stage of this thesis. Special thanks are also due to research assistants Ebru Gökcek, Aslı Numanoğlu, Sibel Başaran, Barlas Ülkü and Özgür Yüncü for their endless support.

Finally, wholehearted thanks are also extended to Mr. Timuçin Hergül for being present in Ankara during the last and the most difficult days of the present study..

TABLE OF CONTENTS

Page

APPENDICES

LIST OF TABLES

TABLE

LIST OF FIGURES

FIGURE

LIST OF SYMBOLS

a' : Adhesion intercept

c : Cohesion intercept (apparent cohesion)

c' : Cohesion intercept in terms of effective stress

L : Length of geosynthetic embedded in soil

P : Pullout force

u : Pore water pressure at the point of interest

w : Width of geosynthetic

δ' : Angle of shearing resistance for the interface

ϕ : Angle of shearing resistance of soil

ϕ' : Angle of shearing resistance of soil in terms of effective stress

σ' : Effective normal stress acting on the interface

σ'_f : Effective normal stress acting on the point of interest

σ_f : Normal stress acting on the point of interest

τ: Pullout resistance

τ_f : Shear strength of soil at a point at a particular plane

CHAPTER I

INTRODUCTION

Since 1970s, the usage of geosynthetics have steadily been increasing in geotechnical applications. The determination of shear strength parameters and their usage is very important for the safety requirements of geotechnical facilities. Although many projects that incorporate geosynthetics are presently being designed and built, an internationally accepted method for testing frictional properties of geosynthetics has not yet been developed.

In this study, the frictional properties of interfaces involving geomembranes and granular soils are tried to be evaluated by means of inclined board (tilting table) tests. The inclined board apparatus was specially designed and manufactured for this purpose. For comparison, similar tests were also performed in the modified direct shear box apparatus. Two types of sand with comparable gradation but having quite different particle roundness were tested against various smooth and rough (textured) geomembranes.

In Chapter 2, an overview of related topics is presented. Chapter 3 gives a brief discussion on the testing methods for the determination of interface friction angle. In Chapter 4, a summary of the previous research on interface friction angle between geosynthetics and soils is presented. Chapter 5 gives the details of the manufactured apparatus, properties of the soil and geomembranes used and the testing procedure. In Chapter 6, the results of the tests and the discussions on these results are presented. Finally, conclusion of the study is given in Chapter 7.

CHAPTER II

AN OVERVIEW OF RELATED TOPICS

2.1 Introduction

In this chapter, a detailed discussion on the geotechnical terms, which will frequently be used in the rest of the text, is given.

The first concept to be explained, is the theory which governs the shear strength parameters, c and ϕ, mainly for granular soils. Next, a brief summary of the geosynthetic types is presented. Finally the importance of interface shear strength parameters in geosynthetic applications is discussed.

2.2 Shear Strength Parameters

The determination of shear strength parameters and their usage is very important for the safety requirements of geotechnical facilities. Although the theory is the same, the terminology for the shear strength parameters for the interfaces with or without geosynthetics is different so that they should be studied separately.

2.2.1 Shear Strength of Soils

The shear strength of a soil is defined as the maximum or limiting value of shear stress that may be induced within a soil mass before the soil yields.

The shear strength was originally expressed by Coulomb (1776) as a linear function of the normal stress as:

$$\tau_f = c + \sigma_f \tan \phi \qquad (2.1)$$

where;

τ_f : Shear strength of soil at a point at a particular plane

c : Cohesion intercept (apparent cohesion)

σ_f : Normal stress acting on the point of interest

ϕ : Angle of shearing resistance of soil

In 1925, Terzaghi revealed that the shear stresses in a soil mass can only be resisted by the skeleton of solid particles and this led to the modification of Equation 2.1 such that:

$$\tau_f = c' + \sigma'_f \tan \phi' \qquad (2.2)$$

and,

$$\sigma'_f = \sigma_f - u \qquad (2.3)$$

where,

τ_f : Shear strength of soil at a point on a particular plane

c' : Cohesion intercept in terms of effective stress

σ'_f : Effective normal stress acting on the point of interest

ϕ' : Angle of shearing resistance of soil in terms of effective stress

u : Pore water pressure at the point of interest

The line represented by Equation 2.2 is called the "Mohr - Coulomb Failure Envelope".

In very broad terms, the angle ϕ is the slope of the common tangent, given by Equation 2.2, which is drawn to the Mohr circles at failure for different states of stress. The stress conditions at failure can be represented by Figure 2.1, where σ_1' and σ_3' are the major and minor effective stresses respectively.

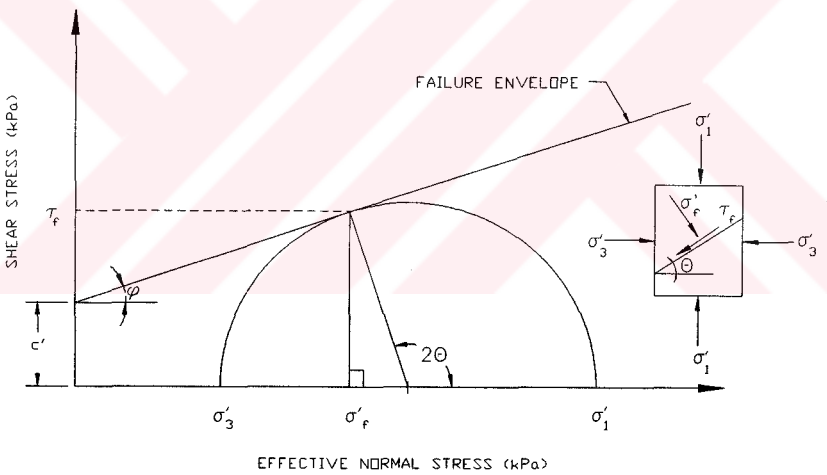

Figure 2.1. Stress Conditions at Failure (After Craig, 1987).

As it can be observed form Figure 2.1, c (or c') is the shear strength intercept when the normal stress is zero. It has the same unit as the shear strength and it simply represents the attractive force between soil particles even if no normal

load is acting on the soil. For granular soils and normally consolidated clays, c is often reported to be equal to zero.

The formulation of the Mohr - Coulomb Failure Envelope makes it easy to be separated into two components such as the frictional resistance (σ_f' tan ϕ') and the cohesion (c'). Neglecting the term "c" from the equation, the simple frictional formula is obtained (Lambe and Whitman, 1979):

$$\tau_f = \sigma_f' \tan \phi' \qquad (2.4)$$

Equation 2.4 refers to a situation where the soil particles are assumed to move along horizontal planes and thus the frictional resistance results only from mineral to mineral contact. In this case, the angle of friction is named as "ϕ_μ". However, as explained by Lambe and Whitman (1979), within actual soils, soil particles are in contact with other soil particles, and planes through the contact points are inclined to the horizontal. In order to have shear failure between particles, it is therefore not only necessary to overcome the mineral - mineral frictional resistance, it is in addition, necessary to make particles move up and over one another.

Hence, the shear resistance of an actual soil mass is made up of two components: (a) the one whose magnitude is controlled by ϕ_μ, and (b) a second component whose magnitude is related to the degree of interlocking. The energy applied to a soil by the external load is used both to overcome the frictional resistance between the soil particles and also to expand the soil against the confining pressures. This tendency of soil to expand is called "dilatancy" and the angle of friction, ϕ, can be expressed as (Das, 1983):

$$\phi = \phi_\mu + \beta \qquad (2.5)$$

where;

ϕ_μ : Angle of sliding friction between mineral surfaces

β : Effect of interlocking

The interlocking concept is schematically represented in Figure 2.2.

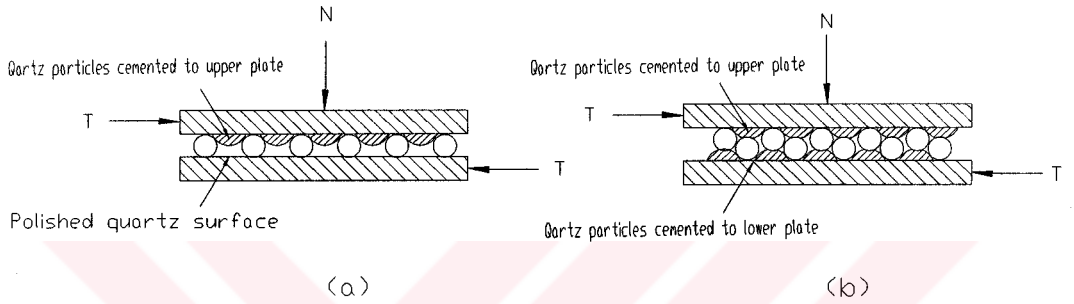

Figure 2.2. Example of Interlocking (a) Smooth Sliding Surfaces, and (b) Highly Interlocked Surfaces (Adopted from Lambe and Whitman, 1979).

Figure 2.3 shows the behavior of loose and dense sands subjected to shear in a direct shear box test. As quoted from Das (1983), the angle of friction,ϕ, can be determined by plotting a graph of the maximum or peak shear stresses versus the corresponding normal stresses (Figure 2.4). The Mohr - Coulomb failure envelope is determined by drawing a straight line through the origin and the points representing the experimental results. The slope of this line will give the peak friction angle, ϕ_p, of the soil. Similarly, the ultimate friction angle ϕ_{cv} can be determined by plotting the ultimate shear stress τ_{cv} versus the corresponding normal stresses as shown in Figure 2.4. The ultimate friction angle ϕ_{cv} represents a

condition of shearing at constant volume of the specimen. For loose sands, the peak friction angle is approximately equal to the ultimate friction angle.

The effects of interlocking and dilatancy are easily followed from Figure 2.3. As stated by Craig (1987), in a dense sand there is considerable degree of interlocking between particles, and before shear failure can take place, the interlocking must be overcome in addition to the frictional resistance at the points of contact. A peak shear strength is observed at a relatively low strain and as interlocking is overcome by time, the shear strength decreases and reaches to a constant value (τ_{cv}). The reduction in the degree of interlocking increases the volume of the specimen during shearing until the specimen becomes loose enough to allow particles to move over and around each other. No further net volume change occurs and the void ratio at this state is called "critical void ratio", denoted by "e_{cv}" (Das, 1983).

In the case of a loose sand, there is no significant particle interlocking to be overcome, and the principal stress difference increases gradually to an ultimate value without a prior peak. At the same time, volume decreases continuously and the void ratio reaches to the critical value "e_{cv}". At this point, the friction angle is denoted by "ϕ_{cv}". For loose sands, the difference between ϕ_{cv} and ϕ_{μ} represents the energy required to rearrange the particles (Craig, 1987).

Table 2.1 gives typical values for the friction angle, ϕ.

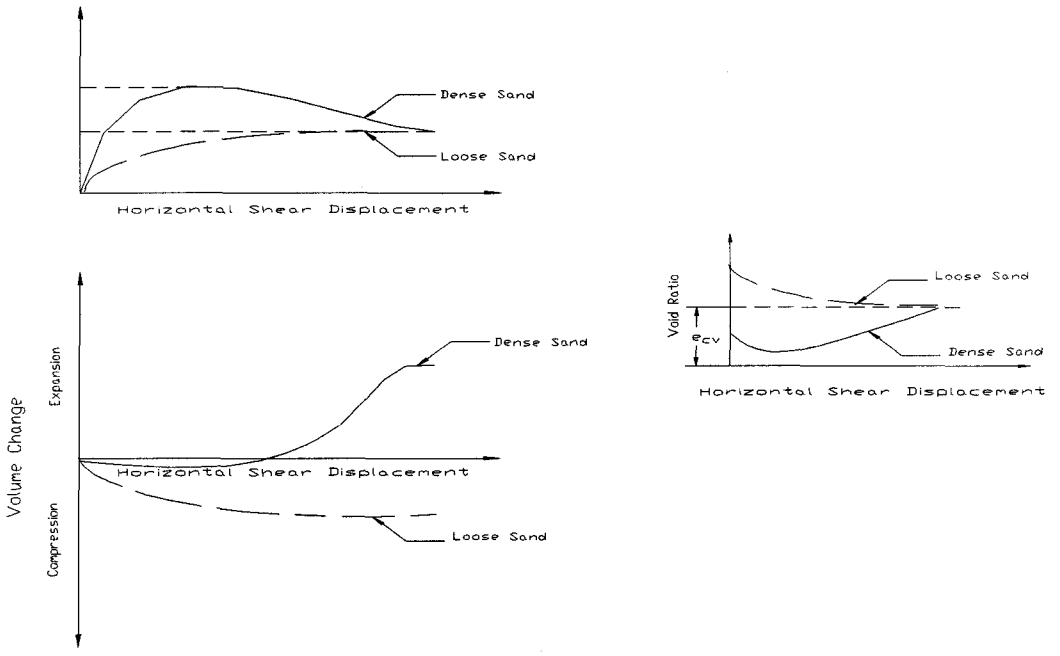

Figure 2.3. Direct Shear Test Results in Loose and Dense Sands (After Das, 1983).

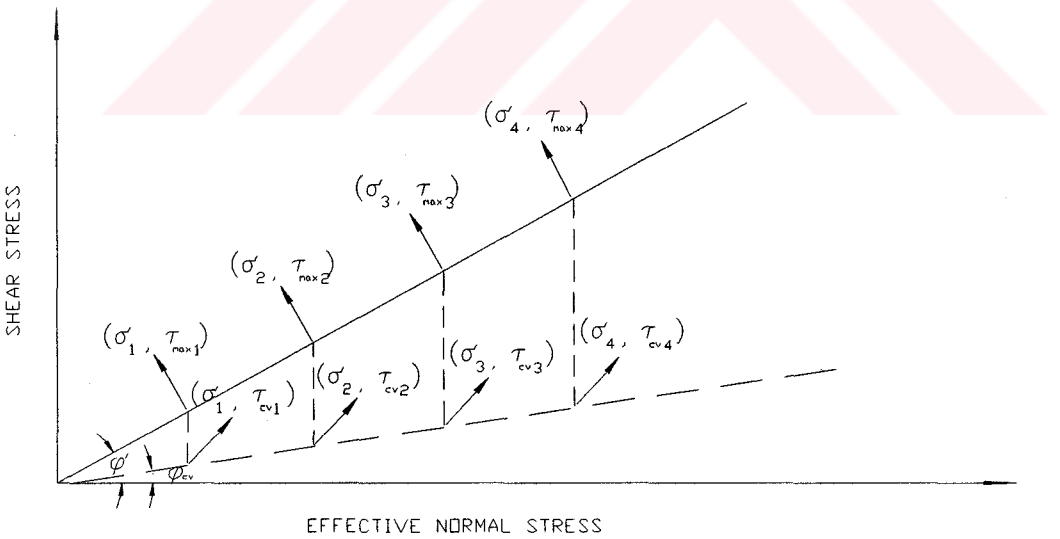

Figure 2.4. Determination of Peak and Ultimate Friction Angles from Direct Shear Test (After Das, 1983).

Table 2.1. Typical Values of ϕ'_p and ϕ'_{cv} for Granular Soils (After Das, 1983).

Type of Soil	ϕ'_p (°)	ϕ'_{cv} (°)
Sand: Round Grains		
Loose	28 - 30	
Medium	30 - 35	26 - 30
Dense	35 - 38	
Sand: Angular Grains		
Loose	30 - 35	
Medium	35 - 40	30 - 35
Dense	40 - 45	
Sandy Gravel	34 - 48	33 - 36
Medium to fine quartz sand	26	32
Feldspar, #25 to 200 sieves	37	42

2.2.2 Shear Strength of Interfaces Involving Geosynthetics

The same rules, governing the shear strength of soils, apply to the shear strength of interfaces involving geosynthetics. In the application of geosynthetics, the friction angle ϕ, is denoted as "δ", and instead of the cohesion intercept c, the adhesion intercept "a" is utilized. As a result, the failure envelope (given by Equation 2.2) takes the form (Ingold, 1991):

$$\tau_f = a' + \sigma' \tan \delta' \qquad (2.6)$$

where;

τ_f : Shear strength of the interface

a' : Adhesion intercept

σ' : Effective normal stress acting on the interface

δ' : Angle of shearing resistance for the interface

2.3 An Overview of Geosynthetics

Since 1970s, the usage of geosynthetics; namely geotextiles, geomembranes, geogrids, geonets, geosynthetic clay liners and geopipes; have steadily been increasing in geotechnical applications mainly because of the following reasons (Koerner, 1994):

(1) They are quality control manufactured in a factory environment

(2) They can be installed rapidly

(3) They generally replace raw material resources

(4) They generally replace difficult designs using natural materials

(5) Their timing is very appropriate

(6) Their use is required by law in some cases

(7) They are generally cost competitive against the natural soil that they replace

(8) They are being actively marketed and are widely available.

The increasing trend in the application of geosynthetics between the years 1970 - 1990 is very well illustrated in Figure 2.5.

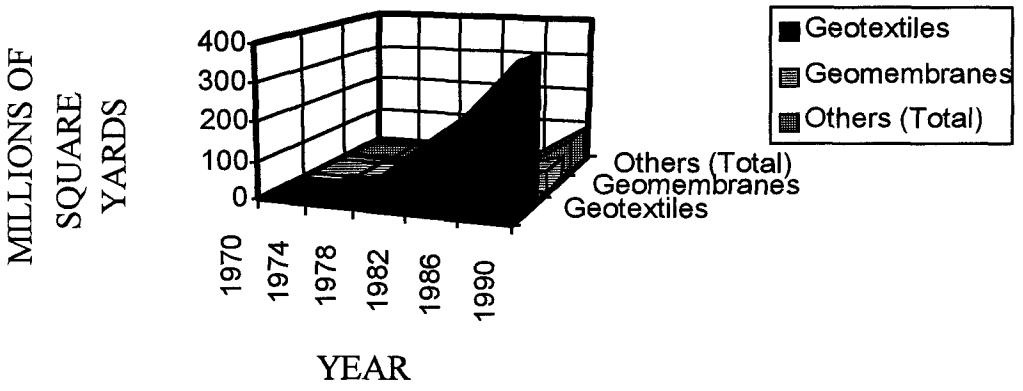

Figure 2.5. Estimated Geosynthetic Market in North America (Adopted from Koerner, 1994).

2.3.1 Raw Materials and Types of Geosynthetics

As quoted from Wasti (1995), type and properties of a geosynthetic will mainly depend on its raw material and its manufacturing process.. Except where biodegradability is required, the raw material for geosynthetics is plastics which are synthetic organic materials, based on carbon, commonly obtained by distillation of crude oil. Two major classes of plastics are given by Koerner (1994) as:

(1) Thermoplastics, which can be repeatedly heated to their softening point, shaped or worked as desired, and then cooled to preserve the remolded shape, and,

(2) Thermosetting plastics for which the above procedure cannot be repeated.

The types of plastic polymers, which are commonly used in the manufacturing process of geosynthetics are listed in Table 2.2. Usually, additives are used together with the polymers to improve their properties.

Table 2.2. Polymers Used in the Manufacturing of Geosynthetics (Adopted from Koerner, 1994).

Polymer	Types of Geosynthetics
Polyethylene (PE)	
High Density Polyethylene (HDPE) Low Density Polyethylene (LDPE) Very Low Density Polyethylene (VLDPE) Chlorosulfinated Polyethylene (CSPE)	Geotextiles, geomembranes, geogrids, geopipe, geonets, geocomposites
Polypropylene (PP)	Geotextiles, geomembranes, geogrids, gocomposites
Polyvinyl Chloride (PVC)	Geomembranes, geocomposites, geopipe
Polyester (PET)	Geotextiles, geogrids
Polyamide (Nylon) (PA)	Geotextiles, geogrids, geocomposites
Polystyrene (PS)	Geocomposites
Ethylene Propylene Diene Monomer (EPDM)	Geomembranes

[a] All of the polymers, except EPDM are thermoplastics. EPDM is a thermosetting polymer.

Basic types of geosynthetics are given in Figure 2.6.

According to ASTM D4439 (Christopher and Holtz, 1985), "geotextile is any permeable textile material used with foundation, soil, rock, earth or any other geotechnical engineering - related material, as an integral part of a man made project, structure or system".

"Woven geotextiles" are the ones manufactured by conventional weaving process and "non-woven geotextiles" are manufacutured by processes other than weaving; namely mechanical bonding (needle-punched types), thermal bonding and chemical bonding. The woven and non-woven geotextiles will usually be abbreviated as "W" and "NW" respectively in the present text.

Although geotextiles are essentially permeable materials, geomembranes are in contrast, are practically impermeable. ASTM D4439 defines geomembranes as "continuous membrane type liners and barriers composed of asphaltic, polymeric or combination there of materials with sufficiently low permeability so as to control fluid migration into a geotechnical related man made project, structure or system". Table 2.3 lists the common types of geomembranes.

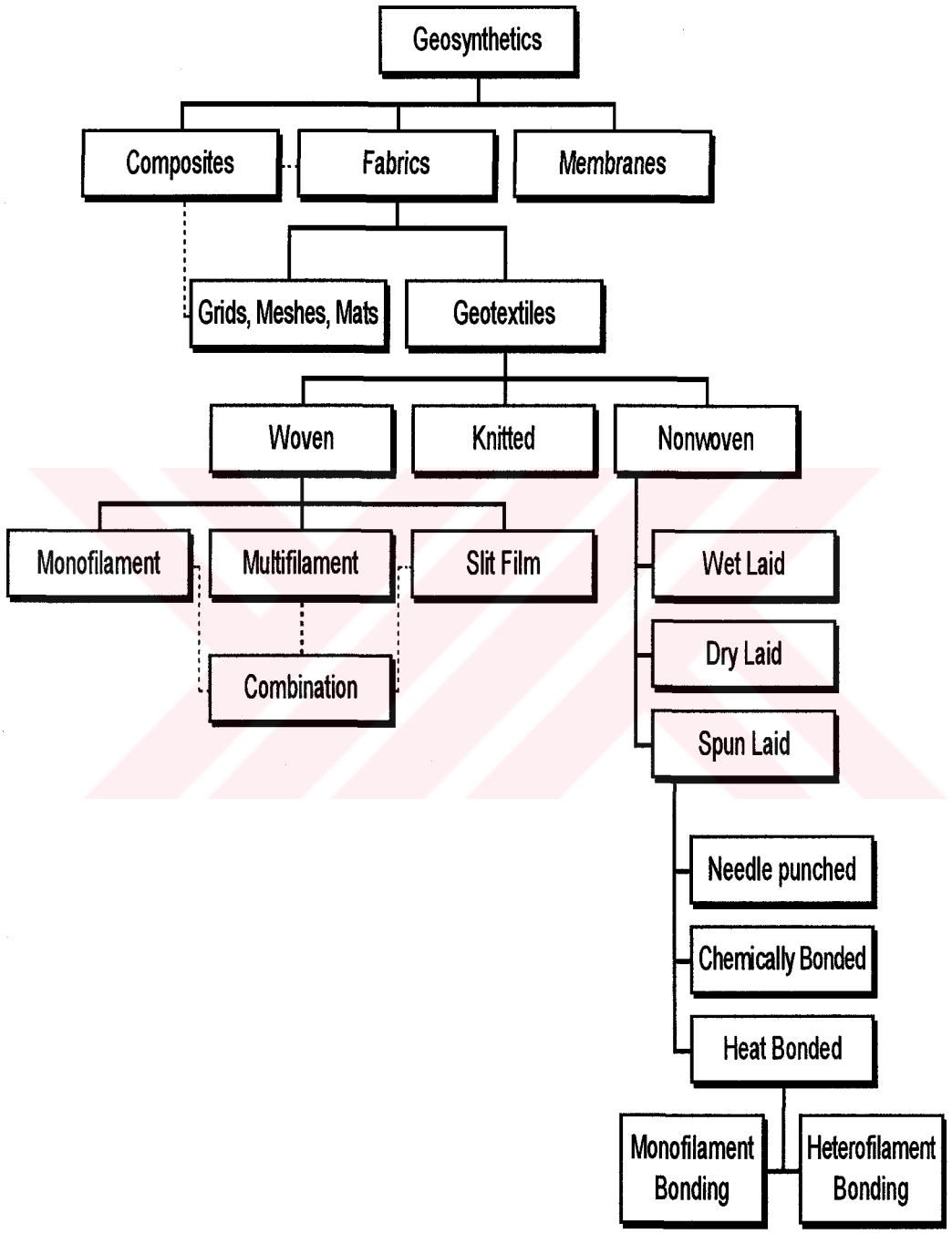

Figure 2.6. Classification of Geosynthetics (After Hausmann, 1990).

Table 2.3. Geomembranes in Current Use (After Koerner, 1994).

A) Most Widely Used
• Polyvinyl chloride (PVC) • Chlorosulphinated polyethylene-reinforced (CSPE-R) • High-density polyethylene (HDPE) • Very low density polyethylene (VLDPE)
B) Less Used
• Ethylene interpolymer alloy-reinforced (EIA-R) • Linear low-density polyethylene (LLDPE) • Chlorinated polyethylene-reinforced (CPE-R)
C) Relatively New
• (Flexible) polypropylene (PP) • Fully cross-linked elastometric alloy (FCEA)

2.3.2 Applications of Geosynthetics and the Use of Interface Shear Strength Parameters

The major functions of geosynthetics and the type of geosynthetics accompanying these applications are given in Table 2.4.

Table 2.4. Major Functions of Geosynthetics

Function	Definition	Geosynthetic
Separation	The synthetic prevents mixing of adjacent dissimilar soils during construction or during repeated external loading of the soil-synthetic system.	Mainly geotextiles, sometimes together with geomembranes
Filtration	The synthetic prevents migration of soil particles without impeding water flow.	Geotextiles
Drainage	The synthetic collects and conveys water in its plane.	Geotextiles, geonets
Reinforcement	The inclusion of the fabric increases the strength of the soil mass, thereby increasing stability or bearing capacity or reducing earth pressures.	Geotextiles, geogrids
Sealing	The synthetic prevents liquid or gas migration in a human - made project, structure or system.	Geomembranes, geotextiles - chemically treated to provide impermeability
Protection	Mechanical protection of geo-membranes against perforation and abrasion.	NW geotextiles

In geotechnical projects involving geosynthetics, one or more of the functions given in Table 2.6 are utilized . Very broadly, the areas of applications include railroads, paved or unpaved roads, retaining walls, slope stabilization, increasing the bearing capacity of foundations and landfill containment systems. Most of these applications involve inclined surfaces where a geosynthetic rests on top of another geosynthetic or soil. Figures 2.7 - 2.9 illustrate the application of one or more types of geosynthetics in geotechnical projects.

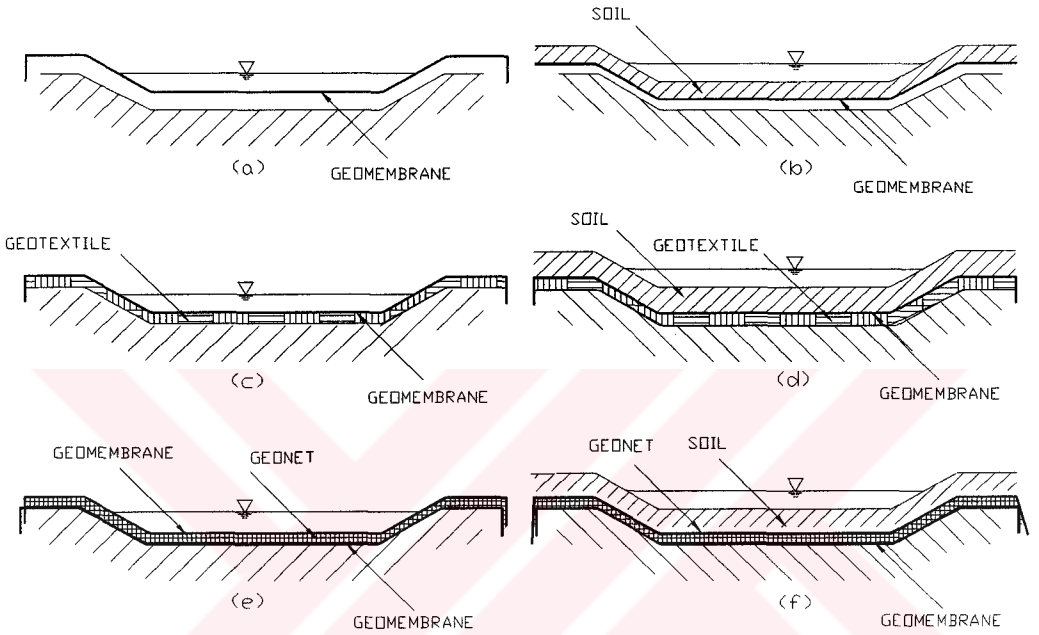

Figure 2.7. Various Types of Geomembrane Liner Systems for Liquid Containment, (a) Single Unprotected Liner System, (b) Liner with Soil Covering, (c) Liner with Geotextile Underliner, (d) Liner with Geotextile Underliner and Overliner with Soil Covering, (e) Double Liner with Geonet Leak Detection between Liners , and , (f) Double Liner with Geonet Leak Detection Between Liners and Soil Covering which may or may not contain a Geotextile or Geogrid as Reinforcement (After Koerner, 1994).

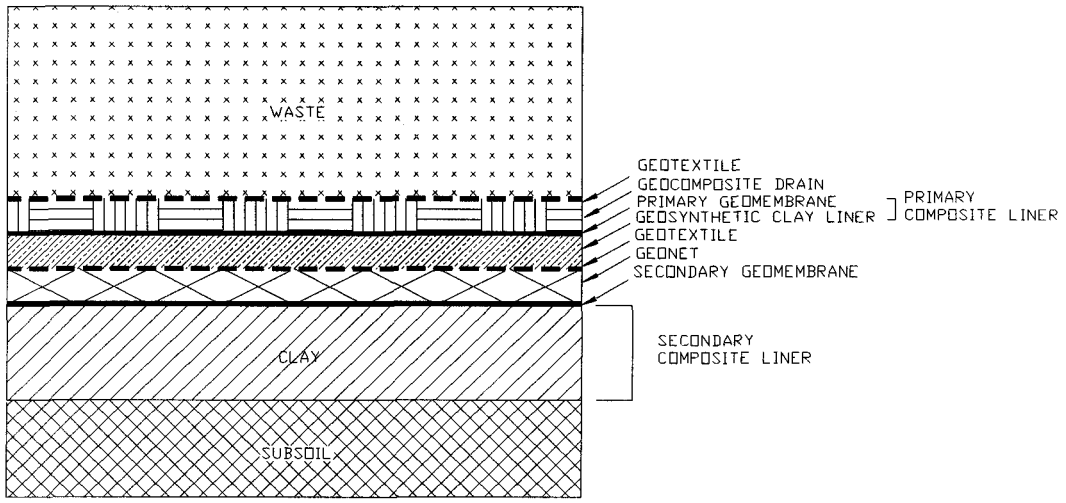

Figure 2.8. **Double Composite Liner for a Waste Containment System (After Koerner, 1994).**

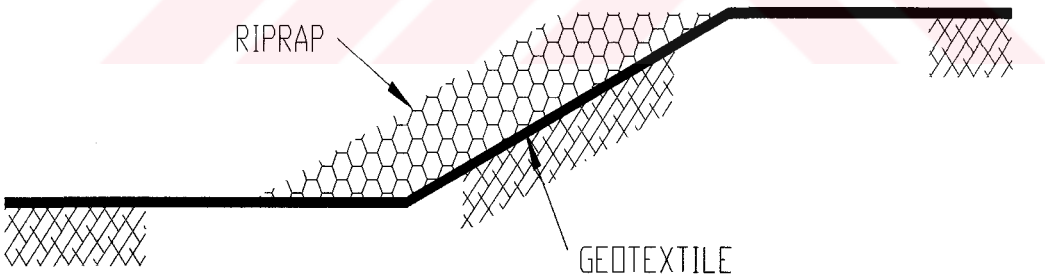

Figure 2.9. **Geotextiles and Riprap as Used for Erosion Control on Slopes (After Cernica, 1995).**

The methods of analysis used for the side slope stability of interfaces involving geomembranes are the infinite slope analysis and the block and wedge analysis. Figures 2.10 and 2.11 present the infinite slope analysis method whereas Figure 2.12 gives the general block and wedge analysis for soil cover of tapered thickness. Figure 2.13 presents a simplified version of the block and wedge analysis given in Sharma and Lewis, 1994 (After Giroud and Beech, 1989) for a cohesionless soil cover of uniform thickness. The details of analysis for the runout and anchor trench shown in Figure 2.12 are explained in Figures 2.14 and 2.15 respectively.

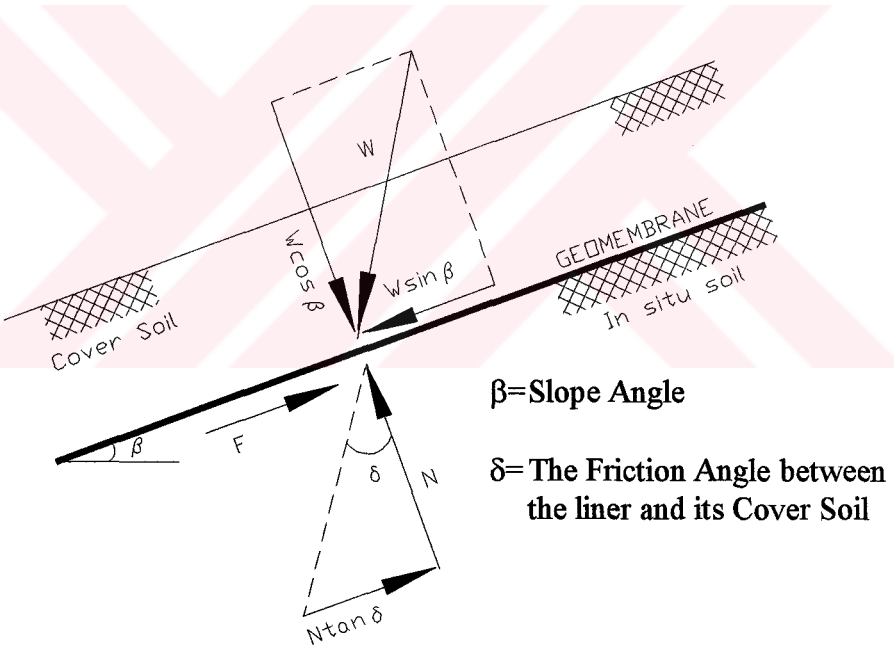

Figure 2.10 Infinite Slope Analysis for Cover Soils on Geomembrane-lined slopes for Uniform Depth of Cover Soil (After Koerner, 1994).

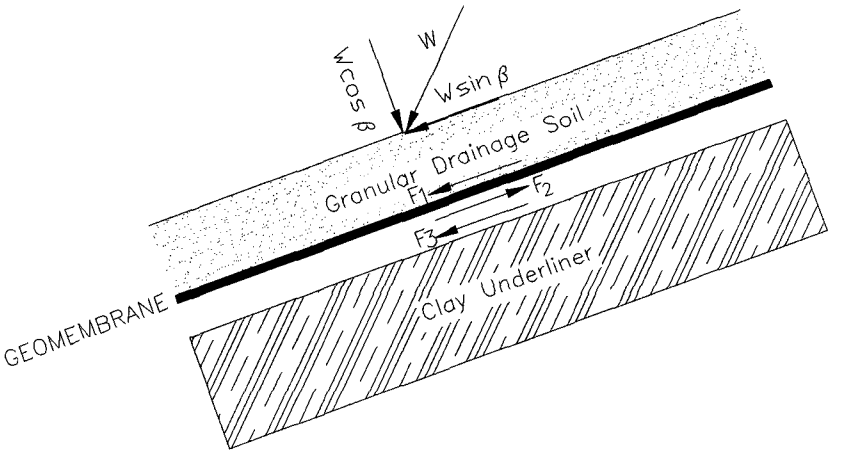

Figure 2.11 Resolution of Shear Stresses for Infinite Slope Analysis in a Geosynthetic-lined Landfill System (Adopted from Koerner, 1994).

The values in Figure 2.11 are defined as follows:

W= The weight of a lift thickness of waste plus the drainage soil,

β= The slope angle

N= W cos β

$F_1 = N \tan \delta_1$

δ_1 =The friction angle of the drainage soil to the upper surface of the geomembrane

$F_2 = N \tan \delta_2$

δ_2 =The friction angle of the lower surface of the geomembrane to the clay underliner

$F_1 - F_2$ =The tensile stress the geomembrane must carry (but only if $F_1 > F_2$).

F_3 = The equal and opposite force to F_2 (which must be carried by the clay).

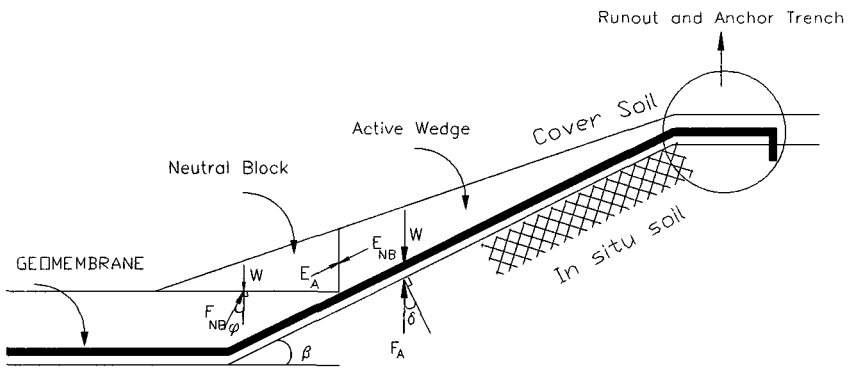

Figure 2.12 Block and Wedge Analysis for Cover Soils on Geomembrane-lined slopes for Non-Uniform (Tapered) Depth of Cover Soil (After Koerner, 1994).

The values in Figure 2.12 are defined as follows:

W_A = The weight of active wedge (area x unit weight)

F_A = The frictional force of cover soil acting on liner (unknown in magnitude but known in direction, which is at an angle δ to the perpendicular to the liner)

δ = The angle of shearing resistance of cover soil to liner

E_A = The force from neutral block acting on active wedge (unknown in magnitude but assumed parallel to cover soil slope)

E_{NB} = The force from active wedge acting on neutral block (equal in magnitude but opposite in direction to E_A)

W_{NB} = The weight of neutral block (area x unit weight)

F_{NB} = The friction force of soil below neutral block (unknown in magnitude, but known in direction, which is at an angle ϕ to the vertical)

ϕ = The angle of shearing resistance of cover soil

The solution involves iterations using a different factor of safety, which applied to the δ and ϕ angles.

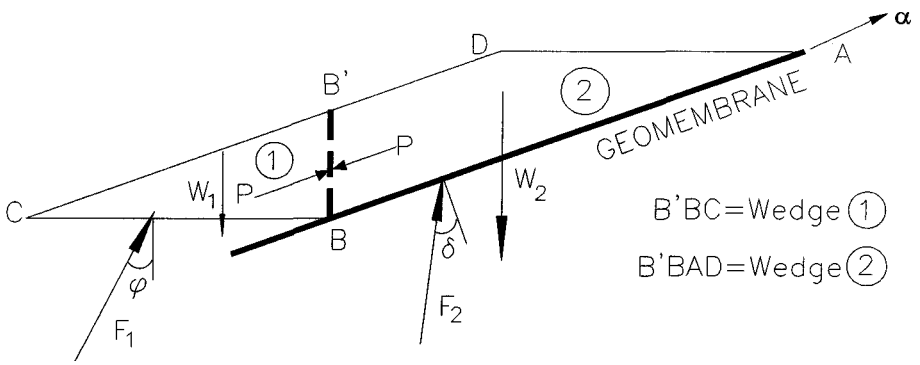

Figure 2.13 Simplified Block and Wedge Analysis for Cohesionless Soils (After Sharma and Lewis, 1994).

The values in Figure 2.12 are defined as follows:

W_1 = Weight of part 1 per unit width perpendicular to the plane of the figure

W_2 = Weight of part 2 per unit width perpendicular to the plane of the figure

F_1 = Force per unit width due to soil friction

F_2 = Force per unit width due to interface friction within the geosynthetic lining system or between the lining system and the soil

δ = The angle of shearing resistance to cover soil to liner

ϕ = The angle of shearing resistance of cover soil

P = Force per unit width transmitted between the two wedges

α= Tension in the geosynthetics located above the slip surface (assumed to be parallel to the slope).

No factor of safety is applied to the δ and ϕ angles. The value of P found from wedge ① is used for wedge ② to find α.

In Figures 2.14 and 2.15, δ is the friction angle between geomembrane and soil, and F_U and F_L are the upper and lower interface friction forces defined in terms of tan δ. F_U is usually assumed to be negligible since the cover soil probably moves with the liner as it deforms.

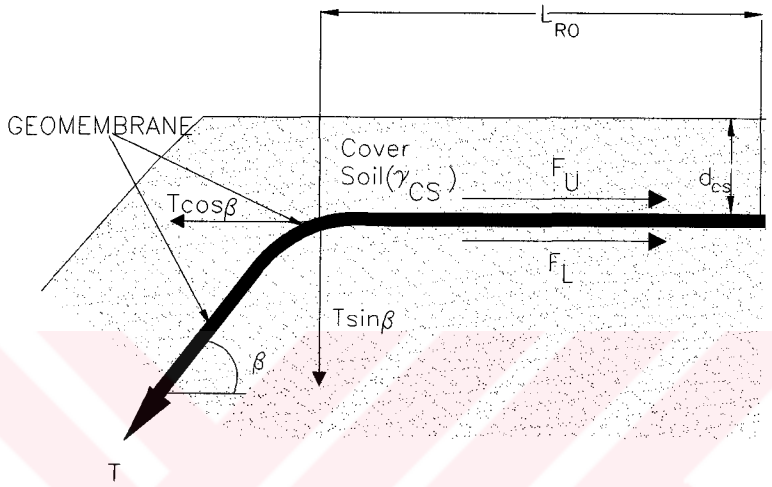

Figure 2.14 Cross Section of Geomembrane Runout Section (After Koerner, 1994)

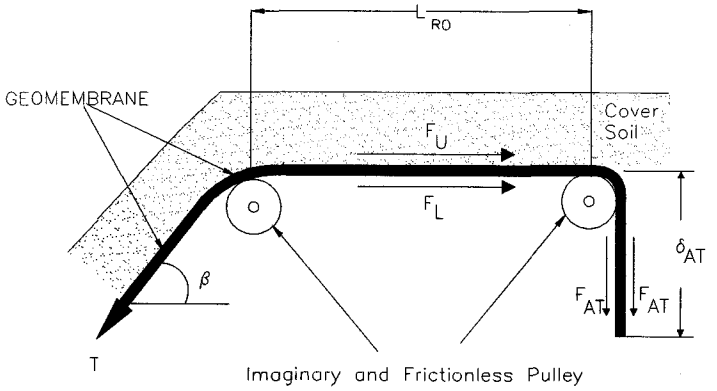

Figure 2.15 Cross Section of Geomembrane runout Section with Anchor Trench (After Koerner, 1994).

CHAPTER III

DETERMINATION OF INTERFACE FRICTION ANGLE

3.1 Introduction

Although many projects that incorporate geosynthetics are presently being designed and built, an internationally accepted method for testing frictional properties of geosynthetics has not yet been developed. As the most critical part of any stability analysis is the determination of friction parameters along an interface, a number of experimental devices has been used in reported works as given in Table 3.1.

In this chapter, the direct shear-box test, the pullout-box test, the inclined board test (also named as Tilting Table" or "Inclined Plane Test" in the literature) and the shaking table test (for dynamic conditions) are discussed. In addition, a brief discussion on the torsional ring-shear test is presented.

Table 3.1. Test Apparatus Used for the Evaluation of Interface Shearing Resistance (After Pasqualini et al.,1995).

REFERENCES	EQUIPMENT	DIMENSION (cm x cm)
Martin et al., 1984	Shear Box	10 x 10
Saxena and Wong, 1984	Shear Box	28 x 28
Koerner et al., 1986	Shear Box	10 x 10
Williams and Houlihan, 1987	Shear Box	30 x 30
Mitchell et al., 1990	Shear Box	7 x 7
Mitchell et al., 1990	Shear Box	5 x 5 and 7 x 7
Mitchell et al., 1990	Pullout Box	43 x 25
O' Rourke et al., 1990	Shear Box	6 x 6
Matichard et al., 1991	Shear Box	10 x 10
Matichard et al., 1991	Half Box Rigid Plane[a]	25 x 25
Matichard et al., 1991	Inclined Board	25 x 25
Matichard et al., 1991	Shear Box	30 x 30
Matichard et al., 1991	Inclined Board	100 x 100
Yegian and Lahlaf, 1992	Shear Box	20 x 20
Yegian and Lahlaf, 1992	Shaking Table	91 x 81
Pasqualini et al., 1993	Shear Box	14 x 14
Pasqualini et al., 1993	Shear Box	7 x 7
Pasqualini et al., 1993	Shear Box	6 x 6 and 10 x 10

[a] No explanation on the test method could be obtained

3.2 Direct Shear Box Test

Interface friction angles between soils and geosynthetics are widely determined in direct shear-box tests (Martin et al., 1984; Sexana and Wong, 1984; Koerner et al., 1986; Williams and Houlihan, 1987; Mitchell et al., 1990; O'Rourke et al., 1990; Seed and Boulanger, 1991; Sharma and Hullings, 1993). Even though nearly 75% of the reported values for soil-geosynthetic or geosynthetic-geosynthetic interfaces are deducted from direct shear-box tests, there is still not a definite method for direct shear testing.

Five basic methods are specified by Ingold (1991) for direct shear tests. The principles of each of these five methods are represented in Figure 3.1.

- Fixed Shear-Box: Employs a standard direct shear-box, in which the geosynthetic is mounted on a rigid block which is placed in the lower half of the shear-box. The upper half of the box is filled with soil that is sheared over the geosynthetic below (Ingold, 1982).

- Partially Fixed Shear-Box: The geosynthetic is laid over soil filling the lower half of the shear-box. One end of the synthetic material is clamped to the lower half of the shear-box and, soil in the upper half is sheared over the interface (Ingold, 1982).

- Free Shear-Box: Is similar to the partially fixed shear-box test except the geosynthetic is free at both ends (Richard and Scott, 1985).

- Large Base Shear-Box: Is similar to the fixed shear-box test except that the lower half of the box has a larger plan dimension than the upper half of the box containing the soil. This method has the advantage that there is a constant contact area between soil and the geosynthetic (Myles, 1982).

- Central Base Shear-Box: This operates on a similar principle as the large base shear-box, except in this case the frictional force generated in the geosynthetic in the lower half is measured over a plan area smaller than the plan area of the soil in the upper half of the box (Brandt, 1985).

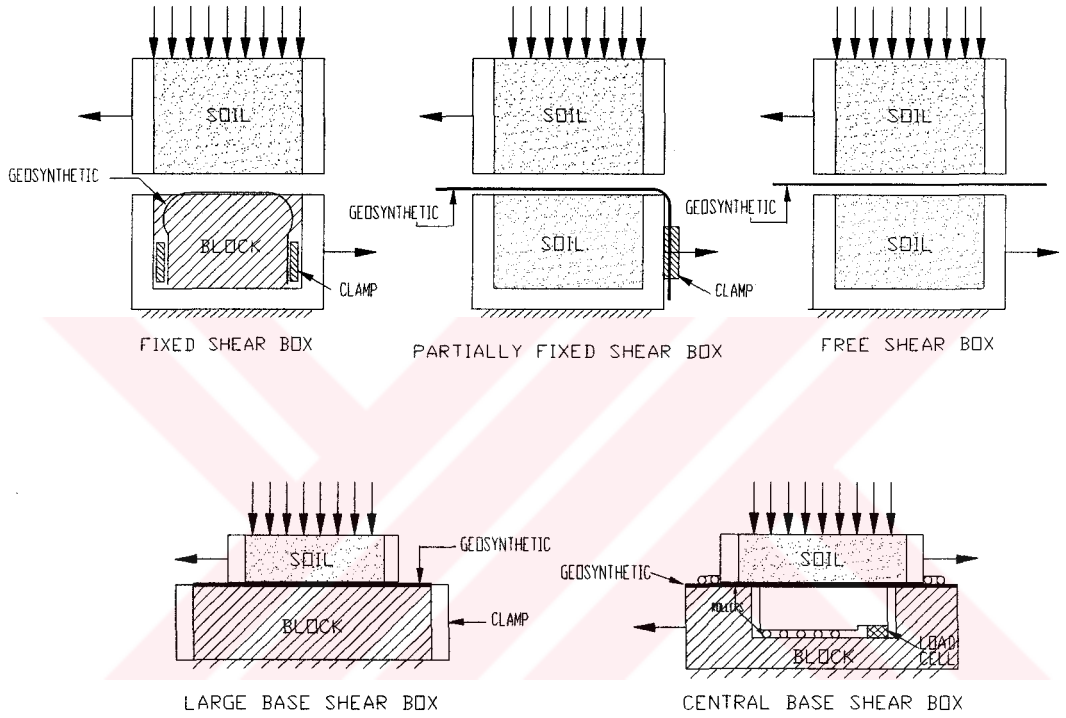

Figure 3.1. Types of Direct Shear Apparatus (After Ingold, 1991).

In BS 6906 (1991), the methodology for determining the frictional resistance of a geosynthetic against soil is given in detail. The test described is mainly similar to the one used for shearing soil-soil interfaces alone. A 30 x 30 cm shear-box is recommended for which the sketch is given in Figure 3.2.

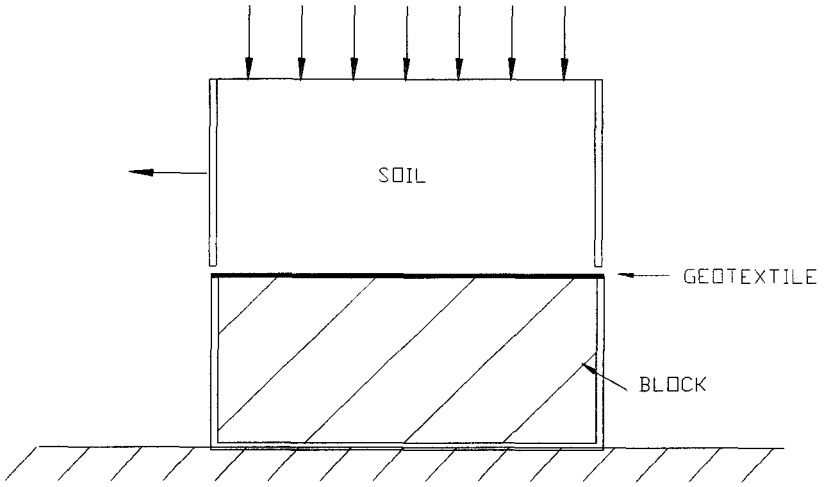

Figure 3.2. Details of the Test (After BS 6906, 1991).

The test is to be performed at a minimum of three different normal stresses. The peak and residual shear stresses obtained are then plotted against their values of normal stress. The slope of the best-fit straight line passing through the points of peak shear stress defines the peak coefficient of friction. Similarly, the slope of the best-fit straight line passing through the points of residual shear stress defines the residual coefficient of friction.

3.3 Pullout-Box Test

Shear strength of interfaces incorporating geosynthetics are often evaluated using pullout-box tests for which the schematic illustration is given in Figure 3.3.

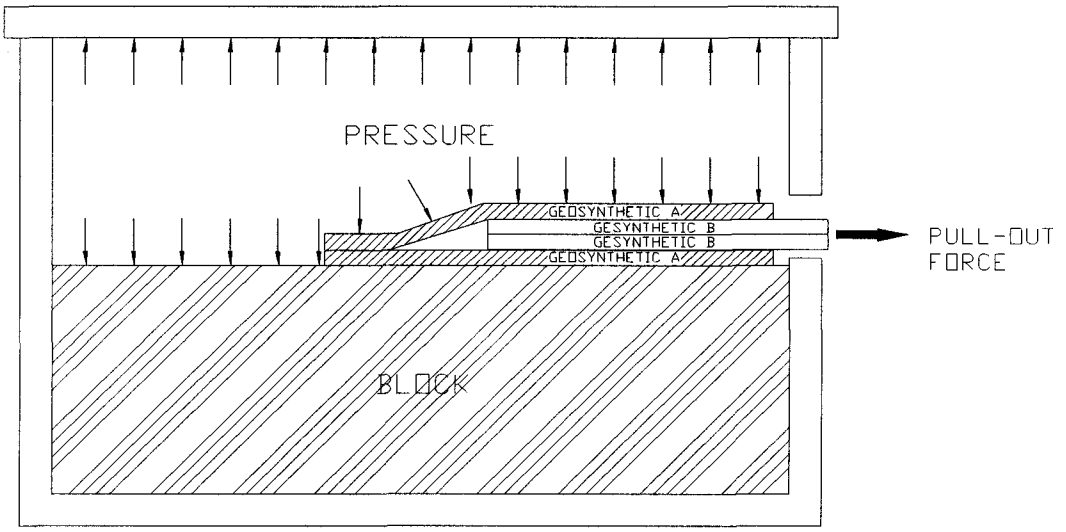

Figure 3.3. Schematic Illustration of Pullout-Box (After Mitchell et al., 1990).

Srinivasa Murthy et al. (1993) stated that pullout tests of different sizes have been conducted by many researchers (Bacot et al., 1978, Schlosser and Elias, 1978; Ingold, 1982, 1984; Sridharan and Singh, 1984, 1986, 1988; Kate et al., 1988, Rao and Pandley, 1988) to distinguish the effects of various parameters of the material tested, but the size of the pullout-box tests are not yet been standardized. From the literature, it is found that, pullout-box size varies from 60x60x20 mm (Rao and Padley, 1988) to 915x915x450 mm (Schlosser and Elias, 1978).

In a pullout-box test, the pullout resistance,τ, i.e. the frictional resistance against sliding, is calculated using Equation 3.1 (Koerner, 1994).

$$\tau = \frac{P}{2wL} \tag{3.1}$$

where;

P = Pullout force

w = Width of geosynthetic

L = Length of geosynthetic embedded in soil

The results of an investigation carried out by Dembicki and Alenowicks (1987) at the University of Gdañsk in Poland, using a 100 x 100 mm shear-box and a large scale pullout-box, indicate that the direct shear test is more suitable than the pullout-box test for the following reasons:

(a) In a pullout-box test shear stresses are not uniformly distributed on the sample before the movement of the sample starts;

(b) Wrinkling can introduce a problem in imposing plane strain conditions especially when thick and soft non-woven geotextiles are utilized;

(c) The measured horizontal force in a pullout-box test consists of two components: i) the force related to the elongation of the free length of the geosynthetic outside the box and, ii) the force related to the shear forces developed inside the box. As a result, the outputs of tensile tests are needed for the precise determination of friction characteristics of the interface;

(d) In a pullout-box test, some part of the geosynthetic is not confined in soil and this part elongates significantly before the relative movement of the synthetic in the soil is initialized.

Similar to item (d), Srinivasa Murthy et al. (1993) reported that the results of pullout-box tests on extensible geosynthetics can represent the interfacial frictional resistance but the results for extensible synthetics under high normal stress are not reliable.

3.4 Inclined Board Test

As explained in Chapter II, the internal angle of shearing resistance ϕ for cohesionless soils is made up of two components:

$$\phi = \phi_\mu + \beta \qquad (3.2)$$

where;

ϕ_μ = Angle of sliding friction between mineral surfaces

β= Effect of interlocking

The dilation theory also applies to interfaces containing a cohesionless soil-geosynthetic combination. Williams and Houlihan (1986) accepted dilation as the primary component of soil-geosynthetic interface friction and proposed that the highest interface friction angles are developed between layers where a significant degree of dilation occurs. As Koutsourais et al. (1991) revealed, for dense cohesionless soil, friction angles under low normal stresses are higher than the values approached under greater normal stress because dense soils under low stresses tend to dilate for which the result is high frictional resistance. According to Ingold (1991), when the normal stress is increased, the ability of soil to dilate to give a high δ', is suppressed and δ' approaches a residual value at higher confining stresses. Consequently, although a straight line failure envelope is assumed for a series of shear-box test results, due to the effects of dilatancy, the true envelope at low stresses curves down and most of the time passes through the origin, with a δ' greater than the one for a straight envelope. In this case, assuming a straight envelope with an adhesion factor may lead to unsafe design.

Figure 3.4 and Figure 3.5 summarize the effects of dilation on the failure envelope.

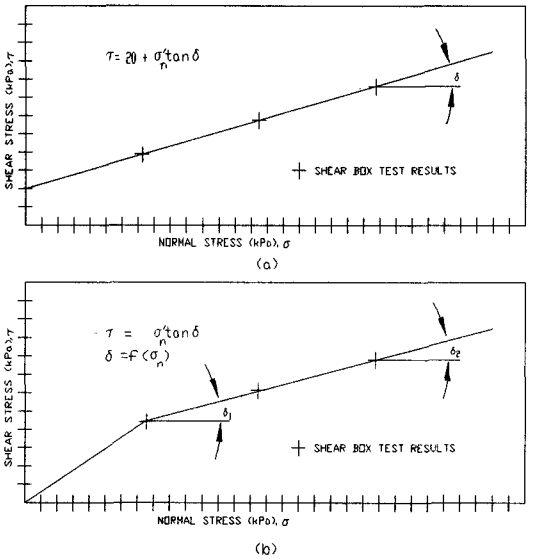

Figure 3.4. Interpretation of Shear-Box Test Results (a) without dilation effect, and (b) with dilation effect (After Ingold, 1991).

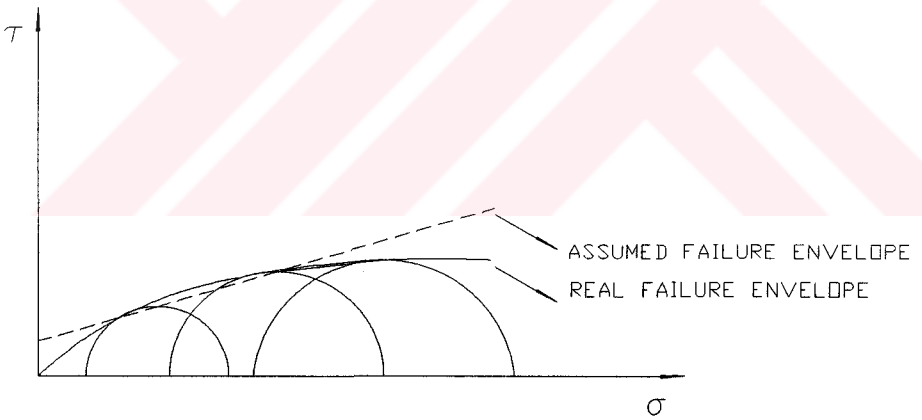

Figure 3.5. Dilation Effects on Mohr-Coulomb Failure Criterion (After Koutsourais et al., 1991).

A similar ambiguity arises for the interpretation of clay-geosynthetic direct shear-box test results. For an undrained test on a saturated clay-geosynthetic interface, the failure envelope is a straight horizontal line with $\delta_u = 0$. If the clay is

partially saturated or heavily consolidated, the failure envelope at lower stresses curves to give a $\delta_u > 0$. At higher normal stresses, the soil sample becomes saturated and the failure envelope reverts to the theoretical one. This bias of the failure envelope to curve towards the origin is sketched in Figure 3.6.

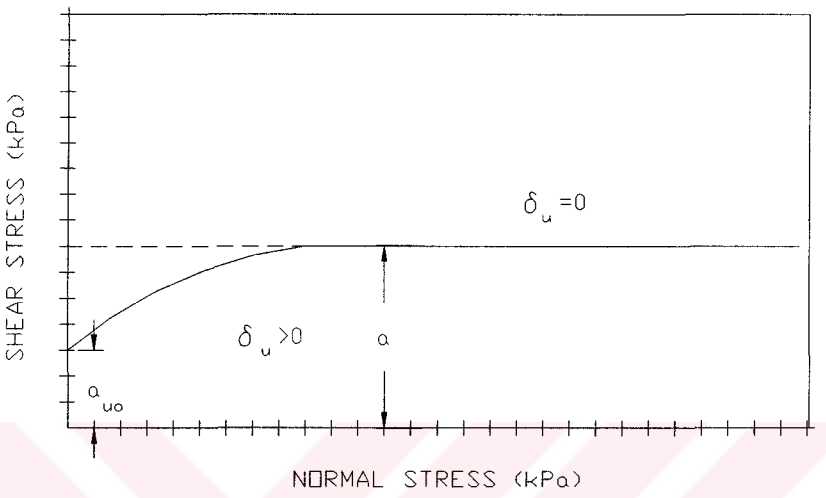

Figure 3.6. Undrained Strength Parameters for a Cohesive Soil-Geosynthetic Interface (After Ingold, 1991).

The tendency of the failure envelope to give a higher δ value under low stresses both for cohesive and for cohesionless soils, requires a detailed analysis of the interface friction characteristics for low normal confinements. Even though this is the real case for a geosynthetic covered by a protective layer, most measurements published were carried out using shear-box tests which are unable to apply low normal stresses (Girard et al., 1990).

Giroud et al. (1990) stated that, particularly with large direct shear-box, the tests under normal stresses below 25 kPa are not accurate. However, as previously pointed out, the Mohr Envelope for nearly all soils is curved at low normal stresses. This necessitates the determination of friction parameters by another

method when the normal stresses are low. Therefore, the shear-box test results should be complemented with inclined board tests.

Inclined board test (Fig. 3.7) is simply composed of a base plate hinged on one side, and a sliding block which is placed on the base plate, with a geosynthetic specimen attached on it. The inclination of the plate is increased by mechanical or electronical means until the block slides and the inclination at which sliding occurs is recorded to determine δ. For an inclined board test, the inclination of the board gives only an apparent friction angle, δ, which is equal to the interface friction angle if the failure envelope is a straight line passing through the origin of axes, i.e. when there is no interface adhesion (a = 0) (Giroud et al., 1990).

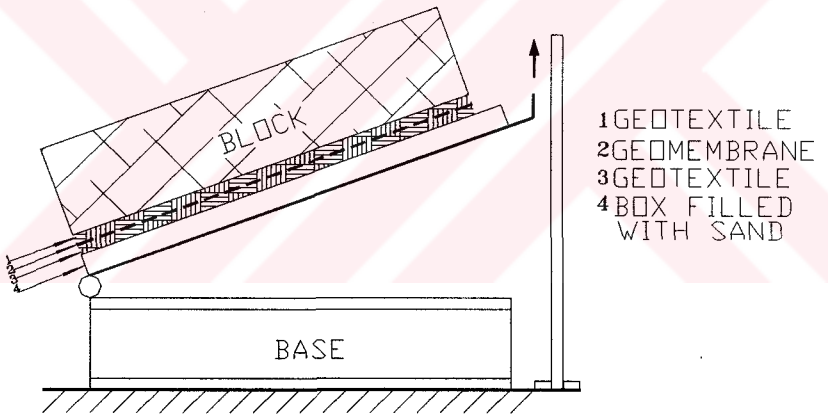

Figure 3.7. The Inclined Board Test Apparatus (After Girard, 1990).

3.5 Shaking Table Test

Nearly all of the shear strength values for geosynthetic-soil and geosynthetic-geosynthetic interfaces given in the literature by Myles (1982), Martin et al. (1984), Saxena and Wong (1984), Williams and Houlihan (1986), Miyamori et al. (1986), Negussey et al. (1989), O'Rourke et al. (1990) and Mitchell et al. (1990) were the results of extensive static tests. These results are directly used for the static stability analysis and design of geotechnical facilities that involve geosynthetics (Yegian and Lahlaf, 1992). Yet, the dynamic behavior of such projects; i.e. their reaction under seismic, blast or other vibrations are not sufficiently studied.

Yegian and Lahlaf (1992) used a shaking table facility and an instrumentation system to evaluate the dynamic friction properties of geosynthetic-geosynthetic interfaces. Figure 3.8 and Figure 3.9 respectively give the schematic representation of the shaking table and free body diagram of the concrete block used in the tests.

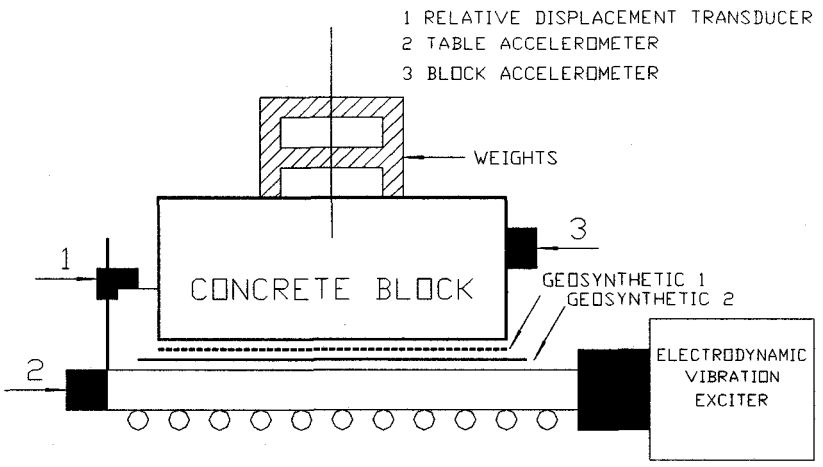

Figure 3.8. Shaking Table Facility (After Yegian and Lahlaf, 1992).

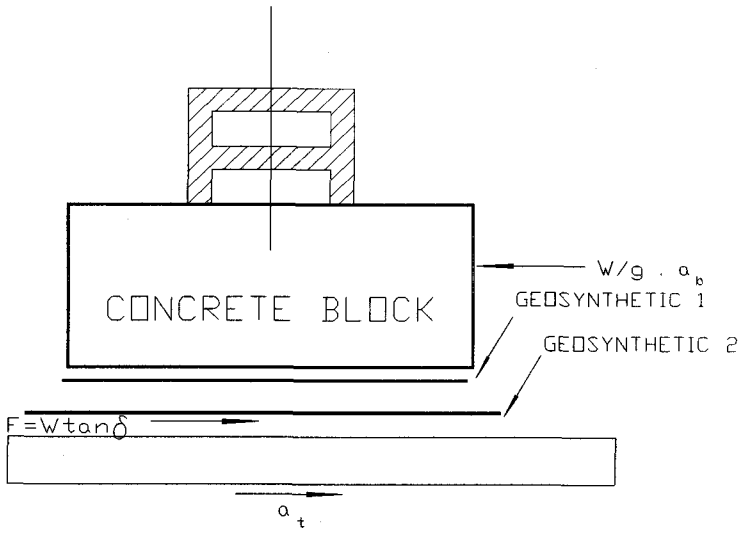

Figure 3.9. Free-Body Diagram of Block (After Yegian and Lahlaf, 1992).

As seen from Figure 3.8, the shaking table had an electrodynamic vibration exciter that gave the table a motion for which the amplitude and the frequency were controlled by a signal generator. A concrete block with the attached weights was placed on the table. The acceleration of the table (a_t) and that of the block (a_b) were measured simultaneously by piezoelectric accelerometers. A linear variable-displacement transducer (LVDT) was used to follow the relative displacement of the block with respect to the table. Knowing the table acceleration and the acceleration it induced to the block; and using the free-body diagram in Figure 3.9, the dynamic angle of friction was obtained through the series of the following equations.

$$F = W \tan \delta \tag{3.3}$$

where;

F = Friction force transmitted from the table to the block

W = Total weight of the concrete block and the attached weights

δ= Geosynthetic-geosynthetic dynamic interface friction angle

The equilibrium of forces gives:

$$W \tan \delta = (W / g)\, a_b \qquad (3.4)$$

where;

a_b = Block acceleration

g = Gravitational acceleration

The dynamic interface friction angle is obtained from Equation 3.4 as:

$$\phi_d = \tan^{-1} (a_b / g) \qquad (3.5)$$

Equations 3.3, 3.4 and 3.5 refer to the instant exactly when the block just starts to move relative to the table, thus giving the peak angle of friction. Immediately after the initiation of the block movement, there is a drop in the measured block acceleration which in turn leads to the residual angle of dynamic interface friction.

3.6 Torsional Ring Shear Test

The cyclic behavior of geosynthetic-soil systems; i.e. their response under continuous shearing, is as important as their behavior under dynamic loading. Continuous shearing phenomenon is essential to mobilize a residual interface strength which can not be obtained in any direct shear box test.

According to Stark and Poeppel (1994); direct shear testing is an effective tool for evaluating the peak interface strength, but, it is not sufficient to maintain an average shear displacement of 40-60 cm which is usually required to obtain the residual interface strength. The shear-box may be reversed a number of times to acquire such large displacements but these reversals do not apply continuous displacement in one direction and thus do not simulate field shearing conditions that lead to residual strength condition.

This problem is overcome by using the ring shear apparatus (Bishop et al., 1971) which tests a circle of soil in a ring, split horizontally at its mid-section, allowing the lower half of the sample to be sheared over a stationary held upper half with no change in contact area between the two faces.

Other advantages of the torsional ring shear apparatus for which the schematic diagram is given in Figure 3.10, are that it provides a constant cross-sectional area during shear, it requires minimum control during the test and it protects the samples against disturbance of particle alignment which is the case in the reversal of the shear-box apparatus.

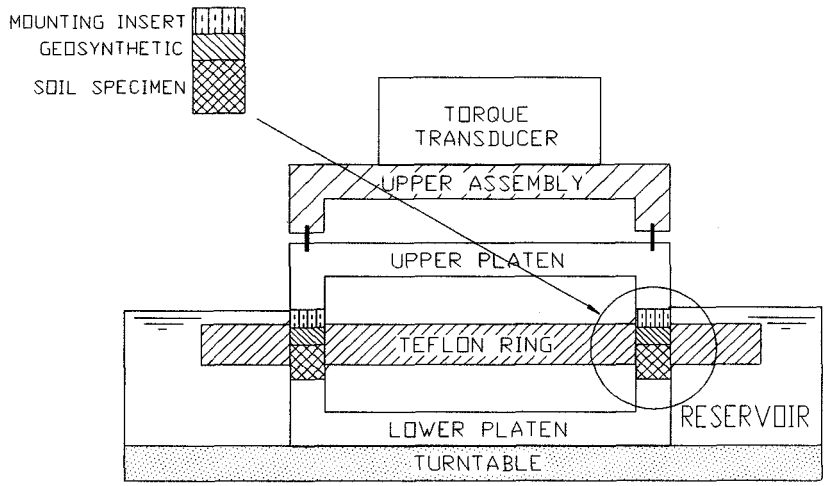

Figure 3.10. Torsional Ring Shear Apparatus (After Evans and Fennick, 1995).

CHAPTER IV

TEST RESULTS FROM THE LITERATURE

4.1 Direct Shear Box Test Results

In the following paragraphs, a summary of various direct shear-box test programs and their results are presented. A more detailed information was given by Takasumi et al. (1991).

Weiss and Batereau (1987) conducted a series of direct shear-box tests using a specially constructed flat shear device. In the test program, 1.5 mm thick PVC or PE geomembranes were used together with a range of geotextiles, the characteristics of which are given in Table 4.1. The geosynthetics were sheared over sand, silt and prefabricated concrete slab. A normal stress range of 5-50 kPa were applied to dry and saturated samples and the test results are given in Table 4.2, Table 4.3 and Table 4.4. The properties of the sand or silt used are not cited.

Table 4.1. Geotextile Properties (After Weiss and Batereau, 1987).

Type	Thickness[a] (mm)	O_{90} (mm)	Polymer fiber
A (NW Geotextile)	2.7	0.07	50% Polyester 50% PVC
B (NW Geotextile)	3.4	0.06	50% Polyester 50% PVC
C (NW Geotextile)	5.2	0.25	100% Polyamide
D (Geomembrane)	3.1	-	100% Polyamide
E (Geomembrane)	3.2	-	100% Polyester
F (Geomembrane)	3.2	-	100% PVC

[a] Under a vertical stress of 20 kN/m^2

[b] Geotextile pore opening size for which 90% of the pore sizes are smaller than that diameter-Apparent opening size in Duth practice.

Table 4.2. Angles of Interfacial Shear (δ) between PE Film and Different Construction Materials (Adopted from Weiss and Batereau, 1987).

Materials in Contact with PE Film	δ (°)	
	Dry	Saturated
Geotextiles (Non-woven)	11 - 14	9
Silt	-	17 - 22
Sand	14 - 24	11 - 22
Prefabricated Concrete Slab	17 - 22	14 - 22

Table 4.3. Angles of Interfacial Shear (δ) between PVC Film and Different Construction Materials (Adopted from Weiss and Batereau, 1987).

Materials in Contact with PVC Film	δ (°)	
	Dry	Saturated
Geotextiles (Non-woven)	17 - 24	14 - 24
Silt	-	19 - 27
Sand	27 - 31	22 - 27
Prefabricated Concrete Slab	27 - 45	27 - 45

Table 4.4. Angles of Interfacial Shear (δ) between Non-woven Geotextiles and Different Construction Materials (Adopted from Weiss and Batereau, 1987).

Materials in Contact with NW Geotextile	δ (°)
	Saturated
Non-woven Geotextile (depends on kind of fibers)	15 - 22
Prefabricated Concrete Slab	
Smooth	24 - 31
Rough	31 - 39
Non-cohesive soil	27 - 35

Fourie and Fabian (1987) used a 60 mm x 60 mm direct shear-box apparatus to investigate the shear strength parameters of several geosynthetic material in contact with a silty clay (CL) with plastic limit (PL) of 14 and liquid

limit (LL) of 27%. The soil samples which were compacted at three different moisture contents were subjected to undrained and drained shear rates of 0.9 mm/min and 0.0033 mm/min respectively.

Two types of geotextiles and a geogrid mesh were used in the tests. The properties of the geosynthetic materials are given in Table 4.5, Table 4.6 and Table 4.7 represent the results of the test program.

Table 4.5. Properties of Geosynthetics (Adopted from Fourie and Fabian, 1987).

	Synthetic Type		
	Geosynthetic A	Geosynthetic B	Geosynthetic C
Polymer Type	Polyester	Polypropylene	Polyethylene
Fabrication	Non-woven Geotextile (needle-punched)	Woven Geotextile	Extruded Geogrid Mesh
O_{90} (mm)	0.094 - 0.06	0.25	8 x 6

Table 4.6. Results of Undrained Shear Tests (After Fourie and Fabian, 1987)

Clay			Non-woven		Woven fabric		Geogrid mesh	
Water content (%)	Normal stress (kPa)	c_u (kPa)	Bond strength (kPa)	Adhesion[a] factor	Bond strength (kPa)	Adhesion factor	Bond strength (kPa)	Adhesion factor
15	50	75	39	0.52	28	0.37	35	0.46
	100	88	75	0.85	60	0.68	65	0.74
	150	98	105	1.07	94	0.96	96	0.98
	250	114	122	1.12	110	0.96	114	1.00
	350	130	153	1.16	117	0.90	120	0.93
17	50	57	38	0.66	30	0.52	58	1.02
	100	75	66	0.88	55	0.73	73	0.98
	150	79	94	1.25	70	0.89	80	1.02
	250	83	-	-	-	-	-	-
19	50	33	56	0.79	18	0.54	20	0.60
	100	36	64	1.50	33	0.92	30	0.88
	150	40	66	1.65	43	1.08	39	0.98

[a] Adhesion Factor = Bond Strength / c_u

Table 4.7. Results of Drained Shear Tests at 15% Water Content (After Fourie and Fabian, 1987).

Clay		Non-woven		Woven fabric		Geogrid mesh	
Normal stress (kPa)	Drained strength (kPa)	Shear stress (kPa)	Adhesion[a] factor	Shear stress (kPa)	Adhesion factor	Shear stress (kPa)	Adhesion factor
50	25	30	1.20	55	2.20	38	1.52
150	72	86	1.19	126	1.75	123	1.70
250	124	158	1.39	190	1.58	183	1.51
350	170	233	1.37	-	-	-	-

[a] Adhesion Factor = Bond Strength/Drained Strength of Clay

According to Fourie and Fabian (1987), the mechanism of drained shearing resistance developed on the clay - geotextile interface does not differ from that of sand - geotextile interface. It apparently does not depend on the transmissivity of the geotextile but instead on the roughness of the geotextile surface and on the stiffness and strength of the geotextile. However, in undrained conditions, the interaction is affected by the transmissivity of the geotextile. If the transmissivity of the geotextile is large enough, the geotextile may partly drain the interface thus increasing the shearing resistance of the clay itself. This leads to an increase in the frictional resistance of the interface. High transmissivity, non - woven geotextiles can therefore effectively be used with clay in both drained and undrained conditions.

Dembicki and Alenowicz (1987) worked with a small (10 cm x 10 cm) and a large (25 cm x 40 cm) direct shear-boxes for their research on a multifilament woven geotextile and a thick needle-punched geotextile. Normal stresses used in the experiments ranged from 25 to 200 kPa. The geosynthetics were sheared against a dry fine sand and the shearing rates were 6 mm/min for the large box and 1 mm/min for the small box which can be accepted as quick-undrained test rates. The results of the experimental program are summarized in Table 4.8 and Table 4.9. Figure 4.1 gives the comparison of Tables 4.8 and 4.9.

Table 4.8. Direct Shear Box Test Results for Woven Geotextile (Adopted from Dembicki and Alenowicz, 1987).

Normal Stress (kPa)	Peak Interfacial Shear Strength (kPa)	
	Large Box	Small Box
25	17.0	15.0
50	32.3	26.7
100	61.22	51.0

Table 4.9. Direct Shear Box Test Results for Non-woven Geotextile (Adopted from Dembicki and Alenowicz, 1987).

Normal Stress (kPa)	Peak Interfacial Shear Strength (kPa)	
	Large Box	Small Box
25	20.6	18.6
50	36.7	33.0
100	67	64.8
200	124.6	112.6

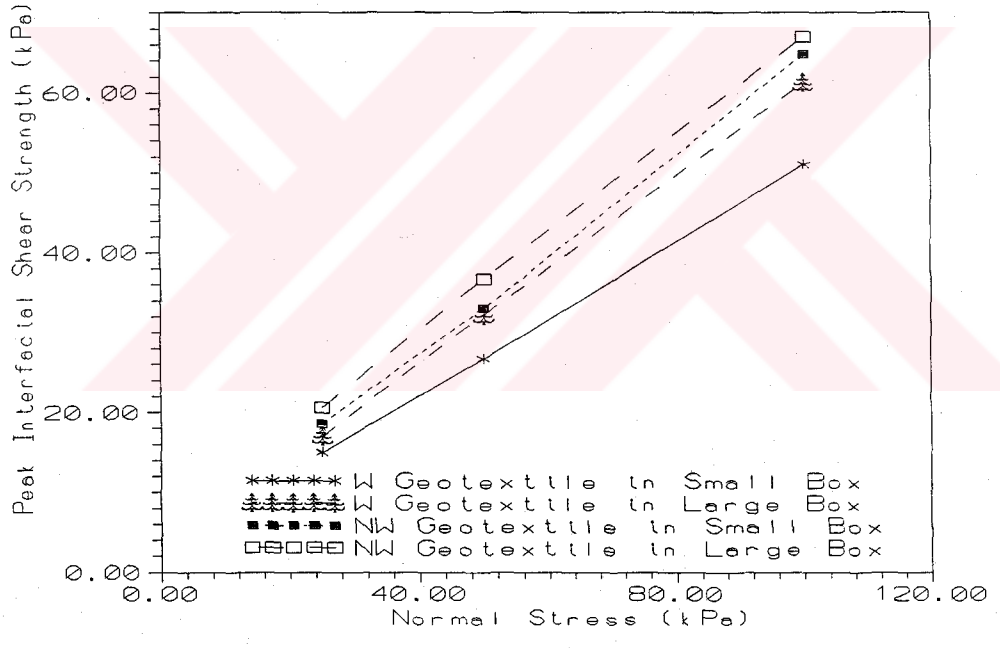

Figure 4.1. Effect of Geotextile Type and Size of Shear Box on the Shear Strength (Adopted from Dembicki and Alenowicz, 1987).

It can be seen from Figure 4.1 that, the non-woven geotextile provided a higher shear strength compared to the woven geotextile under the applied normal

stresses. In addition, it can be observed that, the tests which were performed in a small shear box gave smaller shear strength values when compared with the results from the large box.

Another investigation to evaluate the interface friction characteristics of soils (clay, sand and flyash) and several geosynthetics in various combinations, was made by Koutsourais et al. (1991), using a modified direct shear device with dimensions of 30.5 cm x 30.5 cm. The tests were run at normal stresses ranging from 20 kPa to 62 kPa at shear rates of 0.0025 mm/min to 0.25 mm/min. The tests involving sand and fly ash showed a drained behavior whereas the tests on clay were accepted as undrained.

Characteristics of the soil types that were included in the test program were as given in Table 4.10.

Table 4.10. Characteristics of the Tested Soils (Adopted from Koutsourais et al., 1991).

(1) River sand (SP) (characterized by uniform subangular particles)	(2) Kaoline (CL) (characterized by flat, plate-like particles)	(3) Fly ash (ML) (characterized by rounded particles)
γ_d = 15.0 - 15.4 kN/m^3	γ_w = 18.2 kN/m^3	γ_w = 14.1 kN/m^3
D_{10} = 0.17 mm	w = 30 %	w = 28 %
C_U = 2.8	PL = 27 %, LL = 42 %	D_{10} = 0.0035 mm
e = 0.685	% Clay = 35%	C_U = 4.6
D_R = 80%		% Clay = 5 %

The geosynthetics that were tested included five geotextiles, five geomembranes, one geogrid and one geonet.

The five geotextiles were:

(1) Woven monofilament, polypropylene fabric which was thin and stiff with modest open area, (2) woven slit film polypropylene fabric which was thin and stiff with negligible open area, (3) woven multifilament polyester fabric which was thick and flexible with modest open area, (4) non-woven heat-bonded polypropylene fabric which was thin and relatively stiff with modest porosity, and, (5) non-woven needle-punched polyester fabric which was compressible, thick and flexible with high porosity.

The five geomembranes included:

(1) HDPE that was stiff, hard and smooth, (2) HDPE that was stiff, hard and rough, (3) VLDPE that was medium stiff, hard and smooth, (4) PVC that had medium stiffness, hardness and smoothness, and, (5) CSPE which was reinforced with a fabric scrim and had medium stiffness and roughness with a wavy roughness due to the laminated reinforcement.

The geogrid had thick, flexible ribs of medium smoothness and significant open area, where the geonet was HDPE with a thickness of 5.1 mm.

The results of the experimens are presented in Tables 4.11 - 4.15.

Table 4.11. Geosynthetic versus Sand Interface Friction and Efficiencies[a] (After Koutsourais et al., 1991).

Interface with sand	Normal Stress (kPa)							
	20		35		48		62	
	δ (°)	Eff.	δ (°)	Eff.	δ (°)	Eff.	δ (°)	Eff.
Sand	45	1.0	35	1.0	33	1.0	32	1.0
Non-woven (Needlepunched)	40	0.88	32.5	0.92	30.5	0.92	30	0.93
Non-woven (heat bonded)	37	0.82	32.5	0.92	32.4	0.98	32	1.0
Woven (Monofilament)	31	0.68	29	0.82	28	0.84	28	0.87
Woven (Multifilament)	40	0.88	33.5	0.95	32	0.96	31.5	0.98
Woven (Slit film)	34	0.75	30.5	0.87	30	0.90	30	0.93
HDPE - Smooth	28	0.62	27	0.77	26	0.78	26	0.81
HDPE - Rough	40.5	0.90	33	0.94	31.5	0.95	30	0.93
CSPE	33	0.73	31	0.88	31	0.93	31	0.96
VLDPE	28	0.62	23	0.65	21.5	0.65	21.5	0.67
PVC	33	0.73	30	0.85	30	0.90	30	0.93
Flexible Grid	42	0.93	33	0.94	32	0.96	31.5	0.98

[a] Efficiency (Eff) = δ / ϕ ,where, ϕ is the internal friction of sand

Table 4.12. Geosynthetic versus Fly Ash Interface Friction and Efficiencies[a] (After Koutsourais et al., 1991).

Interface with fly ash	Normal Stress (kPa)							
	20		35		48		62	
	δ (°)	Eff.	δ (°)	Eff.	δ (°)	Eff.	δ (°)	Eff.
Fly Ash	43	1.0	39	1.0	37	1.0	36	1.0
Non-woven (Needlepunched)	44	1.02	39	1.0	37	1.0	36	1.0
Non-woven (heat bonded)	42	0.97	38	0.97	36	0.97	36	1.0
Woven (Monofilament)	35	0.81	33	0.84	32	0.86	31	0.86
Woven (Multifilament)	42	0.97	38	0.97	37	1.0	36	1.0
Woven (Slit film)	40	0.93	36	0.0.92	35	0.94	34	0.94
HDPE - Smooth	33.4	0.77	32	0.82	31	0.83	30.4	0.84
HDPE - Rough	45	1.04	40	1.02	38	1.02	37	1.02
CSPE	39	0.90	36	0.92	35	0.94	34	0.94
VLDPE	28	0.65	24.4	0.62	22.4	0.60	22.4	0.62
PVC	38	0.88	35	0.89	34	0.91	33	0.91
Flexible Grid	42.8	0.99	38	0.97	36	0.97	35	0.97

[a] Efficiency (Eff) = δ / ϕ ,where, ϕ is the internal friction of fly ash

Figures 4.2 to 4.5 schematically present the results of Table 4.11 and 4.12.

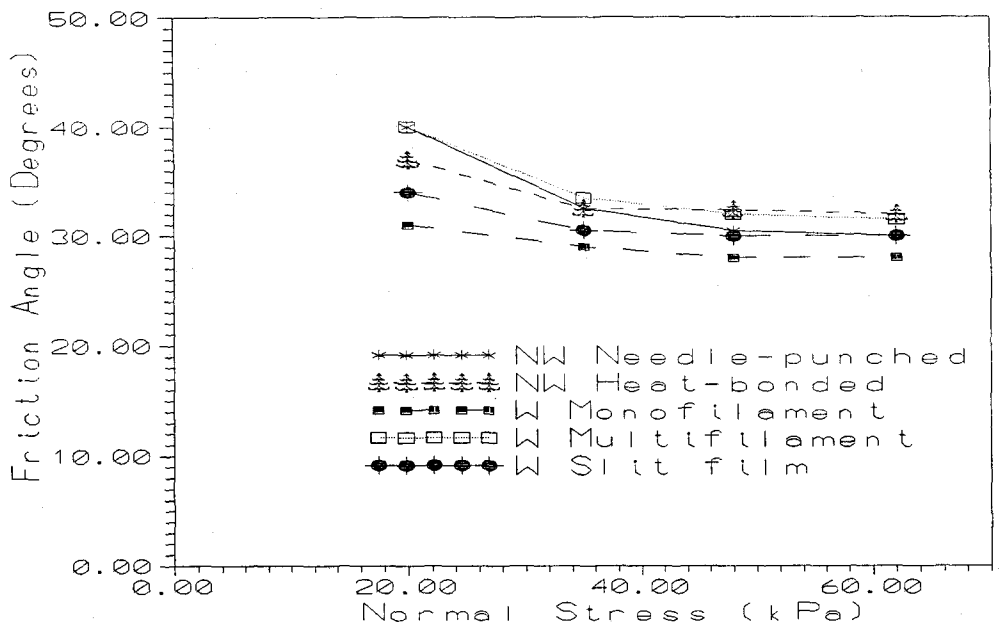

Figure 4.2. Friction Angles for Sand versus Various Geotextile Interfaces (Adopted from Koutsourais et al., 1991).

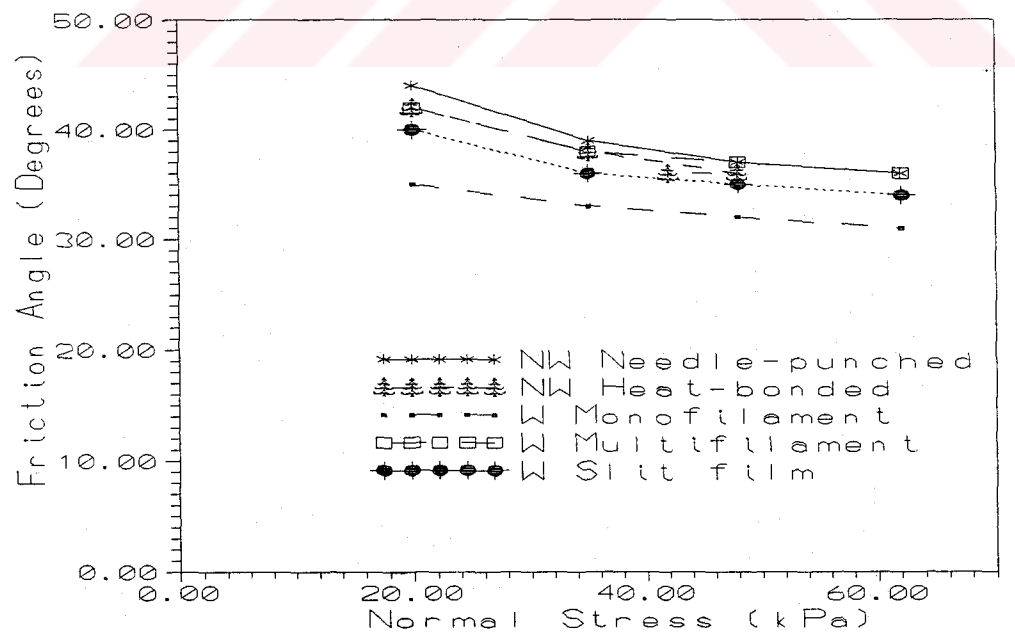

Figure 4.3. Friction Angles for Fly Ash versus Various Geotextile Interfaces (Adopted from Koutsourais et al., 1991).

As seen from Figures 4.2 and 4.3, in general, the performance of the non-woven needle punched geotextile is better than that of other types of geotextiles. The friction angles obtained for the woven multifilament - sand interfaces are also comparable with the former one and any of the two may be utilized for the projects where in-plane drainage ability is not required.

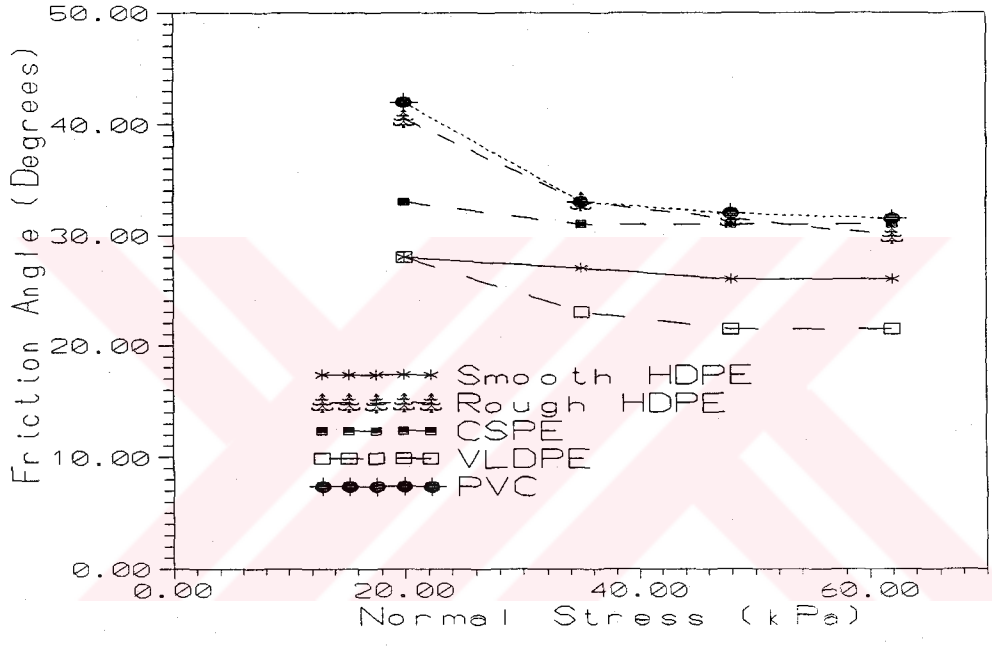

Figure 4.4. Friction Angles for Sand versus Various Geomembrane Interfaces (Adopted from Koutsourais et al., 1991).

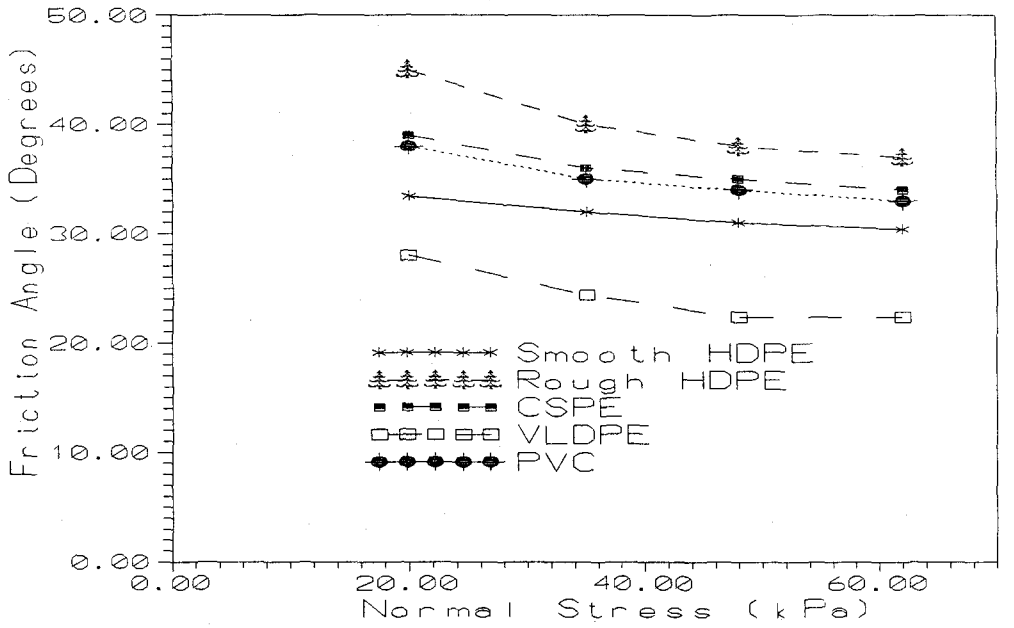

Figure 4.5. Friction Angles for Fly Ash versus Various Geomembrane Interfaces (Adopted from Koutsourais et al., 1991).

As quoted from Koutsourais et al. (1991), for dense cohesionless soils, friction angles under low normal stresses are higher than the values approached under greater normal stresses because, dense soils under low normal stresss tend to dilate resulting in high frictional resistance. When the confinement is increased, the ability to dilate is reduced and the interface friction angle tends to approach a residual value at high normal stresses.

The amount of dilation that occurs at the soil/geosynthetic interface is dependent upon the flexibility and roughness of the geosynthetic. The rougher, more flexible synthetics reveal higher frictional resistances at low normal stresses.

Table 4.13. Geosynthetic versus Kaoline Interface Friction (After Koutsourais et al., 1991).

Interface with Kaoline	Adhesive Intercept, a (kPa)	δ (°)
Kaoline	12.1	6
NW, needlepunched	9.3	15
NW, heat bonded	2.5	17
W, Monofilament	6.2	1
W, Multifilament	9.0	16
W, Slit film	8.6	11
HDPE - Smooth	2.8	5
HDPE - Rough	12.1	11
CSPE	5.2	4
VLDPE	4.1	8
PVC	1.4	6
Flexible Grid	9.6	5

Table 4.14. Geonet versus Geosynthetic Interface Friction (After Koutsourais et al., 1991).

Interface with Geonet	Adhesive Intercept, a (kPa)	δ (°)
NW, needlepunched	-	19
NW, heat bonded	1.4	17
Monofilament	1.4	9
Slit film	1.7	14
HDPE - Smooth	-	13
HDPE - Rough	-	19
CSPE	-	24
VLDPE	1.4	10
PVC	-	13

Table 4.15. Geotextile versus Geomembrane Interface Friction (After Koutsourais et al., 1991).

Geotextile Interface	HDPE (Smooth)		HDPE (Rough)		PVC		CSPE		VLPE	
	δ (°)	a (kPa)	δ (°)	a (kPa)	δ (°)	a (kPa)	δ (°)	a (kPa)	δ (°)	a (kPa)
Woven, slit film	8	2.6	13	1.4	18	-	25	-	11	1.7
Woven,monofilament	7	1.7	9	2.1	18	-	23	3.4	11	1.7
Woven,multifilament	8	2.6	17	4.1	23	-	26	-	10	2.6
NW,heatbonded	9	1.7	16	-	21	-	26	-	12	1.7
NW, needlepunched	10	2.8	15	17.2	26	-	28	-	11	2.8

Results from Table 4.15 show that, the roughened HDPE, PVC and CSPE provided high friction angles with all of the geotextiles, with the exception of the monofilament versus the rough HDPE. On the other hand, the smooth surfaces of the smooth HDPE and VLDPE provided much lower values, 7° - 12°. Although this is the case, one should keep in mind that the adhesion factor and the friction angle are both required to evaluate the shear strength at the boundary between the geosynthetic layers.

Ingold (1991) in his RILEM REPORT 4, published the results of previous research on direct shear-box tests involving geosynthetics. Tables 4.16 - 4.20 summarize his study.

Table 4.16. Soil - Geomembrane Bond Strength Values (After Williams and Houlihan, 1987).

	Geomembrane Type			
	HDPE		PVC	
Soil Type	δ (°)	a' (kPa)	δ (°)	a' (kPa)
Ottawa Sand	19	0.8	26	0.3
Concrete Sand	27	0.7	33	0.6
Sand and 5% Clay	14	0.6	19	0.8
Sand and 10% Clay	17	0.6	19	0.7
Sapprolite	21	0.4	28	0.5
Gulf Coast Clay	25	1.0	23	1.6
Glacial Till	22	0.7	25	1.0

Table 4.17. Sand - Geomembrane Friction Values (After Akbert et al., 1985).

Geomembrane	Sand			
	$\phi = 42°$	$\phi = 41°$	$\phi = 40°$	$\phi = 40°$
PVC - 2	30	34	31	30
PVC - 4	31	20	29	25
EDPM	34	31	31	33
HDPE	25	20	22	22
Sanded Bitumen	34	35	36	38
Smooth Bitumen	41	40	39	36
Rough Bitumen	43	41	38	35

Note Test Temperature: 23°C, Normal Stress: 120 kPa

Table 4.18. Geomembrane - Geotextile Friction Values (After Akbert et al., 1985).

Geomembrane	Friction Angle, δ (°)
Rough Bitumen	30
Smooth Bitumen	13
EPDM	31
Butyl	31
PVC	22
CSPE (Hypalon)	28

Table 4.19. Friction Values at Various Interfaces (After Martin et al., 1984).

a) Soil to Geomembrane Friction Angles (°)

Geomembrane	Concrete Sand ϕ=30°	Ottawa Sand ϕ=28°	Mica Schist ϕ=26°
EPDM	24	20	24
Rough PVC	27	-	25
Smooth PVC	25	-	21
CSPE	25	21	23
HDPE	18	18	17

b) Soil to Geotextile Friction Angles (°)

Geotextile[a]	Concrete Sand ϕ=30°	Ottawa Sand ϕ=28°	Mica Schist ϕ=26°
CZ 600	30	26	25
Typar 3401	26	-	-
Polyfilter X	26	-	-
500 X	24	24	23

[a] The fabric types are brand names of the geotextiles which are commercially available in the market.

c) Geomembrane to Geotextile Friction Angles (°)

Geotextile[a]	EPDM	PVC (Rough)	PVC (Smooth)	CSPE	HDPE
CZ 600	23	23	21	15	8
Typar 3401	18	20	18	21	11
Polyfilter X	17	11	10	9	6
500 X	21	28	24	13	10

[a] The fabric types are brand names of the geotextiles which are commercially available in the market.

In order to show the variety of test results obtained by different researchers, the data from Table 4.16 and Table 4.19 are compared in Figure 4.6. Although the friction angle between Ottawa sand and HDPE , reported by Williams and Houlihan (1987) seems to match with the one given by Martin et al. (1984); the friction angles proposed by the two researchers for the concrete sand and HDPE interface differ by 9°.

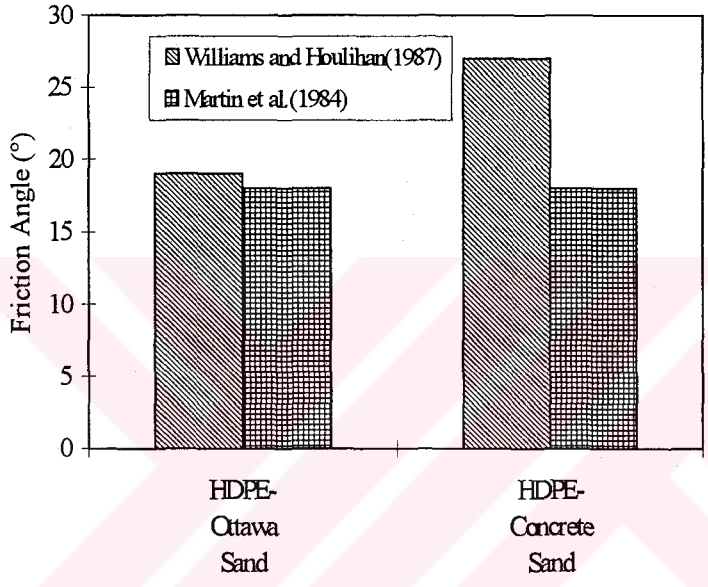

Figure 4.6. Comparison of Friction Angles for the Same Interface from Different Testing Programs

Table 4.20. Geomembrane to Fine-Grained Soil Bond Strengths (After Koerner, 1994).

Soil Type	ML-CL c=9kPa ϕ=38°		CL-ML c=12kPa ϕ=34°		CL c=20kPa ϕ=30°		SP-CH c=25kPa ϕ=24°		CH-SP c=28kPa ϕ=22°	
Geomembrane	a (kPa)	δ (°)	a (kPa)	δ (°)	a (kPa)	δ (°)	a (kPa)	δ (°)	a (kPa)	δ (°)
PVC	8.5	39	3.7	23	14.0	16	7.0	24	12.0	17
EPDM	5.0	33	5.0	23	8.0	23	7.5	20	9.0	18
HDPE	5.0	26	2.0	23	14.0	15	3.0	21	14.0	15
Embossed HDPE	9.0	35	11.0	29	18.0	27	15.0	26	16.0	25

Fishman and Pal (1994), conducted a series of 70 direct shear-box tests to investigate the shear strength of geomembrane - cohesive soil interfaces on a 102 x 102mm square shear-box. Tests were conducted both with smooth and textured HDPE geomembranes in contact with three different cohesive soil types; two glacial tills and a glacial till - bentonite mixture. The rate of shear ranged from 0.005 mm/min to 12.7 mm/min. The soils were all compacted to wet of optimum, however, tests were conducted under conditions of both partial and complete saturation during shear. Soil types that were used and the test conditions are summarized in Table 4.21 and 4.22 respectively. The experiment results are given in Table 4.23.

Table 4.21. Properties of Three Different Clays (After Fishman and Pal, 1994).

	Clay No.1	Clay No.2	Clay No.3
k (m/sec)	7.1×10^{-11}	2.2×10^{-9}	1.8×10^{-10}
c_v (m^2/sec)	1.4×10^{-7}	1.9×10^{-7}	3.8×10^{-8}
G_s	2.7	2.76	2.79
c_u (kPa)	-	217	172
LL (%)	32	37	55
PL (%)	21	25	24

Table 4.22. Test Program (After Fishman and Pal,1994)

	Partially Saturated σ_n (kPa)					Saturated (Rate=1.27 mm/min) σ_n (kPa)					Saturated (Rate=0.015 mm/min) σ_n (kPa)				
	10	34	100	145	320	10	34	100	145	320	10	34	100	145	320
a) Clay 1															
Clay		x		x	x	x	x	x	x	x		x		x	x
Smooth	x	x	x			x	x	x			x	x	x		
Textured	x	x	x			x	x	x			x	x	x		
b) Clay 2						35		69		138					
Clay						x		x		x					
Smooth						x		x		x					
	Saturated														
	Rate=12.7 mm/min			Rate=1.27 mm/min			Rate=0.127 mm/min			Rate=0.0127 mm/min			Rate=0.005 mm/min		
	35	69	138	35	69	138	35	69	138	35	69	138	35	69	138
c) Clay 3															
Clay	x	x	x	x	x	x	x	x	x	x	x	x	x	x	x
Smoooth				x	x	x	x	x	x				x	x	x
Textured				x	x	x	x	x	x				x	x	x

Table 4.23. Summary of Test Results (After Fishman and Pal, 1994)

	Partly Saturated			Saturated (Rate=0.005 mm/min)			Undrained		
	c (kPa)	ϕ_p (°)	ϕ_r (°)	c (kPa)	ϕ_p (°)	ϕ_r (°)	c (kPa)	ϕ_p (°)	ϕ_r (°)
Clay No.1	41	35	35	7	21	21	21	22	22
Clay No.1/Smooth	0	20.5	13.5	3	14	13	0	11	9
Clay No.1/Textured	40	28	24	7	24	22.5	34	19	ID[a]
Clay No.2	-	-	-	-	-	-	28	31	ID
Clay No.2/Smooth	-	-	-	-	-	-	7	16	16
Clay No.3	-	-	-	5	27	27	35	16	16
Clay No.3/Smooth	-	-	-	8	11	11	9	14	14
Clay No.3/Textured	-	-	-	20	22	20	48	24	ID

Mitchell et al. (1990) reviewed the previous research on the famous Kettleman Hills Landfill Liner System and made a more detailed shear strength analysis for the interfaces involved in the Kettleman Hills repository. A modified Karol - Warner direct shear testing apparatus was used to test interface combinations of HDPE liner / geotextile, HDPE liner / geonet, geotextile / geonet, HDPE liner / HDPE liner, HDPE liner/ compacted clay and geotextile / compacted clay. Most of the interfaces were tested both dry and submerged. Normal stresses ranged from 150 to 500 kPa with shear rates of 0.1-1 mm/min. The strength values in Table 4.24 represent the existing data on the strength analysis on the Kettleman Hills and Table 4.25 give the results of the tests conducted by Mitchell et al. (1990). Figure 4.7 compares the available data on Kettleman Hills and the results obtained from the mentioned research.

Table 4.24. Friction Angles or Shear Strengths on Critical Interfaces in the Kettleman Hills Landfill Liner System (After Mitchell et al., 1990).

Interface	Residual Friction Angles (ϕ_r) or Residual Undrained Shear Strength (τ_r) Along Saturated Base	Residual Friction Angle (ϕ_r) Along Dry Slopes
HDPE Liner / Geotextile	8°±1°	9°±1°
HDPE Liner / Geonet	8.5°±1°	8.5°±1°
HDPE Liner/Saturated Clay	45 kPa±12 kPa	-

Table 4.25. Summary of Direct Shear Test Results - Kettleman Hills Repository Liner System Components (Adopted from Mitchell et al., 1990).

Interface Components	Test Conditions	No. of Tests	ϕ_p or τ_p	ϕ_r or τ_r
HDPE / Geotextile	Dry, unpolished[a]	6	12.5 ± 0.7°	10.6 ± 1.2°
HDPE / Geotextile	Dry, partly polished[b]	13	10.6 ± 0.7°	9.8 ± 0.7°
HDPE / Geotextile	Dry, fully polished	4	10.3 ± 0.9°	9.6 ± 0.9°
HDPE / Geotextile	Submerged,unpolished	4	10.4 ± 1.0°	8.4 ± 1.2°
HDPE / Geotextile	Submerged, polished	9	9.3 ±1.0°	8.4 ± 0.9°
HDPE / Clay	As Compacted	3	13.6 ± 2.4°	12.4 ± 1.1°
HDPE / Clay	Saturated	5	50 ± 6 kPa	45 ± 4 kPa
HDPE / Geonet	Dry, transverse[c]	3	9.0 ± 0.25°	7.6 ± 0.3°
HDPE / Geonet	Submerged, transverse	9	8.8 ± 1.2°	8.3 ± 1.2°
HDPE / Geonet	Submerged, aligned[d]	20	7.6 ± 1.3°	6.3 ± 0.9°
Geotextile / Clay	Saturated	3	-	> 24°
Geotextile / Geonet	Dry, aligned	1	> 20°	-
Geotextile / Geonet	Submerged, aligned	5	-	> 10°
HDPE / HDPE	Dry	9	9.9 ± 2.2°	8.8 ± 2.4°
HDPE / HDPE	Submerged	6	9.9 ± 1.8°	9.2 ± 1.9°

[a - b] When HDPE liner/geotextile interfaces are considered, a tendency of the geotextile to polish the HDPE liner is observed. Especially when cyclic shear is applied on a geotextile - geomembrane interface, the peak shear strength is suppressed only in the first cycle. This may be as a result of the "polish effect" of the geotextile on the geomembrane or it is possible that after the first cycle, the fibres of the geotextile is smooth and oriented.

[c - d] The orientation of a geonet relative to its direction of sliding along a HDPE geomembrane influences the interface friction angle. "Aligned shear" means that the geonet ribs are oriented within 15° of the shear direction, "transverse shear" means that the geonet rib orientation is oblique to the shear direction by more than 15°.

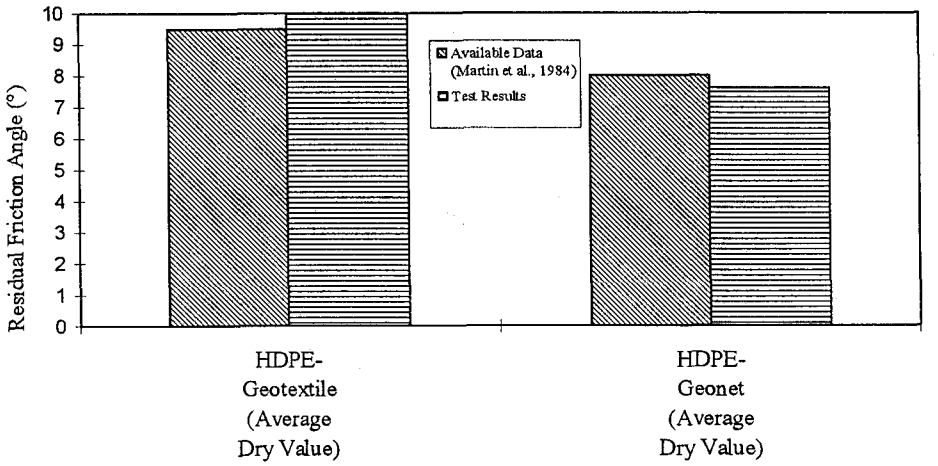

Figure 4.7. Friction Angles for Kettleman Hills Landfill Liner System (Adopted from Mitchell et al., 1990).

Lydick and Zagorsky (1991) made a categorical literature survey on the friction angles of interfaces involving geonets. The data obtained from manufacturers, consulting engineers, third party agencies and owners of waste management facilities are organized and presented in Figure 4.8 and Figure 4.9.

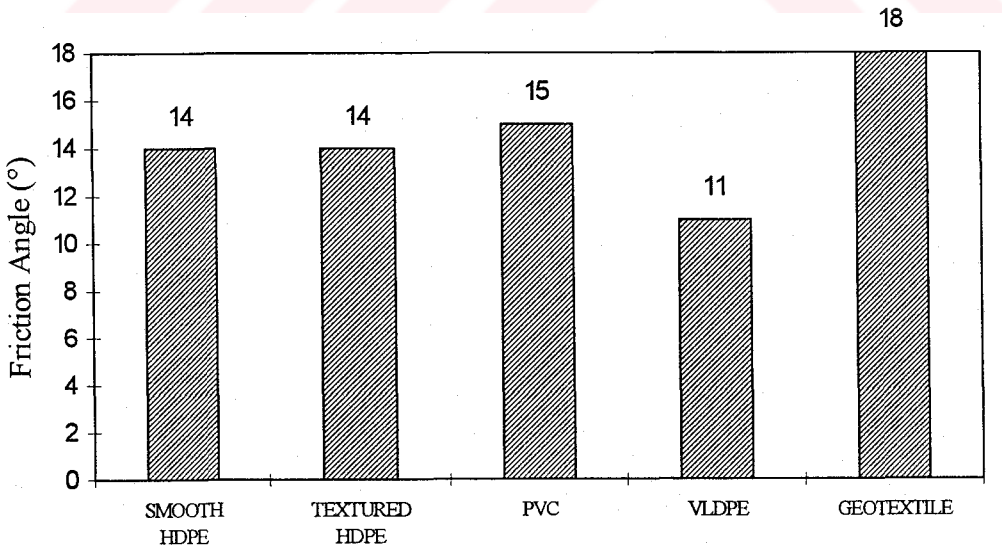

Figure 4.8. Average Friction Angles between Geonets and Other Geosynthetics (After Lydick and Zagorski, 1991).

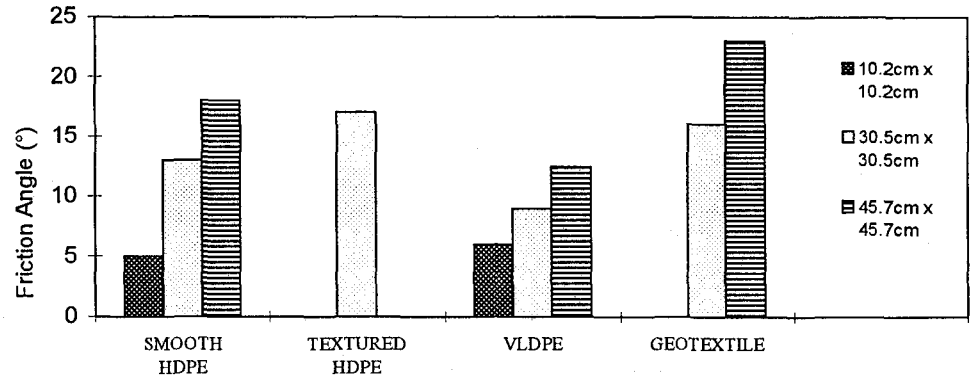

Figure 4.9. Average Friction Angle between Geonets and Other Geosynthetics Relative to Shear-Box Size (After Lydick and Zagorski, 1991).

O'Rourke et al. (1990), investigated the direct shear characteristics of granular soils (Ottawa sand, fluvioglacial sand and calcareous sand) in contact with smooth polymeric materials. A 60 x 60 mm square shear-box was used and the applied shear rates were 0.4 - 0.6 mm/min. Test results for Ottawa sand were compared with data from previous research on Ottawa sand and HDPE. Table 4.26 summarizes the values of the angle of internal friction, δ, determined from different direct shear tests. The friction angles for an Ottawa sand (G_s = 2.66, D_{50} = 0.4 mm and γ_d = 16.5 - 17.0 kN / m^3) sheared over HDPE and PVC are given in Table 27.

Table 4.26. Summary of Direct Shear Test Measurements of Ottawa Sand and HDPE (After O'Rourke et al., 1990).

Reference	Dimensions of Direct Shear Apparatus (mm)	Normal Stress (kN/m^2)	δ (°)
Martin et al. (1984)	100 x 100	14 - 104	18
Sexana and Wong (1984)	280 x 280	69 - 207	19.8
Williams and Houlihan (1987)	305 x 305	3.5 - 69	19
O'Rourke et al. (1990)	60 x60	3.5 - 69	19.1 - 19.4

Table 4.27. Friction Angles for Ottawa Sand Sheared over Various Interfaces (Adopted from O'Rourke et al., 1990).

Material in Contact with Ottawa Sand	δ (°)
Ottawa sand	35
HDPE Lining	19
PVC Lining	30

4.2. Pull - Out Box Test Results

Fourie and Fabian (1987) modified their 60 x 60 mm shear - box to carry out the pull-out tests. The soil which was sheared together with different synthetic materials was a silty clay (CL) with plastic limit (PL) of 14 and liquid limit of 27% at three different moisture contents of 15%, 17% and 19%. The geosynthetics that were used were similar to those given in Table 5. The samples were subjected to pull-out speeds of 0.9mm/min and 0.0033 mm/min for undrained and drained test, the results of which are summarized in Table 4.28 and Table 4.29 respectively.

The undrained shear-box test results for the same testing program was given in Table 4.6. Figure 4.10 illustrates a comparison of Table 4.6 and Table 4.28.

Table 4.28. Results of Undrained Pull-out Tests (After Fourie and Fabian, 1987).

Clay			Non-woven		Woven fabric		Geogrid mesh	
Water content (%)	Normal stress (kPa)	c_u (kPa)	Pull-out Stress (kPa)	Adhesion[a] factor	Pull-out Stress (kPa)	Adhesion factor	Pull-out Stress (kPa)	Adhesion factor
15	15		18		23		20	
	50	75	63	0.84	60	0.81	18	0.24
	150	98	146	1.49	158	1.61	34	0.34
	250	114	158	1.39	165	1.45	40	0.35
17	15		20		30		19	
	50	57	60	1.05	56	0.98	27	0.47
	150	79	114	1.44	92	1.16	33	0.42
	250	83	182	2.16	165	1.99	40	0.48

[a] Adhesion Factor = Pull-out Stress / Undrained Strength of Clay

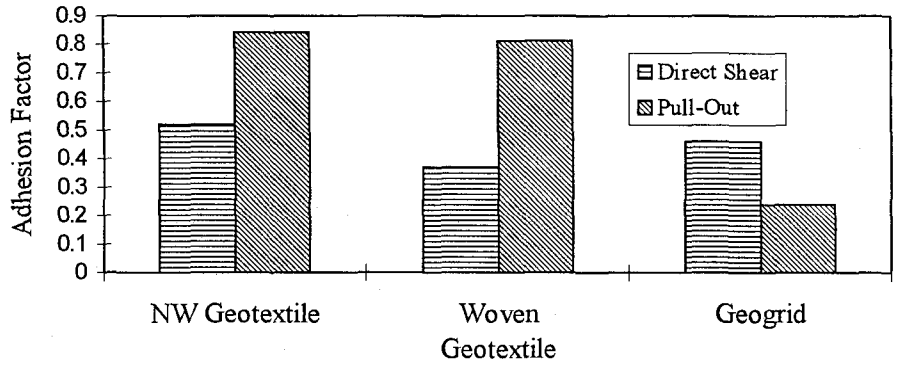

(a)

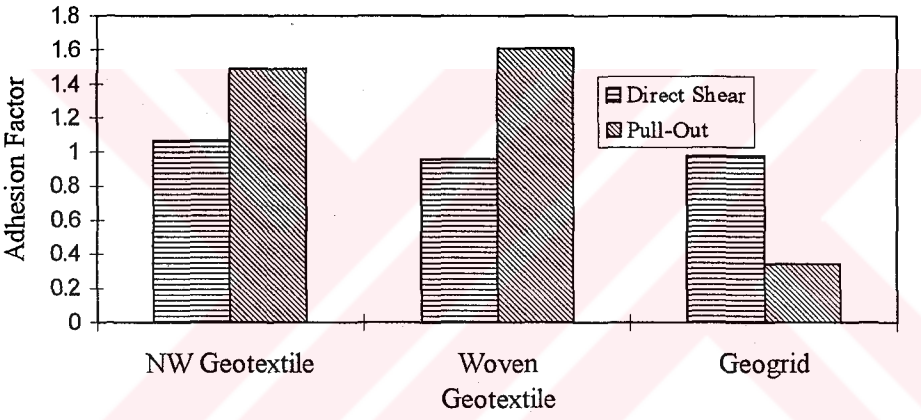

(b)

Figure 4.10. Results of Undrained Direct Shear and Pull-Out Tests for a Water Content of 15%, (a) Normal Stress = 50 kPa, and (b) Normal Stress = 150 kPa (Adopted from Fourie and Fabian, 1987).

A similar denotation to the Figure 4.10 is given in Figure 4.11, by which the adhesion factors from drained direct shear and pull-out tests (Tables 4.7 and 4.29) are compared schematically.

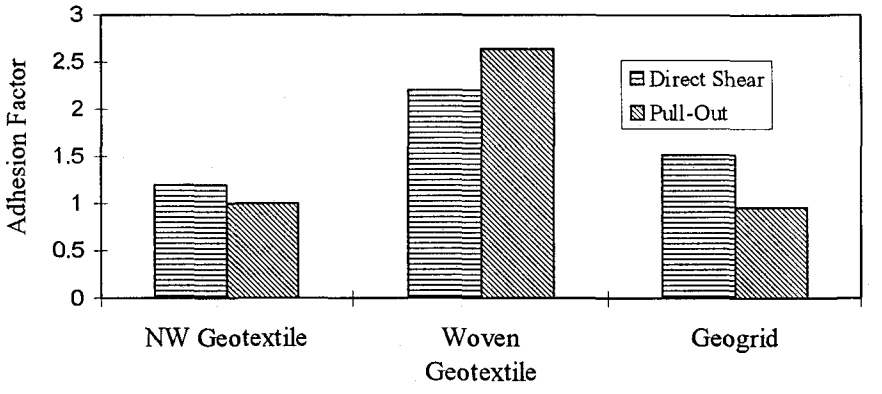

(a)

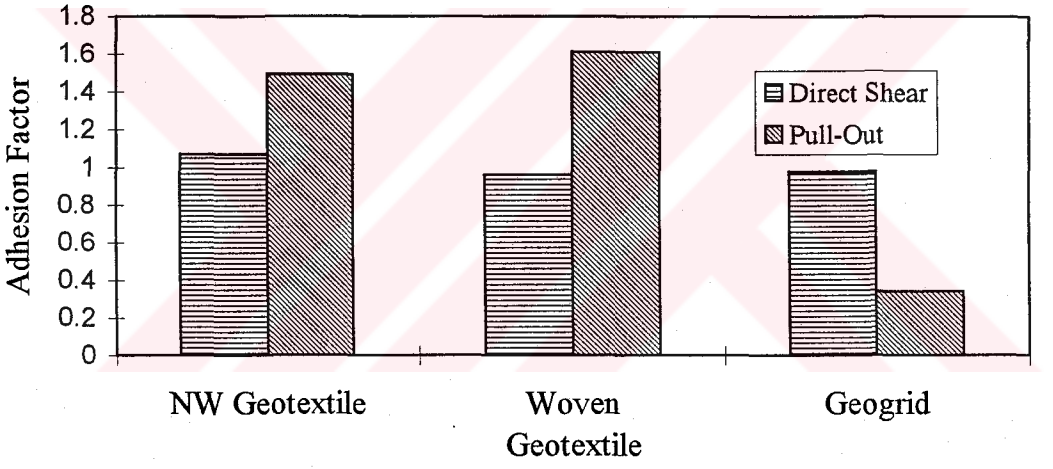

(b)

Figure 4.11. Results of Drained Direct Shear and Pull-Out Tests for a Water Content of 15%, (a) Normal Stress = 50 kPa, and (b) Normal Stress = 150 kPa (Adopted from Fourie and Fabian, 1987).

Table 4.29. Results of Drained Pull-out Tests at 15.0% Moisture Content (After Fourie and Fabian, 1987).

Clay		Non-woven		Woven fabric		Geogrid mesh	
Normal stress (kPa)	Drained strength (kPa)	Pull-out Stress (kPa)	Adhesion[a] factor	Pull-out Stress (kPa)	Adhesion factor	Pull-out Stress (kPa)	Adhesion factor
50	25	25	1.00	66	2.64	24	0.96
150	72	70	0.97	117	1.62	27	0.38
250	124	81	0.62	124	1.00	32	0.28
350	170	92	0.54	-	-	-	-

[a] Adhesion Factor = Pull-out Stress / Drained Strength of Clay

Mitchell et al. (1990), conducted a series of pull-out tests with a constant pull-out rate of 4 mm/min. The results of this test program are given in Table 4.30.

Table 4.30. Pull-out Test Results (After Mitchell et al., 1990).

Interface Components	Test Conditions	No.of Tests	ϕ_r (°)
HDPE / Geotextile	Dry, unpolished[a]	1	9.5
	Dry, polished[b]	1	8.5
	Wet, unpolished	6	7.0 - 10.5
	Wet, polished	2	6.5 - 9.0
HDPE / Geonet	Submerged, transverse[c]	2	8.0 - 9.0
	Submerged, aligned[d]	6	6.0 - 8.0
HDPE / HDPE	Submerged	6	7.0 - 13.5

[a - b] When HDPE liner/geotextile interfaces are considered, a tendency of the geotextile to polish the HDPE liner is observed. Especially when cyclic shear is applied on a geotextile - geomembrane interface, the peak shear strength is suppressed only in the first cycle. This may be as a result of the "polish effect" of the geotextile on the geomembrane or it is possible that after the first cycle, the fibres of the geotextile is smoothed and oriented.

[c - d] The orientation of a geonet relative to its direction of sliding along a HDPE geomembrane influences the interface friction angle. "Aligned shear" means that the geonet ribs are oriented within 15° of the shear direction, "transverse shear" means that the geonet rib orientation is oblique to the shear direction by more than 15°.

The results of the direct shear - box and pull - out tests which were conducted by Mitchell et al. (1990) to portray the Kettleman Hills Failure (Tables 4.25 and 4.29) are represented in Figure 4.12.

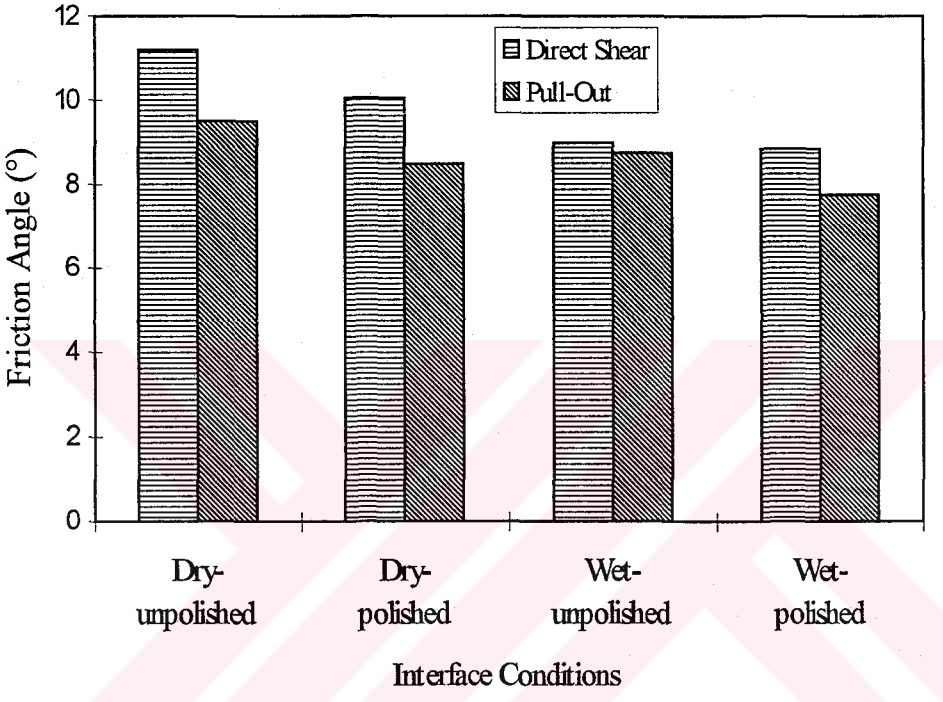

Figure 4.12. HDPE versus Geotextile Friction Angles from Direct Shear-Box and Pull-Out Tests (Adopted from Mitchell et al., 1990).

It may be seen from Figure 4.12 that there is a good agreement between the friction angles determined using the two types of tests. As quoted from Mitchell et al. (1990), this adds confidence to the use of the direct shear box tests for determination of interface strengths.

Srinisava Murthy et al. (1993) investigated the friction angle between sand and a woven geotextile using a pull-out box test for which the dimensions were not indicated. They worked with a uniformly graded sand with γ_d = 15.4 kN/m^3. The

angle of internal friction for the sand was 49°. The tests were conducted under normal stresses of 50 kPa, 75 kPa and 100 kPa and the results are summarized in Table 4.31.

Table 4.31. Friction Angle from Pull-out Tests (°) (Adopted from Srinisava Murthy et al., 1993).

	Normal Stress (kPa)		
Interface	50	75	100
Sand-woven geotextile	45	35	31

4.3. Inclined Board Test Results

A 1.00 x 1.00 m inclined board test was used by Girard et al. (1990) to study the friction angles at geotextile - geomembrane interfaces and the test results are given in Table 4.32. The materials used in the tests are listed below:

-Two types of geomembrane:

(a) One PVC membrane, 1.2 mm thick with one smooth and one slightly rough surface.

(b) One bituminous geomembrane with one rough and one smooth surface (polyester film).

Three types of geotextile:

(a) One non-woven 500g/m^2 geotextile referred to as "A" in Table 31.

(b) Two other non-woven geotextiles, referred to as "B" (300 g/m^2) and "C" (500 g/m^2).

Table 4.32. Friction Angles Attained on the Inclined Plane (After Girard et al., 1990).

Geomembrane	PVC				Bitumen			
Surface	Smooth		Rough		Smooth		Rough	
State	Wet	Dry	Wet	Dry	Wet	Dry	Wet	Dry
A (500 g/m^2)	25°	28°	26°	31°	25.5°	25°	43°	40.5°
B (300 g/m^2)	-	31°	-	-	-	23°	-	-
C (500 g/m^2)	27°	29.5°	27°	31.5°	25.5°	22°	41°	38°

Koutsourais et al. (1991) tested several geosynthetic interfaces using the inclined board test with brand name TMI (Testing Machines, Inc.) Coefficient of Friction Tester. The inclination of the plane was increased at a rate of 1.5±0.5 degrees per second until the weight started to slide at which point, the plane is locked and the angle is noted. The angles of friction obtained from the tests are listed in Table 4.33 and Table 4.34.

Table 4.33. TMI Inclined Board Test Results for Geotextile versus Geomembrane Interface Friction (After Koutsourais et al., 1991).

Geotextile Interface	Smooth HDPE	Rough HDPE	PVC	CSPE	VLDPE
Woven, slit film	18°	17°	23°	25°	22°
Woven, monofilament	21°	14°	22°	23°	22°
Woven, multifilament	21°	25°	29°	27°	22°
Nonwoven, heatbonded	23°	23°	19°	23°	19°
Nonwoven, needlepunched	19°	34°	22°	21°	20°

In order to correlate the results obtained from TMI friction tester to the direct shear box test results, Figure 4.13 is plotted using the data from Table 4.15 and 4.33. As it is clear from the figure, the TMI results are 4-7 degrees less than those obtained by direct shear test for those interfaces whose envelope extends straight through the origin, namely the PVC-Needle-punched and CSPE-Needle-punched interfaces who seem to have a negligible adhesion factor in Table 4.15. In others TMI inclined board tests are 9-19 degrees higher than the direct shear box test results for the other interfaces.

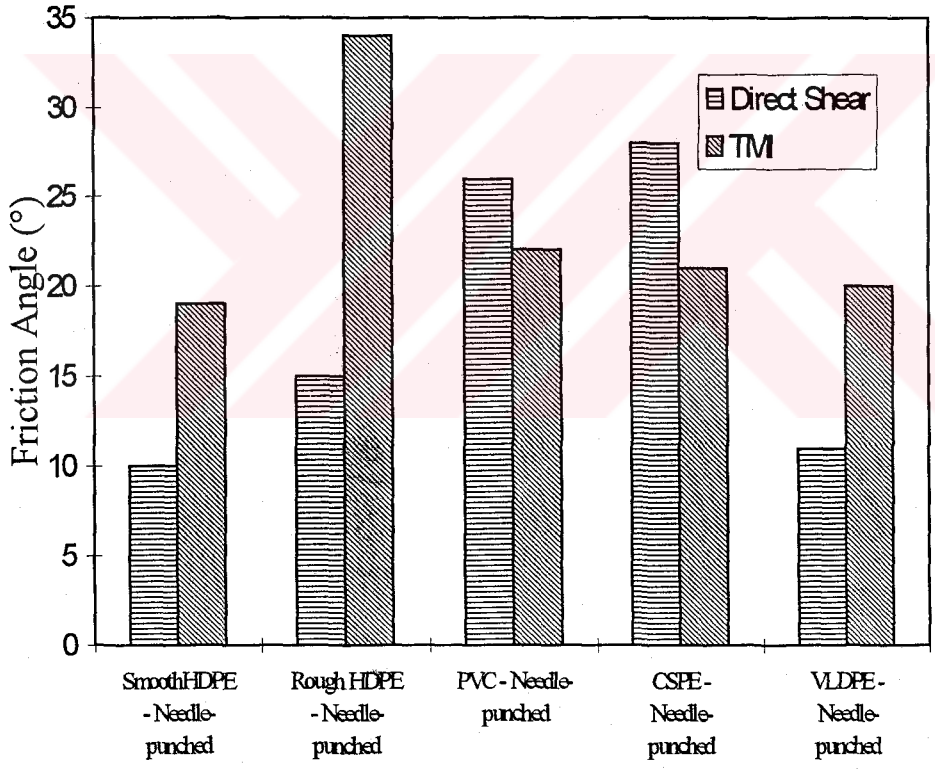

Figure 4.13. Comparison of TMI and Direct Shear Box Test Result (Adopted from Koutsourais et al., 1991).

Table 4.34. TMI Inclined Board Test Results: Geonet versus Geosynthetic Interface Friction (After Koutsourais et al., 1991).

Material in Contact with Geonet	Friction Angle (°)
Geotextile (non-woven, needle- punched)	20
Geotextile (non-woven, heat bonded)	17
Geotextile (woven, monofilament)	14
Geotextile (woven, multifilament)	20
Geotextile (slit film)	14
HDPE Geomembrane (smooth)	16
HDPE Geomembrane (rough)	18
CSPE Geomembrane	24
VLDPE Geomembrane	20
PVC Geomembrane	17

Giroud et al., conducted a series of inclined board tests to determine the friction characteristics between the geomembrane and geonet or non-wowen geotextiles used are described below:

- Smooth and rough 1 mm thick HDPE geomembrane
- A 5mm thick smooth and hard geonet
- A soft geonet
- Polyester needle-punched non-woven geotextile (250 g/m^2).

The tests were performed for normal stresses below 25 kPa, using a rigid block to provide the normal stress and the test results are presented in Table 4.35.

Table 4.35. Measured Interface Strengths (After Giroud et al., 1990).

HDPE Geomembrane	Geonet		Non-woven geotextile
Smooth	19°	15°	-
Rough	14°	10°	48°

4.4 Summary of Results Given in Literature

A brief summary of the range of friction angle values for various interfaces involving geomembranes given in this chapter, is presented in Table 4.36. Figures 4.14, 4.15 and 4.16 schematically represent the minimum and maximum values, reported by different researchers for geomembrane-sand, geomembrane-clay and geomembrane-NW geotextile respectively. The name of the researchers and the testing methods are not cited. The HDPE geomembrane-sand interface angles given in the literature and the results of the present experimental study will comparatively be presented in Chapter 6.

Table 4.36 Range of Reported Friction Angles for Various Interfaces Involving Geomembranes

Type of Geomembrane	Interface Friction Angle Range (°)
Geomembrane-Sand Interfaces	
PE	14-24
PVC	20-34
CSPE	21-31
EPDM	20-34
VLDPE	21.5-28
HDPE (Smooth)	18-28
HDPE (Rough)	30-40.5
Geomembrane-Clay Interfaces	
PVC	6-39
HDPE (Smooth)	5-26
HDPE (Rough)	11-35
Geomembrane-NW Geotextile Interfaces	
PE	9-14
PVC	10-28
CSPE	17-31
EPDM	9-28
HDPE (Smooth)	8-12.5
HDPE (Rough)	15-16

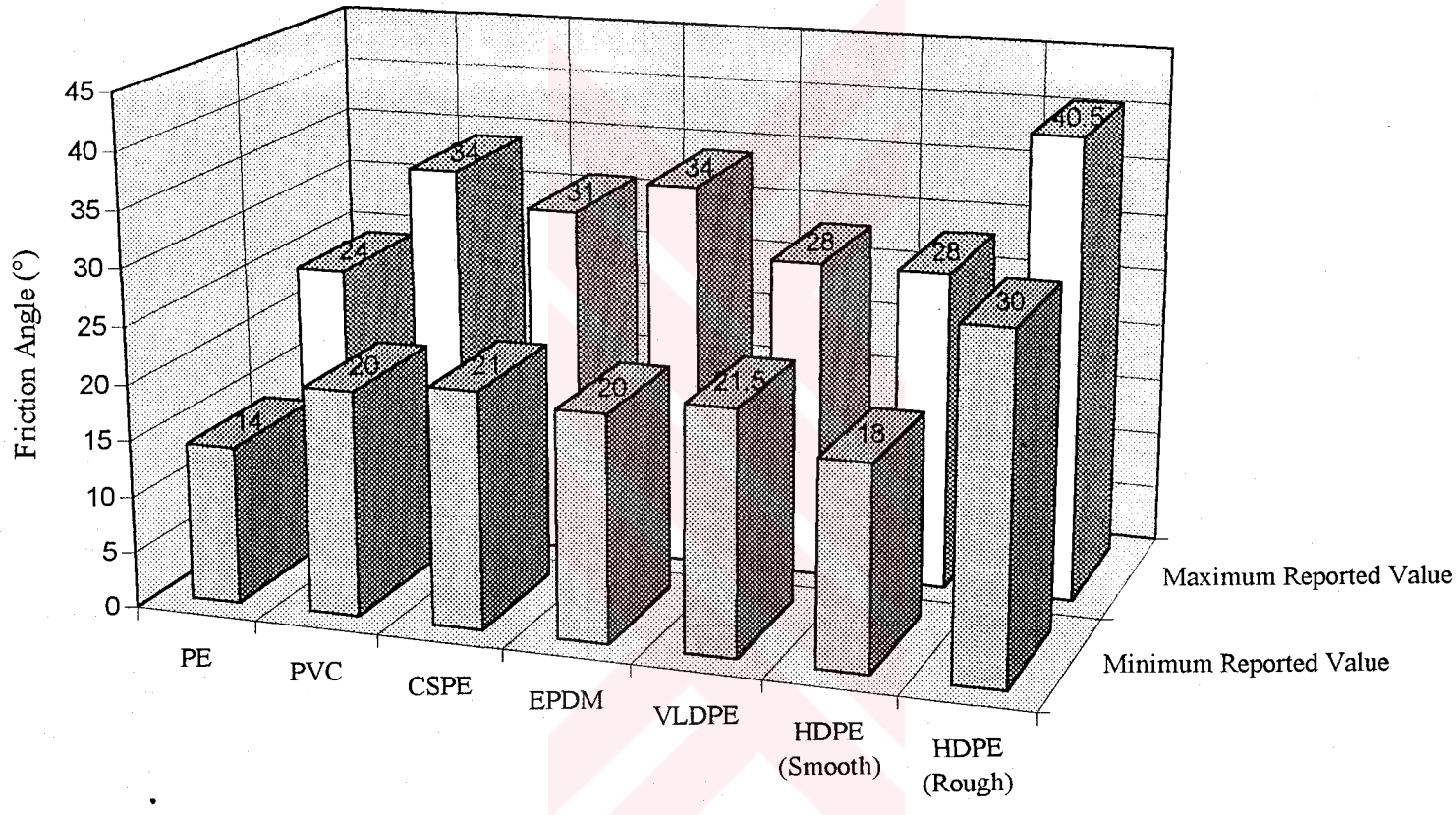

Figure 4.14 Reported Ranges for Sand-Geomembrane Interface Friction Angle

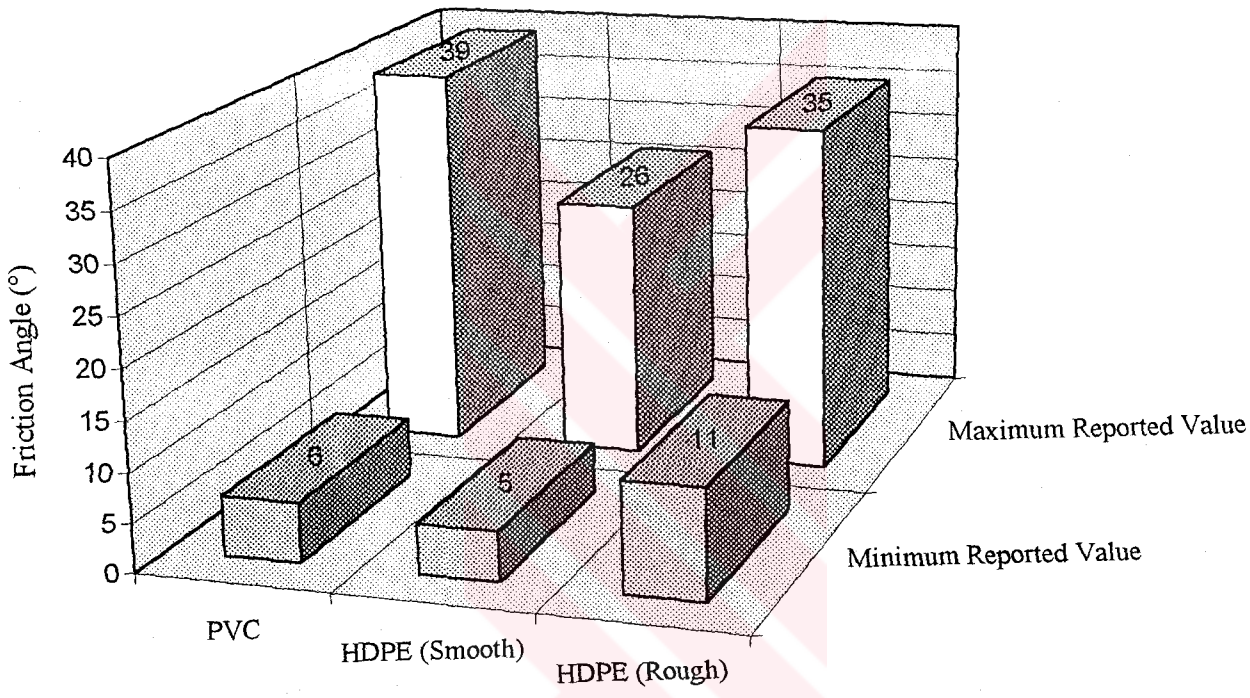

Figure 4.15 Reported Ranges for Clay-Geomembrane Interface Friction Angle

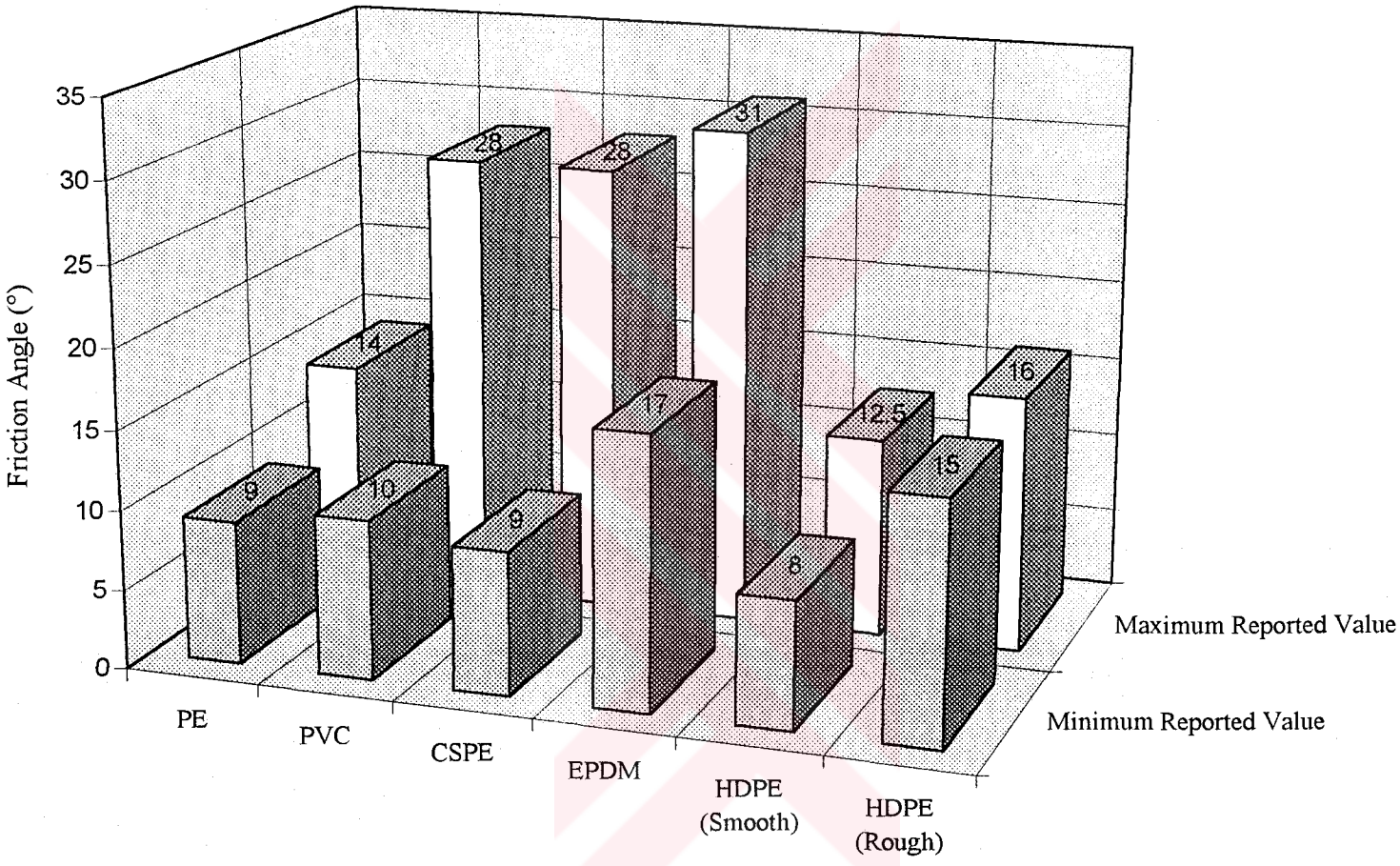

Figure 4.16 Reported Ranges for NW Geotextile-Geomembrane Interface Friction Angle

CHAPTER V

EXPERIMENTAL PROGRAM

5.1 General Information

In the present experimental study, inclined board/tilting table tests were carried out to evaluate geomembrane-sand friction. Different brands of smooth and rough (textured) HDPE (high density polyethylene) geomembranes and two sands of comparable gradation and mean size but having distinctly different degree of particle roundness-namely well rounded Ottawa Sand and angular crushed stone-were used in loose and dense states in the experiments.

Normal stresses were varied in the range of approximately 5-50 kPa on interface areas of 60 x 60 mm, 200 x 200 mm and 300 x 300 mm. Limited number of direct shear box tests were also performed.

5.2 Properties of the Granular Soils Used

Two granular soils were used in the experiments. Soil 1 was Ottawa Sand, available at the METU Soil Mechanics Laboratory; soil 2 was a crushed stone which was sieved to have a similar gradation as the Ottawa sand. Tests were

conducted to determine the grain size distribution curves, specific gravity, maximum and minimum dry densities and the internal friction angles of the soils. The grain size distribution curve is given in Figure 5.1. Tables 5.1 and 5.2 summarize the internal friction angles of the soils and their physical properties respectively.

In the present study, it was considered adequate to assess the limiting densities (or void ratios or porosities) by deposition of dry sand through air. Suggested/adopted procedures for the minimum density determination involve deposition with high intensity and low velocity. A high velocity of fall produces high density with low intensity of deposition (Wasti, 1976). The density obtained by pouring oven dry samples from a small height (<20 mm) into a cylindrical mold (diameter about 100 mm and height about 40 mm) from a funnel having about 25 mm diameter spout is reported as the minimum density. The greatest density obtained as the sand is "rained" in air from increasing heights using a perforated funnel which produces low intensity due to spreading and high falling velocity due to increased falling height is taken as the maximum density.

Table 5.1 Internal Friction Angles for the Soils Used

Soil	State	ϕ (°)
Ottawa Sand	Loose	33
Ottawa Sand	Dense	38
Crushed Stone	Loose	42
Crushed Stone	Dense	46

These values agree with the reported values in literature (Das, 1983). The results given by O'Rourke et al.(1990) for Ottawa Sand with D_{50}=0.4 mm and γ_d=16.5-17.0 kN/m^3 are comparable to the Ottawa Sand used in the present study.

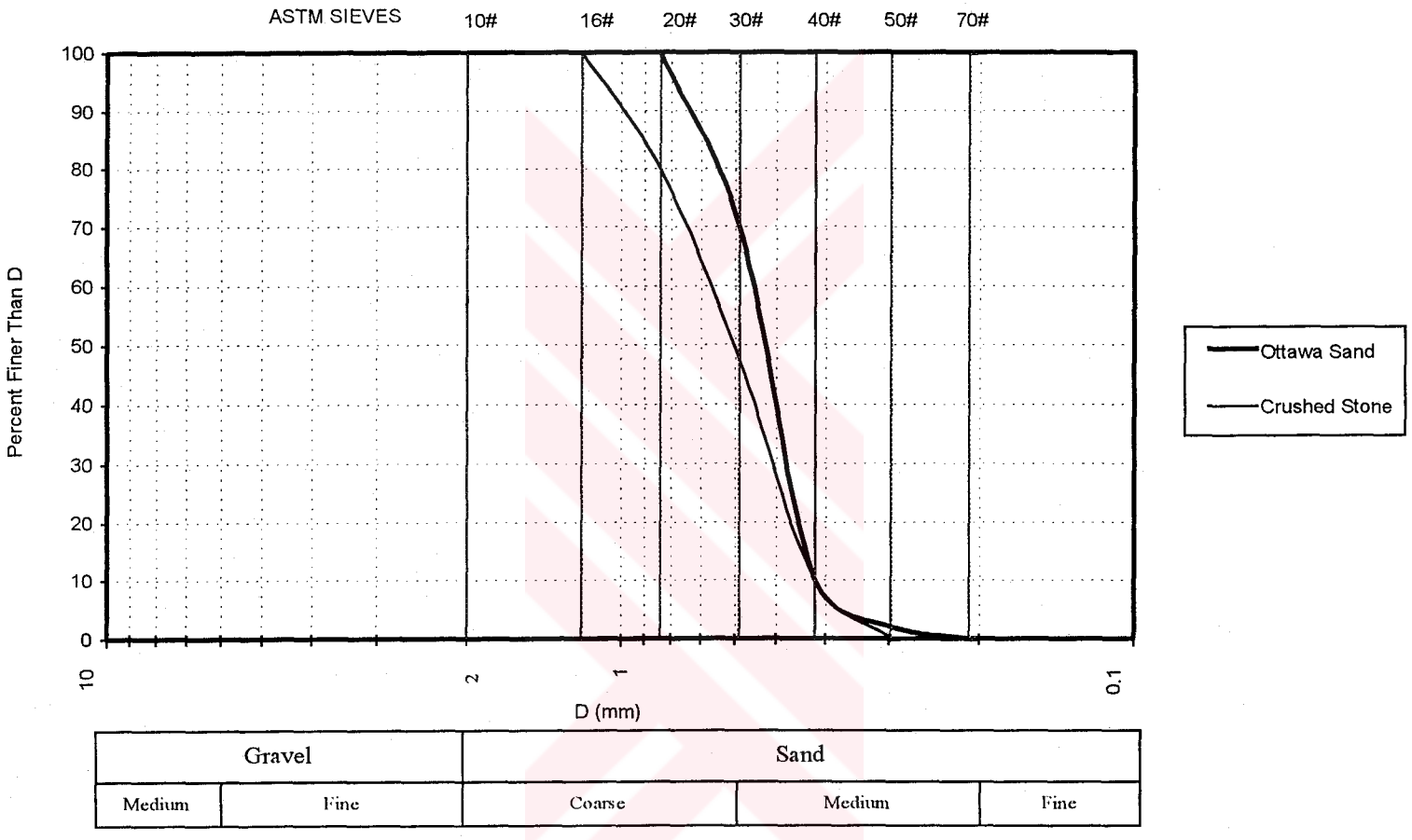

Figure 5.1 Grain Size Distribution Curve

Table 5.2 Physical Properties of the Soils Used

Description	Unified Soil Classification	D_{10} (mm)	D_{30} (mm)	D_{60} (mm)	C_u D_{60}/ D_{10}	C_c $(D_{30})^2/(D_{10}.D_{60})$	G_s	e_{min}	e_{max}	γ_{min}	γ_{max}
Ottawa Sand with Rounded Particles	SP	0.4	0.48	0.55	1.375	1.05	2.65	0.594	0.820	1.456	1.662
Crushed Stone with Highly Angular Particles	SP	0.4	0.52	0.77	1.75	0.97	2.94	1.10	1.226	1.321	1.40

C_u= Coefficient of Uniformity

C_c= Coefficient of Curvature

G_s= Specific Gravity

5.3 Properties of the Geomembranes Used

Three different brands of geomembranes from various manufacturers were utilized in the experiments. They were designated as:

(a) GM(A) with brand name "Werra Plastic": Smooth and rough types

(b) GM(B) with brand name "Fasertechnik-Carbofol": Smooth type only, and,

(c) GM(C) with brand name GSE: Rough type only.

The physical and mechanical characteristics of the membranes, provided by the manufacturers are given in Table 5.3 to Table 5.5.

In the following chapters, the expressions "smooth geomembrane" and "rough geomembrane" will be denoted as "S-GM" and "R-GM" respectively.

Table 5.3 Properties of GM(A)

Property	Method	Unit	Nominal Values
Thickness	Micrometer	mm	1.5
Density	DIN 53479	g/cm^3	0.942
Tensile Properties (each direction)	ASTM D638		
Strength at Break		N/mm^2	33.4
Strength at Yield		N/mm^2	17.9
Elongation at Break		%	528
Elongation at Yield		%	6.6
Initial Tear Force	ASTM D1004	kN/μ	14.7
Puncture Force	DIN 53373	kg	169.1
Environmental Stress Crack Resistance	ASTM D1693	hr	>1000

Table 5.4 Properties of GM(B)

Property	Method	Unit	Nominal Values
Thickness	DIN 53353	mm	>2.5
Density	DIN 53479	g/cm^3	0.939-0.945
Tensile Strength at Yield	DIN 53455	N/mm^2	>15
Tear Resistance	DIN 53515	N/mm	>130
Perforation Resistance	DIN 16726	mm height of fall	>1600

Table 5.5. Properties of GM(C) (Surface Structure: Rough)

Property	Method	Unit	Nominal Values
Thickness	DIN 53353	mm	1.5
Density	DIN 53479	g/cm^3	0.944
Tensile Properties (each direction)	DIN 53455		
Strength at Break		N/mm^2	35
Strength at Yield		N/mm^2	17
Elongation at Break l_0=50 mm		%	700
l_0=64 mm			650
Elongation at Yield l_0=50 mm		%	11
l_0=33 mm			15
Tear Resistance	DIN 53515	N	200
Puncture Resistance	FTMS 101 Method 2065	N	400
Environmental Stress Crack Resistance	ASTM D1693	hr	>1500
Tensile Impact Strength	DIN 53448	mJ/mm^2	800
Low Temperature Brittleness	DIN 53361	° C	<-84

5.4 Experimental Set-Up and Procedure

The conceptual design of the inclined board test apparatus was made by the author. This specially designed apparatus consists of a tilting board which is actually a shallow, rectangular tray and is lifted up by a combination of a hydraulic jack and an air compressor. The complete set-up is mounted on a steel frame. The main features of the apparatus are shown in Figure 5.2.

900 mm high steel frame is made of epoxy polyester painted , 0.8 mm thick cold drawn stainless steel. The tilting board is manufactured from the same material as the steel frame but the bottom of it is reinforced with a special alloy plate to prevent any deflections resulting from the load on it. The tilting board has the dimensions of 600 mm x 490 mm x 25 mm (length x width x depth) and it is hinged along one of the shorter sides to the steel frame under it. On the other shorter side where a ruler is attached, the tilting board is supported at the middle by a hydraulic jack with a ram length of 520 mm, diameter of 85 mm and maximum load capacity of 300 kg. The other dimensions of the steel frame are given in Figure 5.3.

For the lifting system, the combination of an air compressor and a hydraulic jack rather than one of the two was found to be necessary to ensure smooth rising of the board without any speed fluctuations.

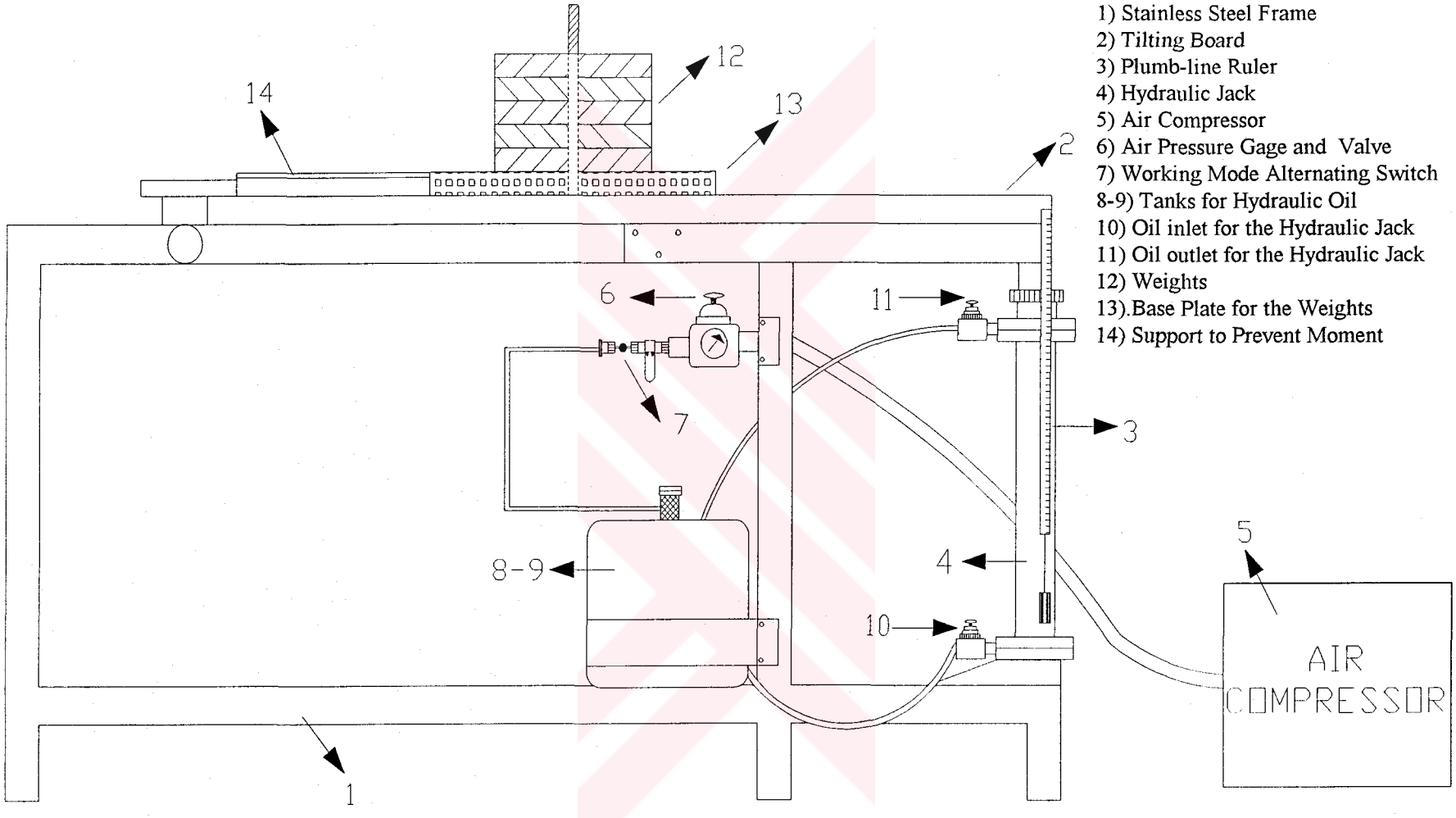

Figure 5.2. Test Apparatus, Schematically

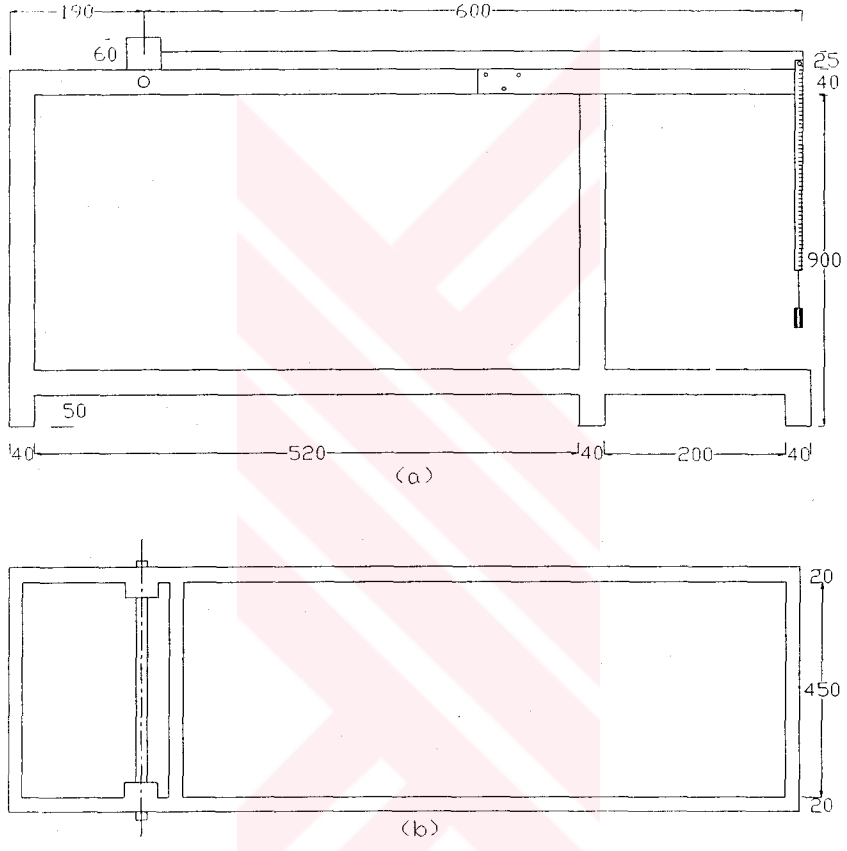

Figure 5.3. Steel Frame with Tilting Board: (a) Side View, and (b) Top View

The functioning of the tilting mechanism is explained by referring to the numbering system given in Figure 5.2.

The air compressor (no.5) is adjusted to start working when the pressure in the system drops below 8 psi, so that the tilting board is lifted up by the same hydraulic force all through the testing period.

The pressurized air coming from the compressor is carried to the air pressure valve (no.6) by which one can adjust the desired working pressure. Under the valve, there is an air pressure gage, indicating the working pressure.

When the pressurized air captured in the valve is released by pressing the working mode alternating switch (no.7), this pressurized air replaces the oil in one of the two tanks (no.8-9), both of which are initially full of hydraulic oil, causing the oil in the tank to move into the other tank. As a chain reaction, the oil in the second tank moves into the hydraulic jack (no.4) causing it to ascend and as a result the tilting board is lifted up.

When it is desired to descend the tilting board, it is enough to pull the alternating switch back to its original position and a reversed course is followed; i.e. the oil flows from the hydraulic jack to the second tank and then to the first tank. The pressurized air in excess is released out of the system from a small hole on the air pressure valve.

During the rising stage, the hydraulic jack is filled by oil coming from the tanks through an inlet tap (no.10) attached to its bottom. This oil is sent out of the hydraulic jack through an outlet tap (no.11) near to its bottom during descending of the tilting board. The flow rate of oil from the inlet tap to the hydraulic jack controls the rising speed of the board, whereas the flow rate of oil from the jack

through the outlet tap affects the descending speed. These flow rates are adjusted by turning the inlet or outlet.

The measurement for the inclination of the board (tray) is done by means of a ruler (no.3), hinged on the free end of the tilting board such that it is free to rotate to keep the plumb-line direction whatever the inclination of the board is. During an experiment, when sliding occurs, the ruler reading is taken to measure the height to which the tilting board raised and knowing the dimensions of the tilting board, it is simple trigonometry to evaluate the angle at the instant when sliding occurs.

Normal loads are applied using dead weights (no.12). The dead weights used for the 200 x 200 mm and 300 x 300 mm experiments were specially cast from lead, each weighing 20 kg, to provide the required normal stresses. These dead weights have the dimensions of 300 x 300 x 20 mm.

Calibration tests were conducted to obtain the correlation between the rising speed and various flow rates through the inlet tap. Assuming the fully closed position as the "null" position, the tap is graded radially by dividing it into five sectors. Calibration curves are drawn for the five different tap openings which are obtained by turning the inlet tap to the next grading division in counter clock wise direction. Although the apparatus has the capability to work at higher rising speeds (when the tap is opened by more than one full turn), the tested rates for which the calibrations are given in Figure 5.4, correspond to the rates used by previous researches; i.e. Girard et al.(1990) and Koutsourais et al. (1991).

A general view of the testing apparatus is given in Figure 5.5.

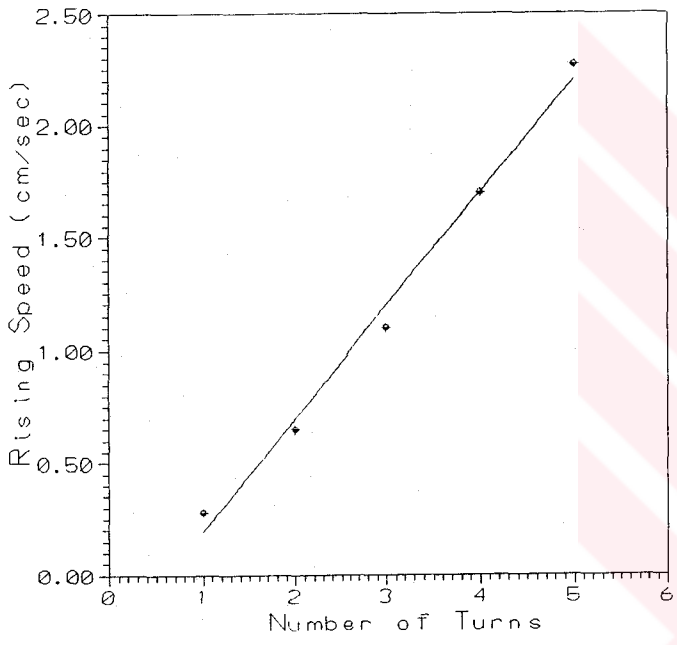

(a)

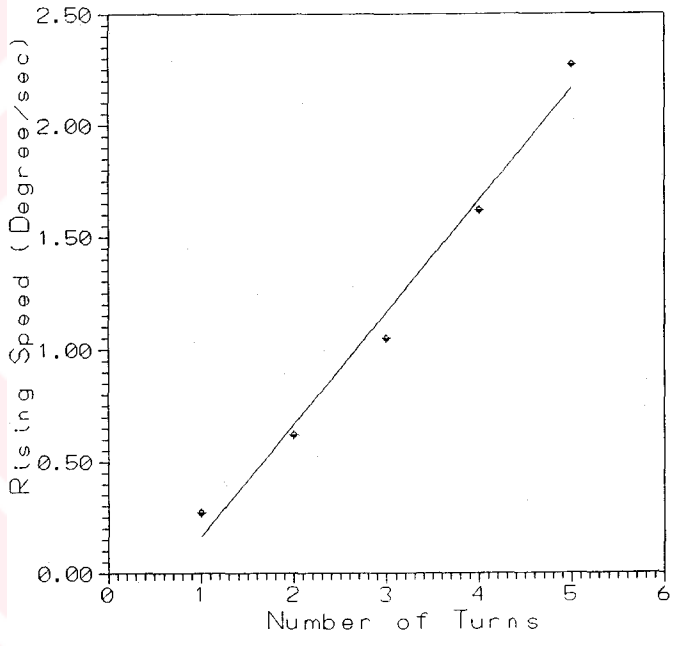

(b)

Figure 5.4. Calibration Curves for the Apparatus: (a) In terms of cm/sec, and (b) In terms of degrees/sec

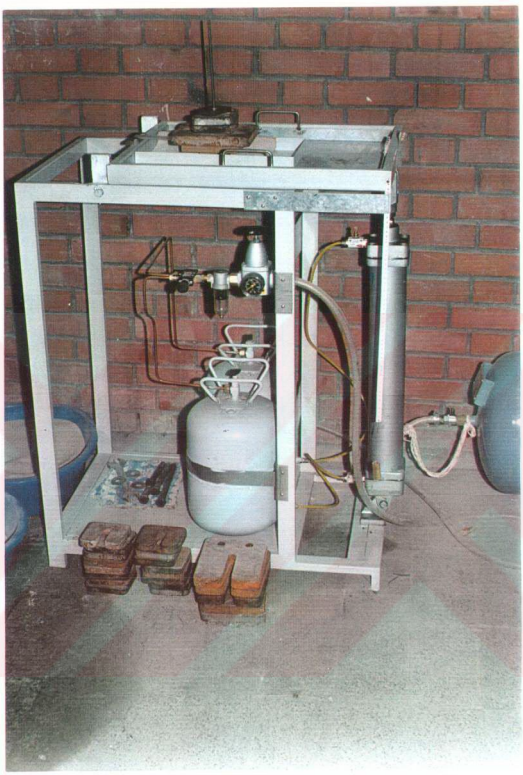

Figure 5.5 A General View of the Inclined Board Test Apparatus

In general, in inclined board or tilting table test to measure soil-geosynthetic friction, a block with dead weights on it and geosynthetic fixed at its bottom area, is placed on a layer of soil. The tilting board is lifted up till the block slides on the soil surface.

In the present study, the following details had to be incorporated to the procedure:

(1) For the tests conducted on 60 x 60 mm interfaces, a smaller tray (having dimensions of 400 x 250 x 30 mm) was placed into the original tray of the board to minimize the loss of time and material during placing the soil into the tray. For the tests performed on 200 x 200 mm and 300 x 300 mm interfaces, the original tray was utilized.

(2) For the experiments on 60 x 60 mm and 200 x 200 mm interfaces, geomembrane was glued to the bottom of the wooden size adopters, specially made to provide required cross-sectional interface area. The 60 x 60 adopters were then attached to the bottom of a base plate which was constructed to support the standard dead weights. The 200 x 200 mm adopters were directly fixed to the 300 x 300 mm dead weights without using a base plate, where as, for the 300 x 300 mm tests, geomembrane was glued onto the lowest dead weight without using any size adopter. The size adopter for the 60 x 60 mm tests is presented in Figure 5.6.

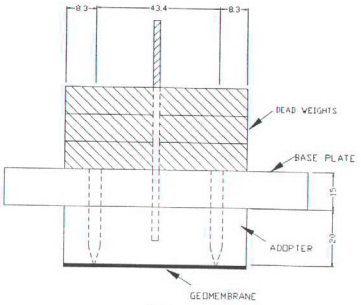

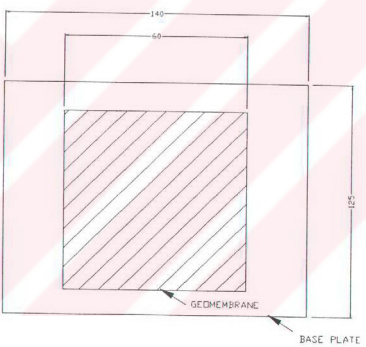

Figure 5.6 Adopters: (a) Side View and, (b) Bottom View

(3) The base plate used for the 60 x 60 mm interfaces had dimensions of 125 x 140 x 15 mm. To prevent the sliding of the weights on the base plate or on top of each other, they were secured tightly between a small wooden stopper and the base plate by means of a long screw (Figure 5.7). The preliminary experiments on 60 x 60 mm interfaces revealed that, the height of the dead weight column situated on the base plate, caused the system to rotate on one edge of the adopter and the system failed, especially at high inclinations of the tilting board. This moment effect was tried to be minimized by installing a plexiglas rectangular strip on the base plate, which leaned against a ball bearing on the steel frame to prevent any extra friction. A detailed illustration of the strip and ball bearing combination are given in Figure 5.8.

(4) To prevent the sliding of sand grains on the surface of the metal trays rather than on the geomembrane-sand interface, a thick paper was stuck to the bottom of the tray and sand particles were glued to the paper to have a high frictional resistance and then the layer of sand was placed above it. The friction angle between sand-glued surface and sand (loose or dense) is about the same as the friction angle of the sand at the dense state (Wasti, 1976) which is much larger than the expected geomembrane-sand interface angle (to verify and quantify this, special direct shear tests were performed which will be discussed in Section 5.5).

(5) The layer of sand placed had to be a thin layer of about 5 mm thickness (which is approximately 10 x D_{50}) since the block tended to sink and tilt to one side and topple over as the board was lifted, if the sand layer was thick. The schematic representation of 5 mm thick sand layer and interfaces is illustrated in Figure 5.9 for loose and dense states of soil.

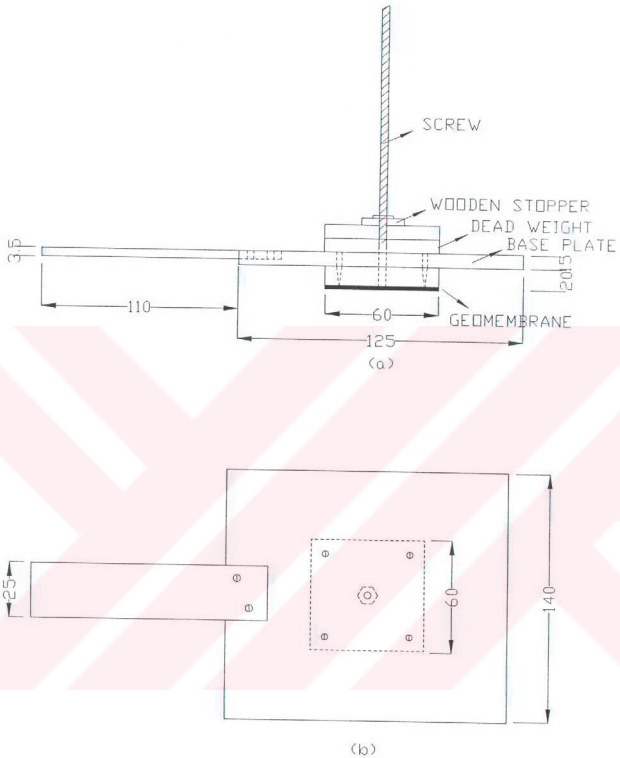

Figure 5.7 Base Plate: (a) Side View, and (b) Top View

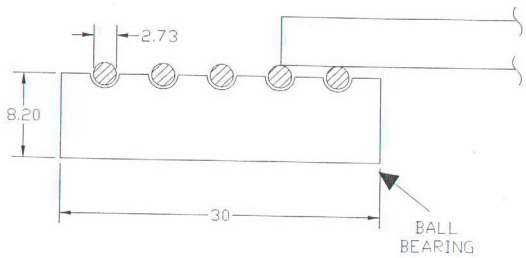

(a)

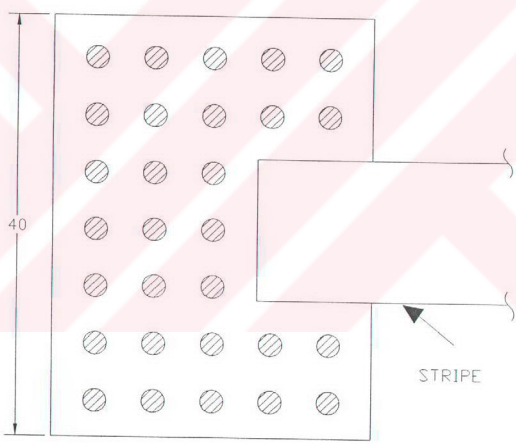

(b)

Figure 5.8 Strip and Ball-Bearing (a) Side View and, (b) Top View

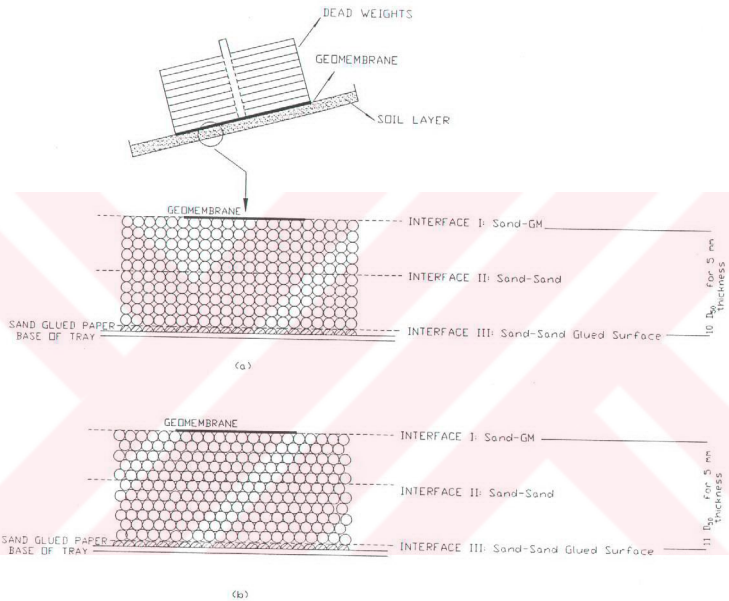

Figure 5.9 Schematic Representation of Interfaces in Inclined Board Tests: (a) Loose State, and (b) Dense State

Figures 5.10 to 5.13 present photographs from the experiments for 60 x 60 mm and 300 x 300 mm experiments.

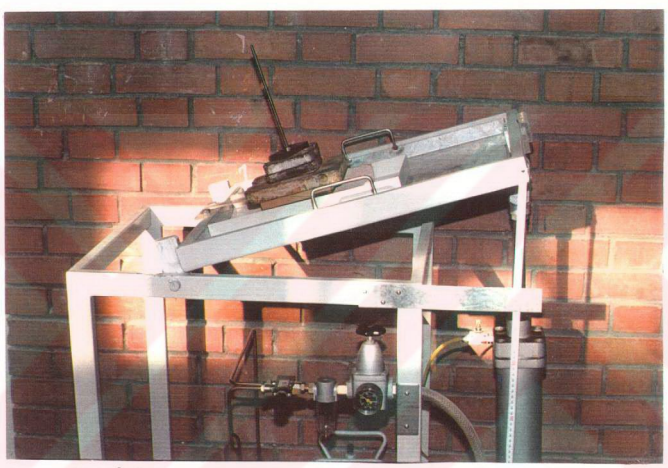

Figure 5.10 A Snap-Shot From the 60 x 60 mm Experiment (Front View)

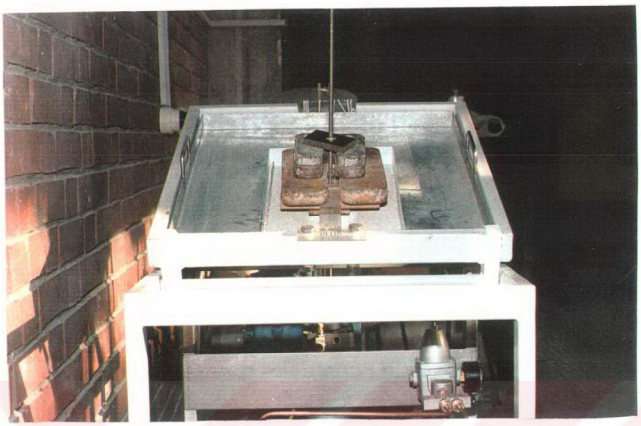

Figure 5.11 A Snap-Shot From the 60 x 60 mm Experiment (Side View)

Figure 5.12 A Snap-Shot From the 300 x 300 mm Experiment

Figure 5.13 A Snap-Shot From the 300 x 300 mm Experiment (Side View)

5.5 Schedule of Experiments

A total of 520 inclined board tests were carried out at 60 x 60 mm, 200 x 200 mm and 300 x 300 mm interface areas. Tests on 300 x 300 mm interfaces were performed at rising speeds of 1, 1.65 and 6.5 degrees/second to decide on the rate effect if any. As almost no effect was detected, the rising rate of 6.5 degrees/second was adopted in all the rest of the tests performed; and this rate was in between the two reported values in the previous work.

Tests were repeated three times for the 60 x 60 mm interfaces and two times for 200 x 200 mm and 300 x 300 mm interfaces. Fresh soil layer was used for

each experiment, whereas fresh geomembrane was glued on the adopters for each new set of experiments, consisting of two or three repeatings as mentioned above.

For the 60 x 60 mm and 200 x 200 mm tests, normal stress range was 5-50 kPa; for the 300 x 300 mm tests, the capacity of the apparatus allowed a normal stress range of 5-25 kPa to be applied.

In addition to the inclined board tests, a total of 32 "fixed shear box" type modified direct shear box tests (see Section 3.2) were carried out in which a wooden block was placed in the lower half of the 60 x 60 mm standard direct shear test apparatus and filling the upper half with the soil used. The shearing rate was 6mm/sec.

For the initial tests in the direct shear box apparatus , geomembrane was glued to the top of the wooden block and the interface friction angles between various geomembranes and granular soils used, were measured to correlate them with the inclined board test results.

Also, special direct shear box tests were conducted in which granular soil was glued to the top of the wooden block and the interface was sheared to verify that the friction angle between sand-glued surface and sand (loose or dense) is about the same as the friction angle of the sand at dense state which is in turn much larger than the geomembrane-sand interface angles measured in the direct shear box tests mentioned above. This verification proved that the sliding took place along "Interface-I (See Figure 5.9) in the inclined board tests conducted in the present experimental study.

The lists of inclined board and modified direct shear box tests are given in Tables 5.6 and 5.7 respectively.

Table 5.6 Interfaces Tested In the Inclined Board Test Apparatus

Soil Used	Density	Geomembrane	Size (mmxmm)	Normal Stress (kPa)	Rate (°/sec)	No. of Tests	Total No. of Tests
Crushed Stone	Dense	S-GM(A) S-GM(B) R-GM(A) R-GM(C)	60x60	5.55-11.10- 16.65-27.75- 33.30-38.85- 44.40-49.95	6.5	3	108
Crushed Stone	Loose	S-GM(A) S-GM(B) R-GM(A) R-GM(C)	60x60	5.55-11.10- 16.65-27.75- 33.30-38.85- 44.40-49.95	6.5	3	108
Ottawa Sand	Dense	S-GM(A) S-GM(B) R-GM(A) R-GM(C)	60x60	5.55-11.10- 16.65-27.75- 33.30-38.85- 44.40-49.95	6.5	3	108
Ottawa Sand	Loose	S-GM(A) S-GM(B) R-GM(A) R-GM(C)	60x60	5.55-11.10- 16.65-27.75- 33.30-38.85- 44.40-49.95	6.5	3	108

Table 5.6 (continued)

Soil Used	Density	Geomembrane	Size (mmxmm)	Normal Stress (kPa)	Rate (°/sec)	No. of Tests	Total No. of Tests
Ottawa Sand	Dense	S-GM(A) R-GM(C)	200x200	10-20-30-45	6.5	2	16
Crushed Stone	Dense	S-GM(A) R-GM(A)	200x200	10-20-30-45	6.5	2	16
Ottawa Sand	Dense	S-GM(A) R-GM(C)	300x300	5-10-15-20-25	6.5	2	20
Crushed Stone	Dense	S-GM(A) R-GM(C)	300x300	5-10-15-20-25	6.5	2	20
Ottawa Sand	Dense	S-GM(A) R-GM(C)	300x300	20-25	1	2	8
Ottawa Sand	Dense	S-GM(A) R-GM(C)	300x300	20-25	1.65	2	8

Total = 520

Table 5.7 Interfaces Tested in the Modified Direct Shear Box Apparatus

Soil Used	Density	Interface	Normal Stress (kPa)	No. of Tests	Total No. of Tests
Ottawa Sand	Dense	S-GM(A)	14, 25, 50, 100, 200	2	10
Ottawa Sand	Dense	R-GM(C)	14, 25, 50, 100, 200	2	10
Crushed Stone	Loose	S-GM(A)	14, 25, 50	2	6
Crushed Stone	Loose	R-GM(C)	14, 25, 50	2	6
Crushed Stone	Dense	S-GM(A)	14, 25, 50, 100, 200	2	10
Crushed Stone	Dense	R-GM(C)	14, 25, 50, 100, 200	2	10
Ottawa Sand	Loose	Sand Glued Surface	14, 25, 50, 100, 200	2	10
Ottawa Sand	Dense	Sand Glued Surface	14, 25, 50, 100, 200	2	10
Crushed Stone	Loose	Crushed Stone Glued Surface	14, 25, 50, 100, 200	2	10
Crushed Stone	Dense	Crushed Stone Glued Surface	14, 25, 50, 100, 200	2	10
				Total =	**92**

CHAPTER VI

EXPERIMENTAL RESULTS AND DISCUSSION

In this chapter, the results of inclined board tests and "fixed type" direct shear box tests are given and discussed.

6.1 Inclined Board Test Results

The results of the inclined board tests, outlined in Table 5.6, are given in Figures 6.1 to 6.4. The data points for these tests are given in Tables A.1 to A.24 in Appendix A.

The lines given in Figures 6.1 to 6.4 are drawn by linear regression analysis to find the sliding angle,δ, and the point having coordinates of (0,0) is not included in the analyses.

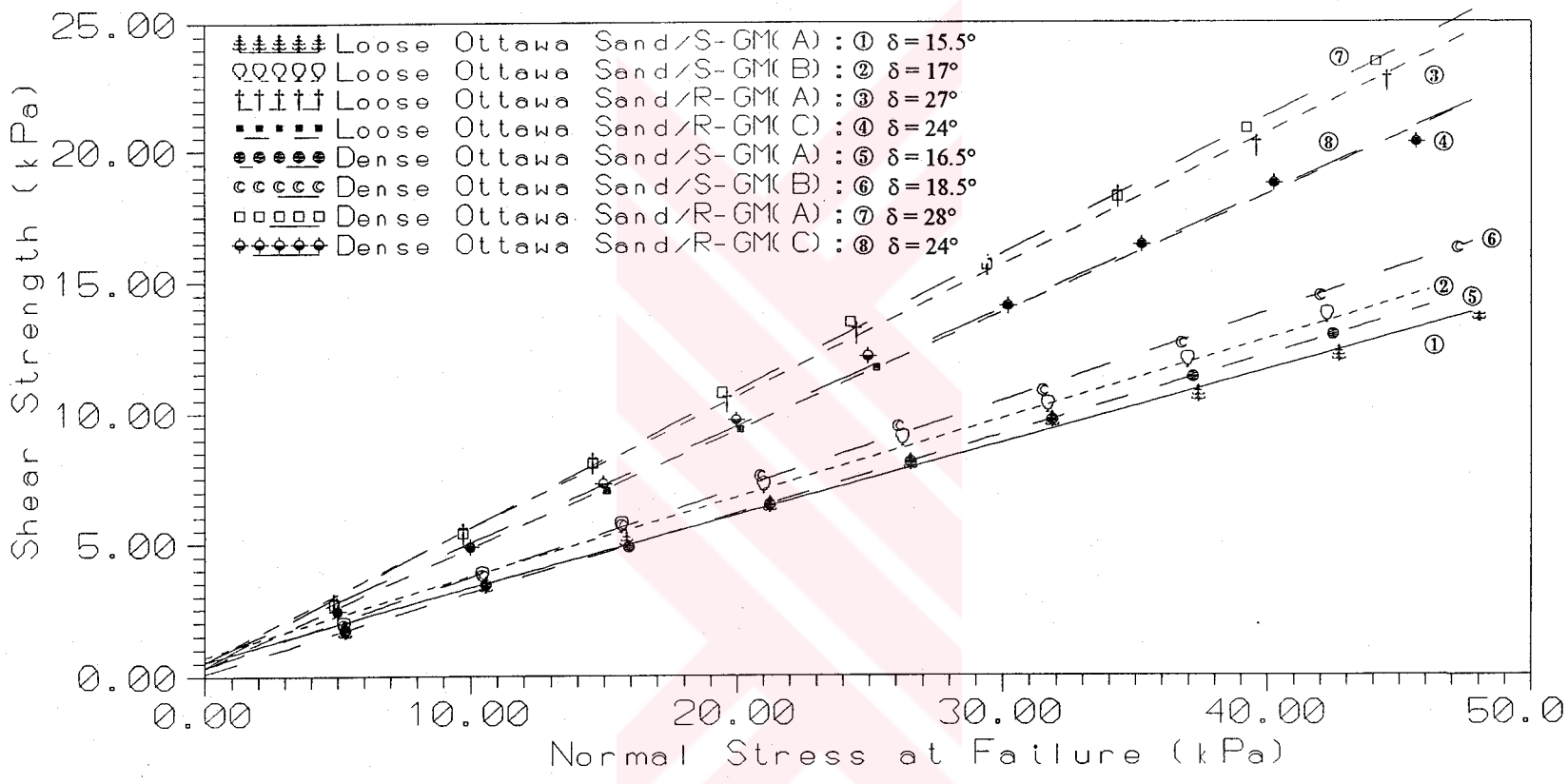

Figure 6.1 60 x 60 mm Inclined Board Test Results on Interfaces Involving Ottawa Sand

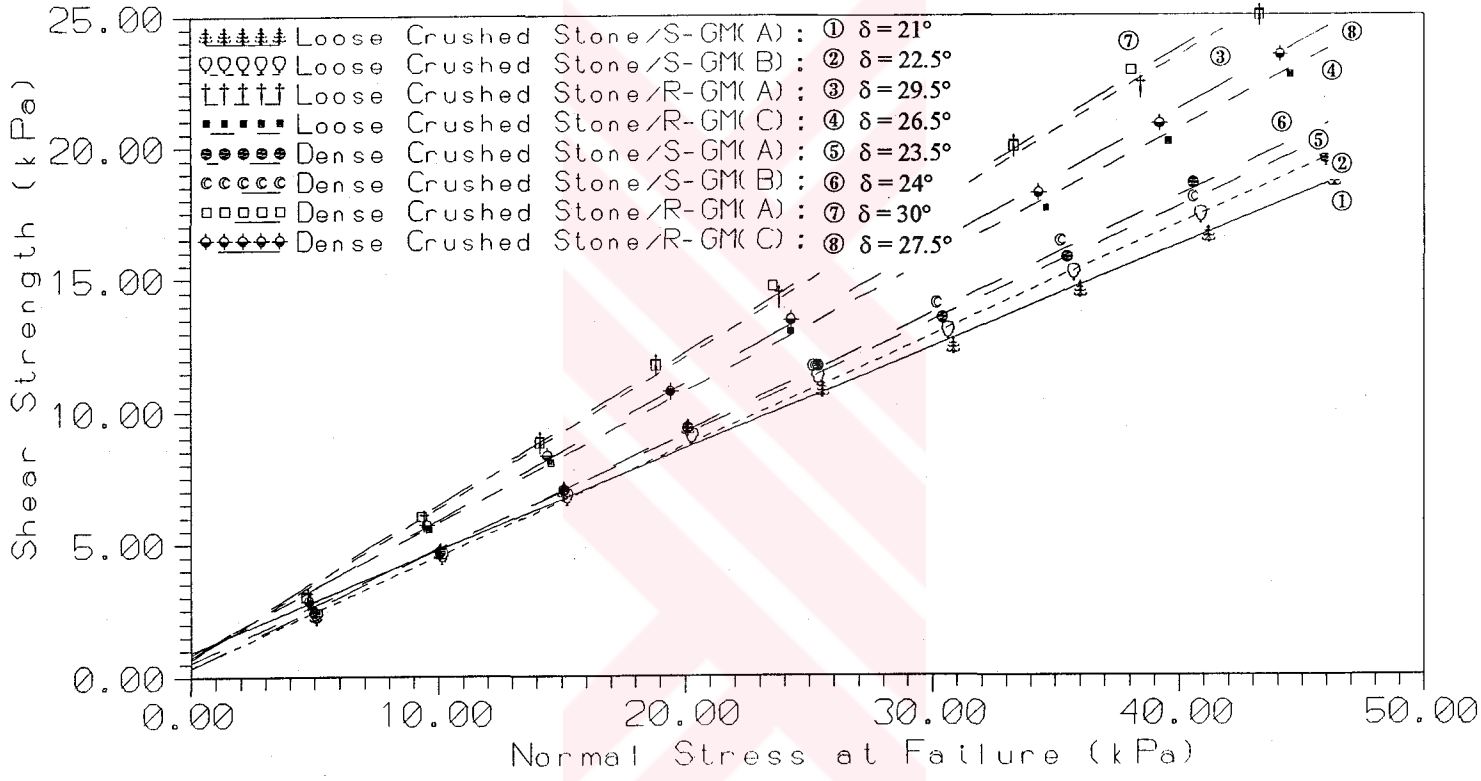

Figure 6.2 60 x 60 mm Inclined Board Test Results on Interfaces Involving Crushed Stone

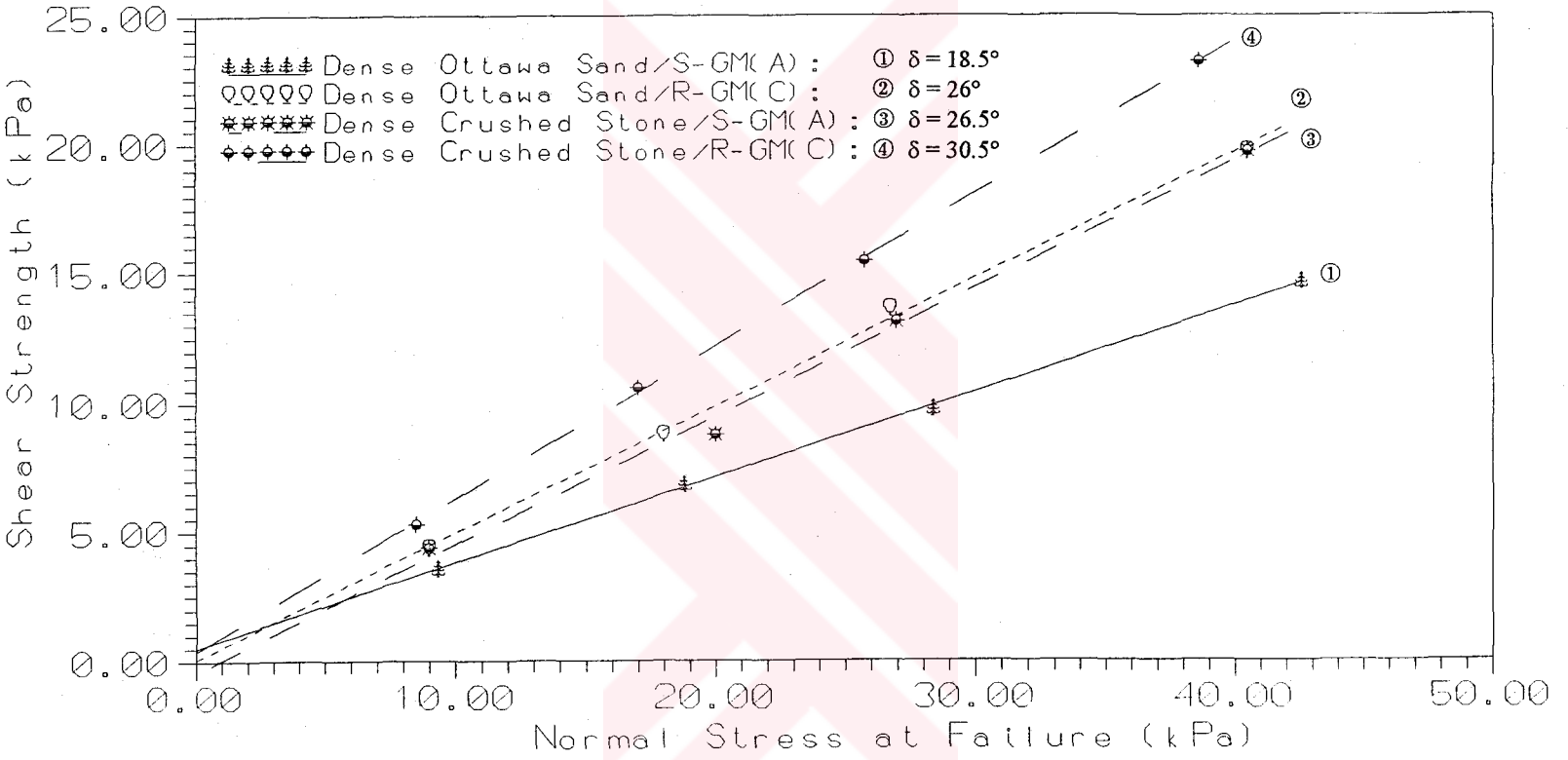

Figure 6.3 200 x 200 mm Inclined Board Test Results

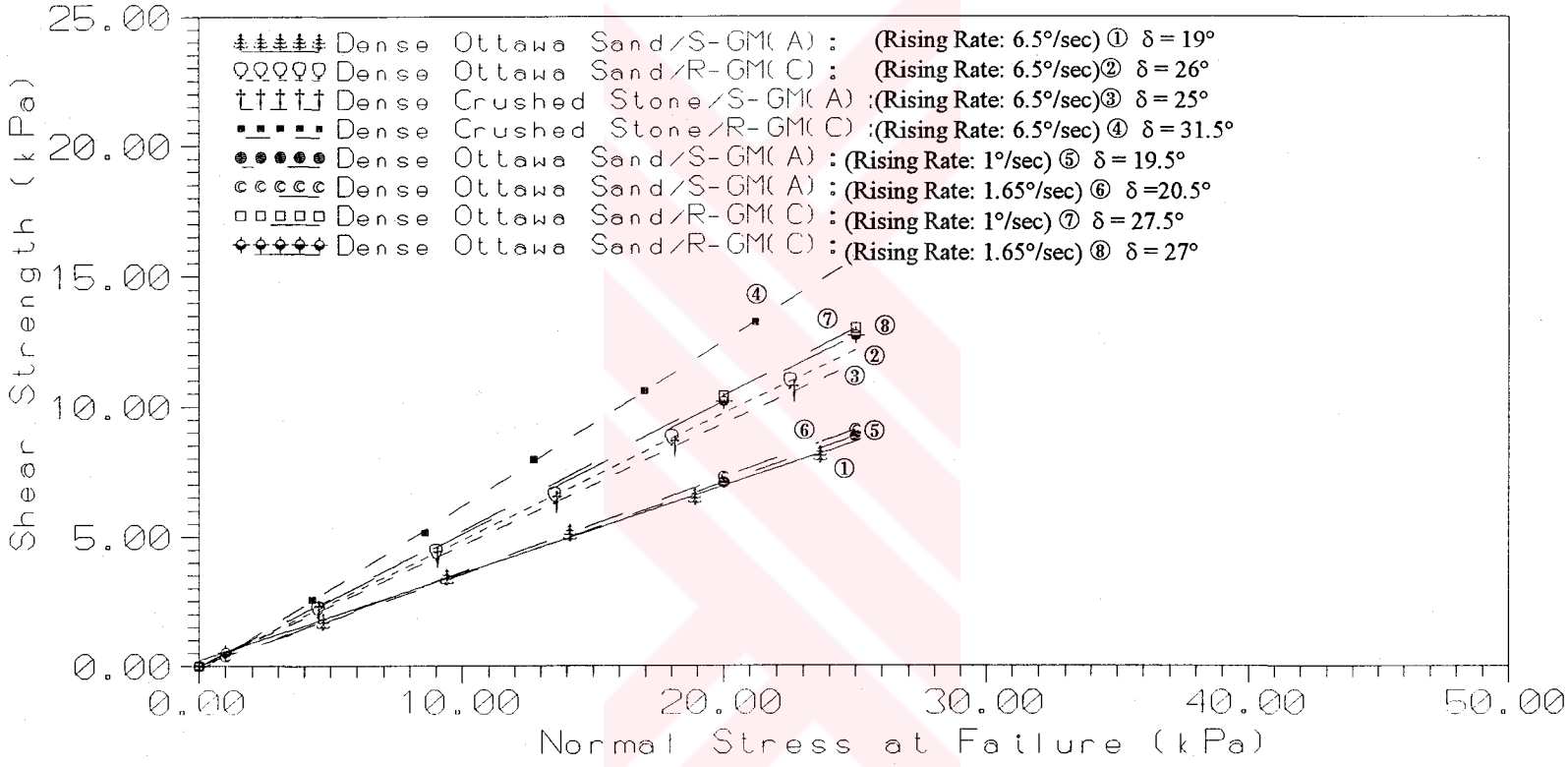

Figure 6.4 300 x 300 mm Inclined Board Test Results

The following points are observed from Figures 6.1 to 6.4:

1. Although the (0,0) point was not taken into consideration in the regression analysis, the curves nearly passed through the origin, i.e., the adhesion ,a, was always smaller than 1 kPa, even a maximum of -1 kPa was observed; so the adhesion intercept was assumed to be negligible.
2. The sliding angles (δ) varied from 15.5° for loose Ottawa Sand/Smooth Geomembrane interfaces to 30.5° for dense crushed stone/Rough Geomembrane interfaces.
3. Interfaces involving very angular crushed stone always gave higher sliding angles (δ) than the interfaces involving well rounded Ottawa Sand.
4. Interfaces involving rough geomembrane always gave higher sliding angles (δ) than the interfaces involving smooth geomembrane.
5. Interfaces involving the rougher geomembrane, namely R-GM(A) gave higher sliding angles than R-GM(C) with relatively lower degree of roughness.
6. The comparison of curves ① - ⑤, ② - ⑥, ③ - ⑦, and ④ - ⑧ both in Figures 6.1 and 6.2 (the figures for the 60 x 60 inclined board tests), showed that the density of the soil layer did not have a remarkable effect on the sliding angle of the interface, neither in the interfaces involving Ottawa Sand nor the ones involving crushed stone (the maximum difference was 1.5° for Ottawa Sand and 2.5° for crushed stone). For this reason the inclined board tests on 200 x 200 mm and 300 x 300 mm interfaces were conducted only on dense soil layer.
7. The comparison of curves ① - ⑤ - ⑦ and ② - ⑥ - ⑧ in Figure 6.4 showed that the rising rate of the inclined board did not have an important effect on the sliding angles obtained.

The summary of the results excluding tests with so called "loose" samples and tests with rates other than 6.5 degrees/sec are given in Table 6.1.

Table 6.1 Summary of Inclined Board Test Results

	Ottawa Sand				Crushed Stone			
Interface Area (mm^2)	Smooth GM(A)	Smooth GM(B)	Rough GM(A)	Rough GM(C)	Smooth GM(A)	Smooth GM(B)	Rough GM(A)	Rough GM(C)
60 x 60	16.5°	18.5°	28°	24°	23.5°	24°	30°	27.5°
200 x 200	18.5°	-	-	26°	26.5°	-	-	30.5°
300 x 300	19°	-	-	26°	25°	-	-	31.5°

The examination of the data given in Table 6.1 shows that the experimental values are quite consistent except one (i.e. the value corresponding to crushed stone, smooth GM(A) and 300 x 300 mm interface area) which appears to have been measured a few degrees too low. In Figure 6.5, the results given in Table 6.1 are plotted for smooth GM(A) and rough GM(C) for both soils and three different interface areas.

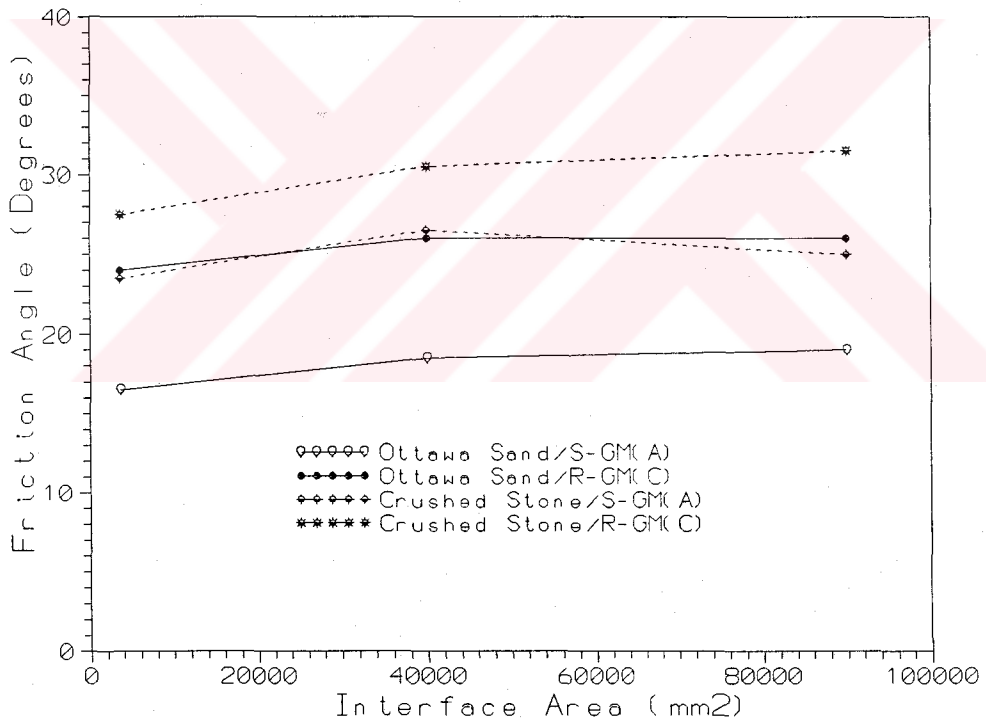

Figure 6.5 Friction Angle versus Interface Area in Inclined Board Tests

The following statements can be given on Table 6.1 and Figure 6.5:

1. It appears that on the average about 3 degrees larger δ values are obtained when the interface area is increased, and values found for 200x 200 mm and 300 x 300 mm interface areas seem to be closer to each other. In any case, in the inclined board tests generally large areas are tested. The inclusion of small area of 60 x 60 mm area in the present study was to compare the results with shear box test with 60 x 60 mm area. It may be proposed that for similar materials, a relatively large area, for instance a minimum of 200 x 200 mm area is to be employed.

2. It is found that the interface friction angles of granular soils with rounded particles are much more sensitive to changes in the surface roughness of the geomembrane and even to the changes in the brand of the geomembrane than the soils with angular grains. For example δ for smooth GM(A) and rough GM(C) differed by 7-7.5° for the Ottawa Sand whereas this was 4° (excluding the above mentioned inconsistent value) for the crushed stone. Similarly smooth GM(A) and GM(B) gave 2° difference for the Ottawa Sand and 0.5° for the crushed stone; rough GM(A) and GM(C) resulted in 4° difference in δ values for the Ottawa Sand and 2.5° for the crushed stone.

The results given in Table 6.1 and the are also presented in terms of efficiencies ($\tan \delta/\tan \phi$) in Table A.25 in Appendix A. In Appendix B, a simple check against effect of overturning in the inclined board test is explained

6.2 Direct Shear Box Test Results

Figures 6.6 and 6.7 present typical direct shear box test results for dense Ottawa Sand against smooth GM(A) whereas the corresponding curves against rough GM(C) interface are given in Figures 6.8 and 6.9.

The results of the direct shear box tests, outlined in Table 5.7 are presented in Table 6.2, The remaining direct shear test data are given in Appendix B.

Table 6.2 Summary of Direct Shear Box Test Results

Soil Used	Density	Geomembrane	Friction Angle	Difference*
Ottawa Sand	Dense	S-GM(A)	22°	5.5°
Ottawa Sand	Dense	R-GM(C)	32°	8°
Crushed Stone	Loose	S-GM(A)	29.5°	-
Crushed Stone	Dense	S-GM(A)	31°	7.5°
Crushed Stone	Loose	R-GM(C)	34°	-
Crushed Stone	Dense	R-GM(C)	37°	9.5°

* Difference in friction angles obtained from direct shear box tests and inclined board tests

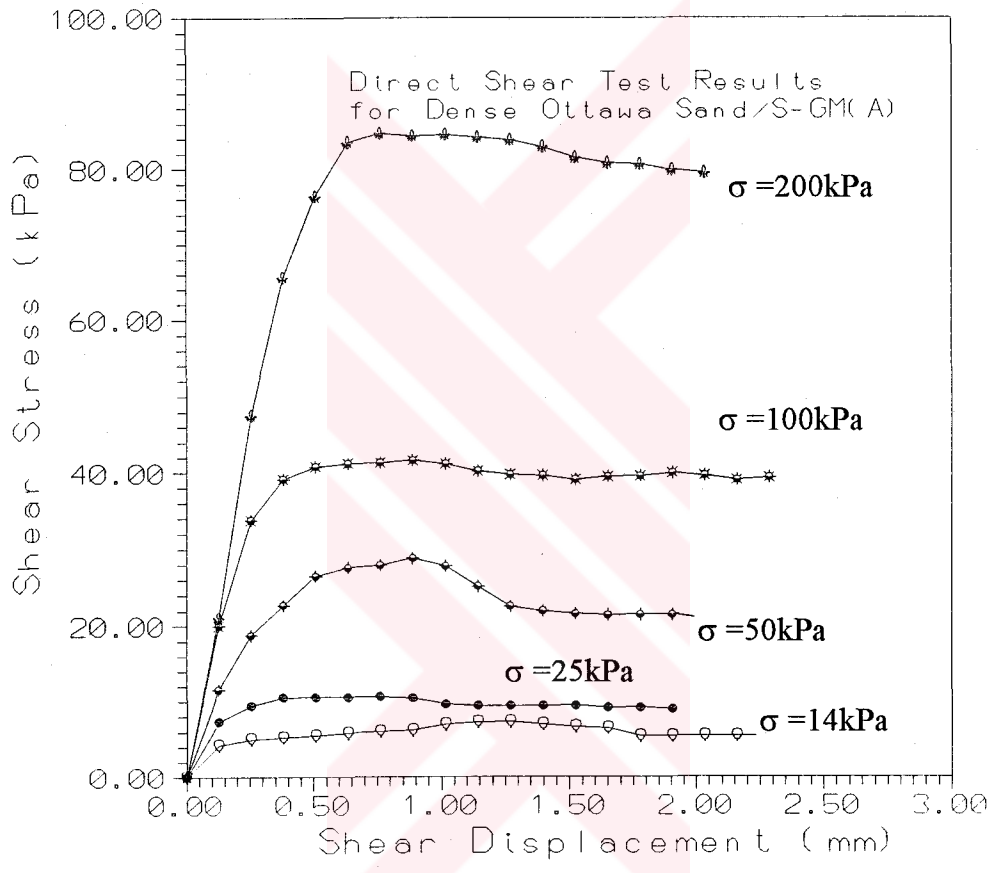

Figure 6.6 Direct Shear Box Test Results for Dense Ottawa Sand/S-GM(A)

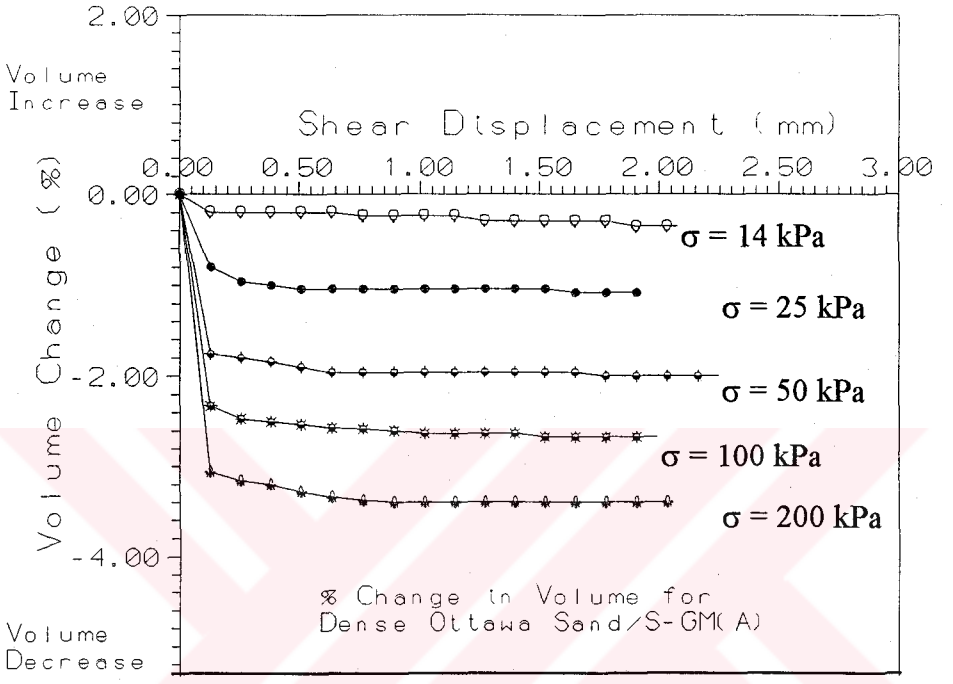

Figure 6.7 Δ Volume (%) for Dense Ottawa Sand/S-GM(A)

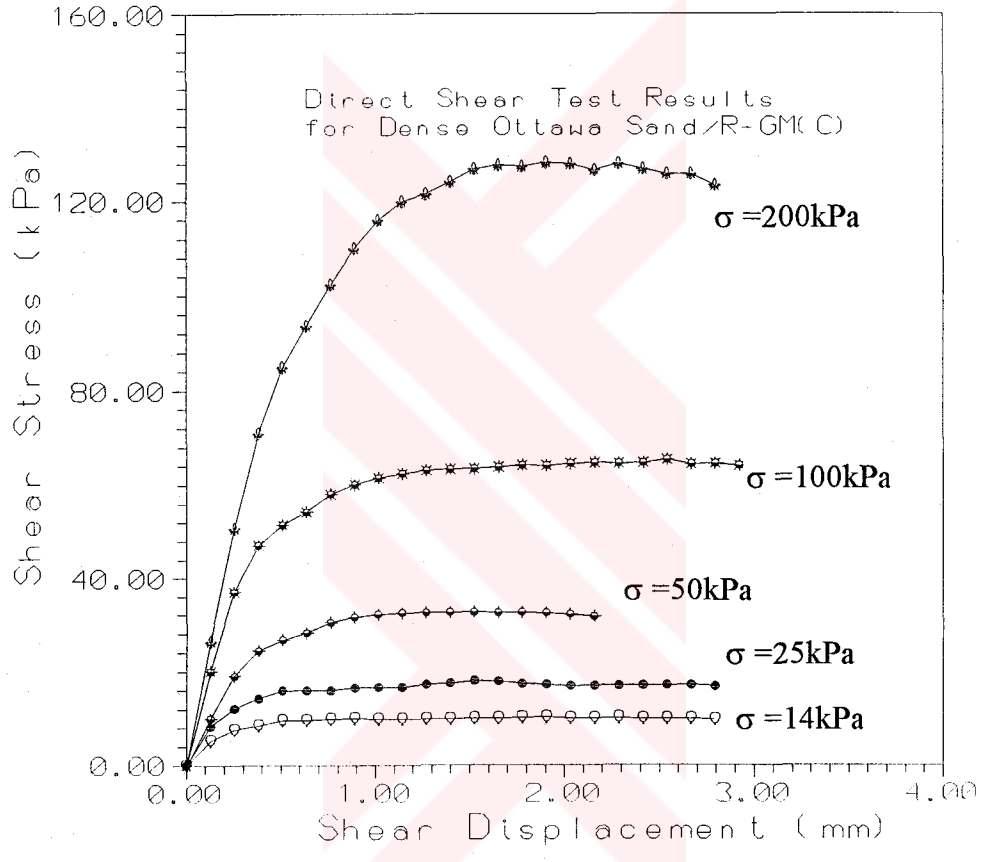

Figure 6.8 Direct Shear Box Test Results for Dense Ottawa Sand/R-GM(C)

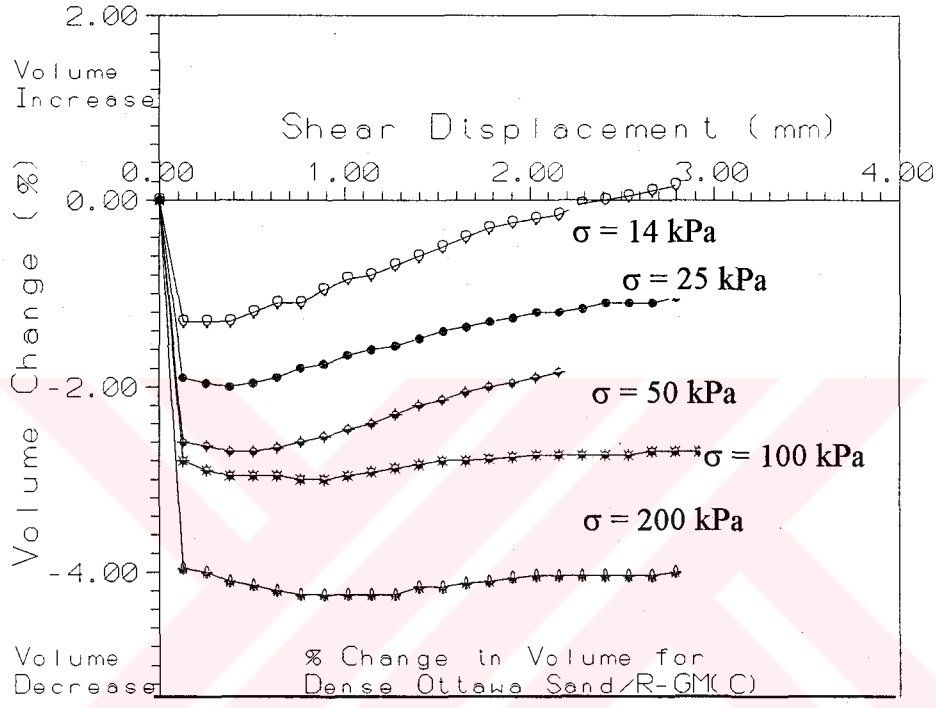

Figure 6.9 Δ Volume (%) for Dense Ottawa Sand/R-GM(C)

Table 6.2 shows that "fixed" shear tests yielded about 5 to 10 degrees higher interface friction angles than the corresponding inclined board tests; the difference being greater for the crushed stone. In order to check if "dilatancy" or "interlocking" during shearing could explain the larger friction angles in shear box tests; volume change (determined from sample thickness changes) versus shearing displacement plots have been examined. It was seen that all tests exhibited contraction during shearing except very small expansion after initial contraction at very low normal stresses; which excluded that possibility. The fact that 5-10° higher angles in shear box tests have been reported for geomembrane-geotextile interfaces where dilatancy is out of question, may suggest that the different sliding mechanism involved in the inclined board test gives lower limit of interface angles.

The improvement in the interface friction due to the increased surface roughness of the geomembrane was 10 degrees for the Ottawa Sand and smaller namely 6 degrees for the crushed stone (Table 6.2). The values are different but the trend is the same in the inclined board tests where these differences were 7.5 and 4 degrees respectively for the Ottawa Sand and the crushed stone.

Girard et al.(1990). state that the inclined board tests reveal more realistic friction angles than the direct shear box tests. After a series of direct shear, inclined board and field tests on slopes involving geomembranes and geotextiles, Girard et al. (1990) concluded that the inclined board results are still greater than the real field conditions and a factor of safety must be applied to the results of both tests for design purposes although the factor of safety that should be used for the inclined board tests are smaller than the one needed to modify the direct shear box results.

It must be also added that neither in the inclined board nor in the direct shear tests carried out in the present study, it was not possible to detect a break in the failure envelope as mentioned before. It is thought that standard direct shear

testing is not suitable for testing under low normal stresses which enables "the break" to be assessed, and dilation was not observed in tests anyway. On the other hand, in inclined board tests, the dilation effect probably did not exist at all.

A comparison of friction angles obtained from the two different tests in the present experimental study together with the direct shear test results for interfaces involving sand and geomembrane from the literature are given in Figure 6.10 which shows that the values obtained in the present study lies between the minimum and maximum limits presented by different researchers.

An important point that should be stated is that, for natural soils, the design values should be closer to the friction angles obtained for crushed stone since the Ottawa Sand represents an extreme case where the sand particles are highly rounded.

The results given in Table 6.2 are also presented in terms of efficiencies ($\tan\delta/\tan\phi$) and adhesion in Table C.1 in Appendix C.

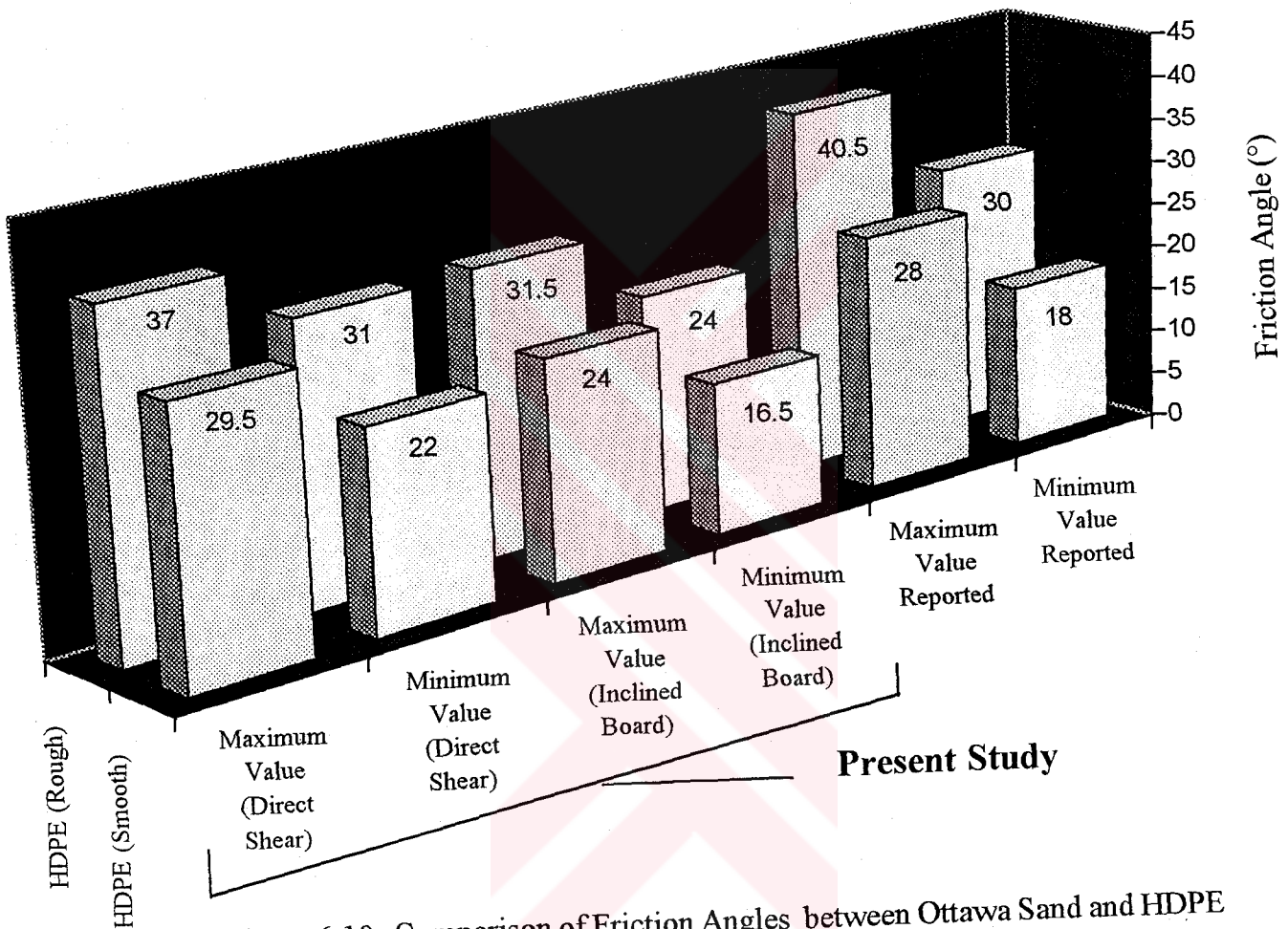

Figure 6.10 Comparison of Friction Angles between Ottawa Sand and HDPE from the Literature and Present Study

CHAPTER VII

CONCLUSIONS

The following conclusions can be drawn from the inclined board and direct shear box tests, carried out using two sands; Ottawa Sand with well rounded particles and crushed stone with very angular particles; and smooth and rough (textured) geomembranes of different brand names.

1. Angularity of the sand particles and increased surface roughness of the geomembrane improves the sand-geomembrane interface shear strength to a similar extend.

2. In the case of crushed stone (of which particles may have comparable angularity to that of most natural sands), the difference in the interface friction angle between sand and the rough and smooth geomembrane is considerably less than the one found for the Ottawa Sand with well rounded particles. In other words, the degree of the geomembrane is greater in the case of rounded particles..

3. Inclined board tests yield consistently smaller interface friction angles for both soils and all the geomembranes used. Reported values though very few support this finding and the inclined board test results are considered to be more realistic.

REFERENCES

Akbert, S.Z., Hammamji, Y., and Lafleur, J., 1985. "Frictional Characteristics of Geomembranes, Geotextiles and Geomembrane-Geotextile Composites", Proc. 2nd. Canadian Symposium on Geotextiles and Geomembranes, Edmonton, Alberta, pp.209-217.

Bacot, J., Iltis, M., Lareal, P., Paumier, T., and Sanglerat, G., 1978. "Study of the Soil Reinforcement Friction Coefficient", Proc. of the Symposium on Earth Reinforcement, ASCE, Pittsburgh, PA, USA, pp.157-185.

Bishop, A.W., Green, G.E., Garga, V.K., Andresen, A., and Brown, J.D., 1971. "A New Ring Shear Apparatus and Its Application to the Measurement of Residual Strength", Geotechnique, Vol.21, No.4, pp.273-328.

BS 6906, 1991. "Methods of Test for Geotextiles. Part 8: Determination of Sand-Geotextile Frictioanl Beahavior by Direct Shear", pp.1-8.

Cernica, J.N., 1995. Geotechnical Engineering: Foundation Design, John Wiley and Sons Inc., U.S.A.

Christopher, B.R., and Holtz, R.D., 1985. Geotextile Engineering Manual-Course Text, National Highway Institute, Federal Highwway Administration, Washington, U.S.A.

Craig, R.F., 1987. Soil Mechanics, 4th. ed., Chapman and Hall, London, Great Britain.

Daniel, D.E., 1991. "Compacted Clay and Geosynthetic Clay Linings", Proc. XV CGT, Italy.

Das, M.B., 1983. Advanced Soil Mechanics, McGraw-Hill Inc., U.S.A.

Dembicki, E., and Alenowickz, J., 1987. "Determination of Frictional Properties of Geotextiles", Journal of Geotextiles and Geomembranes, Vol.6, No.4, pp.307-314.

Evans, M.D., and Fennick, T.J., 1995. "Geosynthetic/Soil Friction Angles Using a Rotation Shear Device", ASTM Geotechnical Testing Journal, Vol.18, No.2, pp.271-275.

Fishman, K.L., and Pal, S., 1994. "Further Study of Geomembrane/Cohesive Soil Interface Shear Behavior", Journal of Geotextiles and Geomembranes, Vol.13, pp.571-590..

Fourie, A.B., and Fabian, K.J., 1987. "Laboratory Determination of Clay-Geotextile Interaction", Journal of Geotextiles and Geomembranes, Vol.6, No.4, pp.275-294.

Girard, H., Fischer, S., and Alonso, E., 1990. "Problems of Friction Posed by the Use of Geomembranes on Dam Slopes-Examples and Measurements", Journal of Geotextiles and Geomembranes, Vol.9, No.2, pp.129-143.

Giroud, J.P., Swan, Jr.R.H., Richer, P.J., and Spooner, P.R., 1990. "Geosynthetic Landfill Cap: Laboratory and Field Tests, Design and Construction", Proc. 4th. International Conference on Geotextiles, Geomembranes and Related Products, Balkema, Rotterdam, pp.493-498.

Hausmann, M.R., 1990. Engineering Principles of Ground Modification, McGraw-Hill Inc., U.S.A.

Ingold, T.S., 1982. "Some Observations on the Laboratory Measurement of Soil-Geotextile Bond", ASTM Geotechnical Testing Journal, Vol.5, No.3/4, pp.57-67.

Ingold, T.S., 1984. "A Laboratory Investigation of Soil Geotextile Friction", Journal of Ground Engineering, Vol.17, pp.21-28.

Ingold, T.S., 1991. "Rilem Report 4: Friction Testing", Geomembranes, Identification and Performance Testing, Chapman and Hall, Cambridge, Great Britain, pp.176-203.

Kate, J.M., Rao, G.V., and Tyagi, S.K., 1988. "Evaluation of Soil-Reinforcement Friction", Indian Geotechnical Journal, Vol.18, pp.153-160.

Koerner, R.M., 1994. Designing with Geosynthetics, 3rd. ed., Prentice Hall Inc., New Jersey, U.S.A.

Koerner, R.M., Martin, J.P., and Koerner, G.R., 1986. "Shear Strength Parameters between Geomembranes and Cohesive Soils", Journal of Geotextiles and Geomembranes, Vol.4, No.1, pp.21-30.

Koutsourais, M.M., and Sprague, C.J., 1991. "Interfacial Friction Study of Cap and Liner Components for Landfill Design", Journal of Geotextiles and Geomembranes, Vol.10, No.5/6, pp.531-548.

Lambe, T.W., and Whitman, R.V., 1979. Soil Mechanics, John Wiley and Sons, U.S.A.

Lydick, L.D., and Zagorski, A.Z., 1991. "Interface Friction of Geonets: A Literature Survey", Journal of Geotextiles and Geomembranes, Vol.10, pp.549-558.

Martin, J.P., Koerner, R.M., and Whitty, J.E., 1984. "Experimental Friction Evaluation of Slippage between Geomembranes, Geotextiles and Soils", Proc. International Conference on Geomembranes, Denver, Co, IFAI, St.Paul, MN, pp.191-196.

Mitchell, J.K., Seed, R.B., and Seed, H.B., 1990. "Kettleman Hills Waste Landfill Slope Failure-I:Liner System and Properties", Journal of Geotechnical Engineering, ASCE, Vol.116, No.4, pp.647-668.

Myles, B., 1982. "Assesment of Soil-Fabric Friction by Means of Shear", Proc. 2nd. International Conference on Geotextiles and Geomembranes, Las Vegas, Vol.3, pp.787-791.

Negussey, D., Wijewickreme, W.K.D., and Vaid, Y.P., 1989. "Geomembrane Interface Friction", Canadian Geotechnical Journal, Vol. 26, No.1, pp.165-169.

O'Rourke, T.D., Druchel, S.J., and Netrevali, A.N., 1990. "Shear Strength Characteristics of Sand-Polymer Interfaces", Journal of Geotechnical Engineering, ASCE, Vol.115, No.8, pp.1118-1133.

Pasqualini, E., Roccato, M., and Sani, D., 1995. "Waste Disposal by Landfill", GREEN'93 Sarsby(ed.) , Balkema, Rotterdam, pp.349-356.

Rao, G.V., and Pandley, S.K., 1988. "Evaluation of Geotextile-Soil Friction", Indian Geotechnical Journal, Vol.18, pp.77-105.

Richards, E.A., and Scott, J.D., 1985. "Soil-Geotextile Frictional Properties", 2nd. Canadian Symposium on Geotextiles and Geomembranes, Edmonton, Alberta, pp.13-24.

Saxena, S.K., and Wong, Y.T., 1984. "Frictional Characteristics of Geomembranes", Proc. International Conference on Geomembranes, Denver, CO, IFAI, St.Paul, MN, pp.187-190.

Schlosser, F., and Elias, V. ,1978. "Friction in Reinforced Earth", Proc. oc the Symposium on Earth Reinforcement, ASCE, Pittsburgh, PA, USA, pp.753-763.

Seed, R.B., and Boulanger, R.W., 1991. "Smooth HDPE-Clay Liner Interface Shear Strengths - Compaction Effects", Journal of Geotechnical Engineering", ASCE, Vol.117, No.4, pp. 686-693.

Sharma, H.D., and Houllings, D.E., 1993. "Direct Shear Testing for HDPE/Amended Soil Composites", Proc. Geosynthetics'93, Vancouver, Canada, ASCE, New York, pp.1469-1481.

Sridharan, A., and Singh, H.R., 1984. "Friction Coefficient in Reinforced Earth", Proc. of the Indian Geotechniccal Conference, Calcutta, Indian Geotechnical Society, New Delhi, pp.43-47.

Sridharan, A., and Singh, H.R., 1986. "An Experimental Study on Mild Steel as Soil Reinforcement" Indian Geotechnical Journal, Vol. 16, pp.334-345.

Sridharan, A., and Singh, H.R., 1988. "Effect of Soil Parameters on Friction Coefficient between Soil and Reinforcement" Indian Geotechnical Journal, Vol. 18, pp.323-339.

Srinisava Murthy, B.R., Sridharan, A., and Bindumadhava, 1991. "Evaluation of Interface Frictional Resistance", Journal of Geotextiles and Geomembranes, Vol.12, pp.235,253.

Stark, T.D., and Poeppel, A.R., 1994. "Landfill Liner Interface Strengths from Tortional-Ring Shear Tests", Journal of Geotechnical Engineering, ASCE, Vol.120, pp.597-615.

Takasumi, D.L., Green, K.R., and Holtz, R.D., 1991. " Soil-Geosynthetics Interface Strength Characteristics: A Review of State-of-the-Art Testing Procedures", Proc. of Geosynthetics'91, IFAI, Atlanta, GA, pp.87-100.

Wasti, Y., 1995. Application of Geosynthetics: Lecture Notes.

Weiss, W. and Batereau, C., 1987. "A Note on Planar Shear between Geosynthetics and Construction Materials", Journal of Geotextiles and Geomembranes, Vol.5, No.1, pp.63-67.

Willams, N.D., and Houlihan, M., 1986. "Evaluation of Friction Coefficients between Geomembranes, Geotextiles and Related Products", Proc. of 3rd. International Conference on Geotextiles, Vienna, OIAV, Austria.

Williams, N.D., and Houllihan, M., 1987. "Evaluation of Interface Friction Properties between Geeosynthetics and Soil", Proc. Geosynthetics'87, New Orleans, LA, IFAI, St.Paul, MN, pp.616-627.

Yegian, M.K., and Lahlaf, A.M., 1992. "Dynamic Interface Shear Strength Properties of Geomembranes and Geotextiles", Journal of Geotechnical Engineering, ASCE, Vol.118, pp.761-779.

APPENDIX A

DATA POINTS FOR THE INCLINED BOARD TEST

Table A.1 Friction Characteristics for Loose Sand-SGM(A) : 60 x 60 mm

Normal Stress at Horizontal State (kPa)	Sliding Angle (°)	Normal Stress at Failure (kPa)	Shear Strength (kPa)
5.55	18	5.28	1.72
11.10	18	10.56	3.43
16.65	18	15.84	5.15
22.20	17	21.23	6.49
27.75	17	26.54	8.11
33.30	17	31.84	9.74
38.85	16	37.35	10.71
44.40	16	42.68	12.24
49.95	16	48.02	13.77

Table A.2 Friction Characteristics for Dense Sand-SGM(A) : 60 x 60 mm

Normal Stress at Horizontal State (kPa)	Sliding Angle (°)	Normal Stress at Failure (kPa)	Shear Strength (kPa)
5.55	18	5.28	1.72
11.10	18	10.56	3.43
16.65	17	15.92	4.87
22.20	17	21.23	6.49
27.75	17	26.54	8.11
33.30	17	31.84	9.74
38.85	17	37.15	11.36
44.40	17	42.46	12.98
49.95	17	47.77	14.60

Table A.3 Friction Characteristics for Loose Sand-SGM(B) : 60 x 60 mm

Normal Stress at Horizontal State (kPa)	Sliding Angle (°)	Normal Stress at Failure (kPa)	Shear Strength (kPa)
5.55	20	5.22	1.90
11.10	20	10.43	3.80
16.65	20	15.65	5.70
22.20	19	21.00	7.22
27.75	19	26.24	9.03
33.30	18	31.67	10.30
38.85	18	36.95	12.00
44.40	18	40.23	13.72
49.95	17	47.77	14.60

Table A.4 Friction Characteristics for Dense Sand-SGM(B) : 60 x 60 mm

Normal Stress at Horizontal State (kPa)	Sliding Angle (°)	Normal Stress at Failure (kPa)	Shear Strength (kPa)
5.55	20	5.22	1.90
11.10	20	10.43	3.80
16.65	20	15.65	5.70
22.20	20	20.86	7.59
27.75	20	26.08	9.49
33.30	19	31.49	10.84
38.85	19	36.73	12.65
44.40	19	41.98	14.46
49.95	19	47.22	16.26

Table A.5 Friction Characteristics for Loose Crushed Stone-SGM(A) : 60 x 60 mm

Normal Stress at Horizontal State (kPa)	Sliding Angle (°)	Normal Stress at Failure (kPa)	Shear Strength (kPa)
5.55	25	5.03	2.35
11.10	25	10.06	4.69
16.65	25	15.09	7.04
22.20	25	20.12	9.38
27.75	23	25.54	10.84
33.30	22	30.86	12.47
38.85	22	36.02	14.55
44.40	22	41.17	16.63
49.95	22	46.31	18.71

Table A.6 Friction Characteristics for Dense Crushed Stone-SGM(A) : 60 x 60 mm

Normal Stress at Horizontal State (kPa)	Sliding Angle (°)	Normal Stress at Failure (kPa)	Shear Strength (kPa)
5.55	26	4.99	2.43
11.10	25	10.06	4.69
16.65	25	15.09	7.04
22.20	25	20.12	9.38
27.75	25	25.35	11.73
33.30	24	30.42	13.54
38.85	24	35.50	15.80
44.40	24	40.56	18.60
49.95	23	45.98	19.52

Table A.7 Friction Characteristics for Loose Crushed Stone-SGM(B) : 60 x 60 mm

Normal Stress at Horizontal State (kPa)	Sliding Angle (°)	Normal Stress at Failure (kPa)	Shear Strength (kPa)
5.55	24	5.07	2.26
11.10	24	10.14	4.51
16.65	24	15.21	6.77
22.20	24	20.28	9.03
27.75	24	25.35	11.29
33.30	23	30.65	13.01
38.85	23	35.76	15.18
44.40	23	40.87	17.35
49.95	23	45.98	19.52

Table A.8 Friction Characteristics for Dense Crushed Stone-SGM(B) : 60 x 60 mm

Normal Stress at Horizontal State (kPa)	Sliding Angle (°)	Normal Stress at Failure (kPa)	Shear Strength (kPa)
5.55	25	5.03	2.35
11.10	25	10.06	4.69
16.65	25	15.09	7.04
22.20	25	20.12	9.38
27.75	25	25.15	11.73
33.30	25	30.18	14.07
38.85	25	35.21	16.42
44.40	24	40.46	18.06
49.95	24	45.63	20.32

Table A.9 Friction Characteristics for Loose Sand-RGM(A) : 60 x 60 mm

Normal Stress at Horizontal State (kPa)	Sliding Angle (°)	Normal Stress at Failure (kPa)	Shear Strength (kPa)
5.55	29	4.85	2.69
11.10	29	9.71	5.38
16.65	29	14.56	8.07
22.20	28	19.60	10.42
27.75	28	24.50	13.03
33.30	28	29.40	15.63
38.85	28	34.30	18.24
44.40	27	39.56	20.16
49.95	27	44.51	22.68

Table A.10 Friction Characteristics for Dense Sand-RGM(A) : 60 x 60 mm

Normal Stress at Horizontal State (kPa)	Sliding Angle (°)	Normal Stress at Failure (kPa)	Shear Strength (kPa)
5.55	29	4.85	2.69
11.10	29	9.71	5.38
16.65	29	14.56	8.07
22.20	29	19.42	10.76
27.75	29	24.27	13.45
33.30	28	29.40	15.63
38.85	28	34.30	18.24
44.40	28	39.20	20.84
49.95	28	44.10	23.45

Table A.11 Friction Characteristics for Loose Crushed Stone-RGM(A) : 60 x 60 mm

Normal Stress at Horizontal State (kPa)	Sliding Angle (°)	Normal Stress at Failure (kPa)	Shear Strength (kPa)
5.55	32	4.71	2.94
11.10	32	9.41	5.88
16.65	32	14.12	8.82
22.20	32	18.83	11.76
27.75	31	23.79	14.29
33.30	31	28.54	17.15
38.85	31	33.30	20.00
44.40	30	38.45	22.20
49.95	30	43.26	24.98

Table A.12 Friction Characteristics for Dense Crushed Stone-RGM(A) : 60 x 60 mm

Normal Stress at Horizontal State (kPa)	Sliding Angle (°)	Normal Stress at Failure (kPa)	Shear Strength (kPa)
5.55	33	4.65	3.02
11.10	33	9.31	6.04
16.65	32	14.12	8.82
22.20	32	18.83	11.76
27.75	32	23.53	14.71
33.30	31	28.54	17.15
38.85	31	33.30	20.00
44.40	31	38.06	22.87
49.95	30	43.26	24.98

Table A.13 Friction Characteristics for Loose Sand-RGM(C) : 60 x 60 mm

Normal Stress at Horizontal State (kPa)	Sliding Angle (°)	Normal Stress at Failure (kPa)	Shear Strength (kPa)
5.55	26	4.99	2.43
11.10	26	9.98	4.87
16.65	25	15.09	7.04
22.20	25	20.12	9.38
27.75	25	25.25	11.73
33.30	25	30.18	14.07
38.85	25	35.21	16.42
44.40	25	40.24	18.76
49.95	24	45.63	20.32

Table A.14 Friction Characteristics for Dense Sand-RGM(C) : 60 x 60 mm

Normal Stress at Horizontal State (kPa)	Sliding Angle (°)	Normal Stress at Failure (kPa)	Shear Strength (kPa)
5.55	26	4.99	2.43
11.10	26	9.98	4.87
16.65	26	14.96	7.30
22.20	26	19.95	9.73
27.75	26	24.94	12.16
33.30	25	30.18	14.07
38.85	25	35.21	16.42
44.40	25	40.24	18.76
49.95	24	45.63	20.32

Table A.15 Friction Characteristics for Loose Crushed Stone-RGM(C) : 60 x 60 mm

Normal Stress at Horizontal State (kPa)	Sliding Angle (°)	Normal Stress at Failure (kPa)	Shear Strength (kPa)
5.55	30	4.81	2.78
11.10	30	9.61	5.55
16.65	29	14.56	8.07
22.20	29	19.42	10.76
27.75	28	24.27	13.03
33.30	27	29.67	16.48
38.85	27	34.62	17.64
44.40	27	39.56	20.16
49.95	27	44.51	22.68

Table A.16 Friction Characteristics for Dense Crushed Stone-RGM(C) : 60 x 60 mm

Normal Stress at Horizontal State (kPa)	Sliding Angle (°)	Normal Stress at Failure (kPa)	Shear Strength (kPa)
5.55	31	4.76	2.86
11.10	31	9.51	5.72
16.65	30	14.42	8.33
22.20	29	19.42	10.76
27.75	29	24.27	13.45
33.30	29	29.12	16.14
38.85	28	34.30	18.24
44.40	28	39.20	20.84
49.95	28	44.10	23.45

Table A.17 Friction Characteristics for Dense Sand-SGM(A) : 200 x 200 mm

Normal Stress at Horizontal State (kPa)	Sliding Angle (°)	Normal Stress at Failure (kPa)	Shear Strength (kPa)
10	21	9.33	3.58
20	20	18.79	6.84
30	19	28.37	9.77
45	19	42.55	14.65

Table A.18 Friction Characteristics for Dense Sand-RGM(C) : 200 x 200 mm

Normal Stress at Horizontal State (kPa)	Sliding Angle (°)	Normal Stress at Failure (kPa)	Shear Strength (kPa)
10	26	8.99	4.38
20	26	17.98	8.77
30	27	26.73	13.62
45	26	40.45	19.73

Table A.19 Friction Characteristics for Dense Crushed Stone-SGM(A) : 200 x 200 mm

Normal Stress at Horizontal State (kPa)	Sliding Angle (°)	Normal Stress at Failure (kPa)	Shear Strength (kPa)
10	26	8.99	4.38
20	26	19.98	8.76
30	26	26.96	13.14
45	26	40.45	19.72

Table A.20 Friction Characteristics for Dense Crushed Stone-RGM(C): 200 x 200 mm

Normal Stress at Horizontal State (kPa)	Sliding Angle (°)	Normal Stress at Failure (kPa)	Shear Strength (kPa)
10	32	8.48	5.30
20	32	16.96	10.60
30	31	25.72	15.45
45	31	38.57	23.18

Table A.21 Friction Characteristics for Dense Sand-SGM(A): 300 x 300 mm

Normal Stress at Horizontal State (kPa)	Sliding Angle (°)	Normal Stress at Failure (kPa)	Shear Strength (kPa)
5.00	20	4.70	1.71
10.00	20	9.40	3.42
15.00	20	14.10	5.13
20.00	19	18.90	6.51
25.00	19	23.65	8.14

Table A.22 Friction Characteristics for Dense Sand-RGM(C) : 300 x 300 mm

Normal Stress at Horizontal State (kPa)	Sliding Angle (°)	Normal Stress at Failure (kPa)	Shear Strength (kPa)
5.00	26	4.50	2.19
10.00	26	9.00	4.38
15.00	26	13.50	6.57
20.00	26	18.00	8.76
25.00	26	22.50	10.95

Table A.23 Friction Characteristics for Dense Crushed Stone-SGM(A): 300 x 300 mm

Normal Stress at Horizontal State (kPa)	Sliding Angle (°)	Normal Stress at Failure (kPa)	Shear Strength (kPa)
5.00	25	4.53	2.11
10.00	25	9.06	4.22
15.00	25	13.60	6.34
20.00	25	18.13	8.45
25.00	25	22.66	10.57

Table A.24 Friction Characteristics for Dense Crushed Stone-RGM(C) : 300 x 300 mm

Normal Stress at Horizontal State (kPa)	Sliding Angle (°)	Normal Stress at Failure (kPa)	Shear Strength (kPa)
5.00	31	4.29	2.58
10.00	31	8.58	5.15
15.00	32	12.72	7.95
20.00	32	16.96	10.60
25.00	32	21.20	13.25

Table A.25 Summary of Inclined Board Test Results in Terms of Efficiencies[a]

	Ottawa Sand				Crushed Stone			
Interfce Area (mm^2)	Smooth GM(A)	Smooth GM(B)	Rough GM(A)	Rough GM(C)	Smooth GM(A)	Smooth GM(B)	Rough GM(A)	Rough GM(C)
60 x 60	0.38	0.43	0.68	0.57	0.42	0.43	0.56	0.50
200 x 200	0.43	-	-	0.62	0.48	-	-	0.57
300 x 300	0.44	-	-	0.62	0.45	-	-	0.59

[a] Efficiencies given inthis table are calculated as tan δ/ tan ϕ where the angle ϕ is taken from Table 5.1 and refers to the dense state of the soil used.

APPENDIX B

A SIMPLE CHECK FOR OVERTURNING EFFECT IN INCLINED BOARD

A schematic representation of the inclined board at the most critical state (maximum load height and the maximum angle obtained) is given in Figure B.1. Assuming that the strip mounted on the base plate to minimize the overturning effect has maximum possible rigidity and accepting that the ball bearing acts as a roller support, the free body diagram becomes as it is presented in Figure B.1:

* W_{max} =180 N
* δ =30°

- $M_{overturning}$=W x sin δ x H=180 x 0.5 x 0.06 = 5.39 N.m
- $M_{resisting}$=(W x cos δ x 0.03) + P x 0.17 = 4.68 + 0.17 P
- P = (5.39-4.68)/0.17=4.18 N
- $F_{extra\ friction}$ = μ x 4.18

Since μ (coefficient of friction) is very small, the extra friction resulting from the roller support can be eliminated.

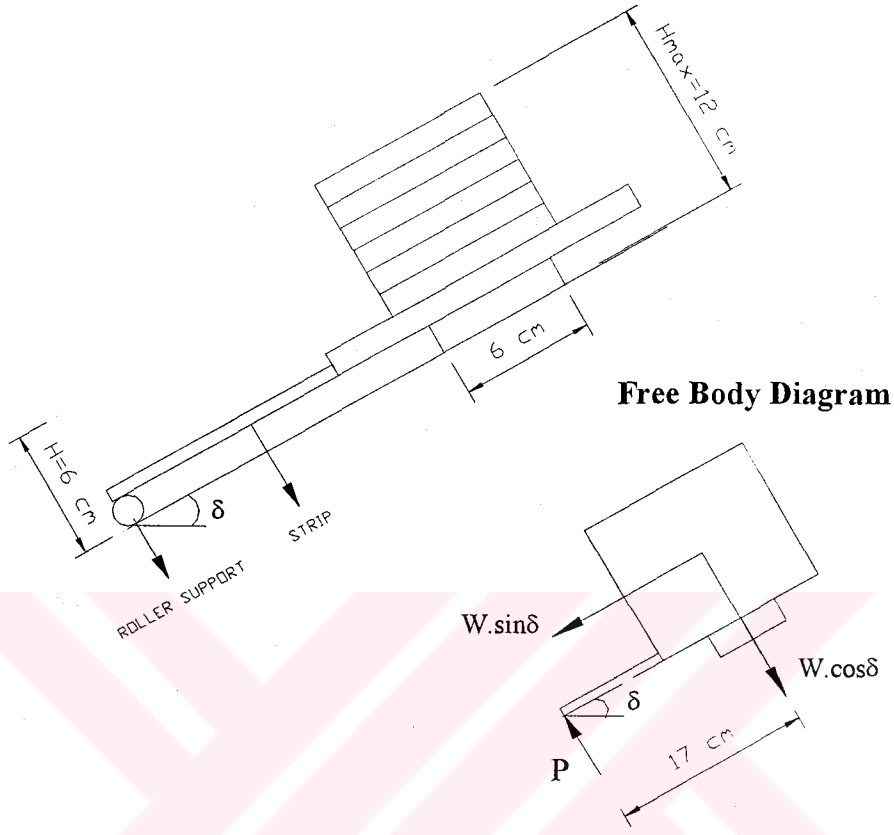

Figure B.1 Schematic Representation and Free Body Diagram of the Inclined Board Test

APPENDIX C

DETAILED INFORMATION ON DIRECT SHEAR BOX TEST RESULTS

Table C.1 Direct Shear Box Test Results inTerms of Efficiencies

Soil Used	Density	Geomembrane	Efficiency[a]	Adhesion (kPa)
Ottawa Sand	Dense	S-GM(A)	0.52	2.76
Ottawa Sand	Dense	R-GM(C)	0.80	1.43
Crushed Stone	Loose	S-GM(A)	0.63	4.33
Crushed Stone	Dense	S-GM(A)	0.58	2.24
Crushed Stone	Loose	R-GM(C)	0.75	3.88
Crushed Stone	Dense	R-GM(C)	0.73	2.89

[a] Efficiencies given inthis table are calculated as tan δ/ tan ϕ where the angle ϕ is taken from Table 5.1.

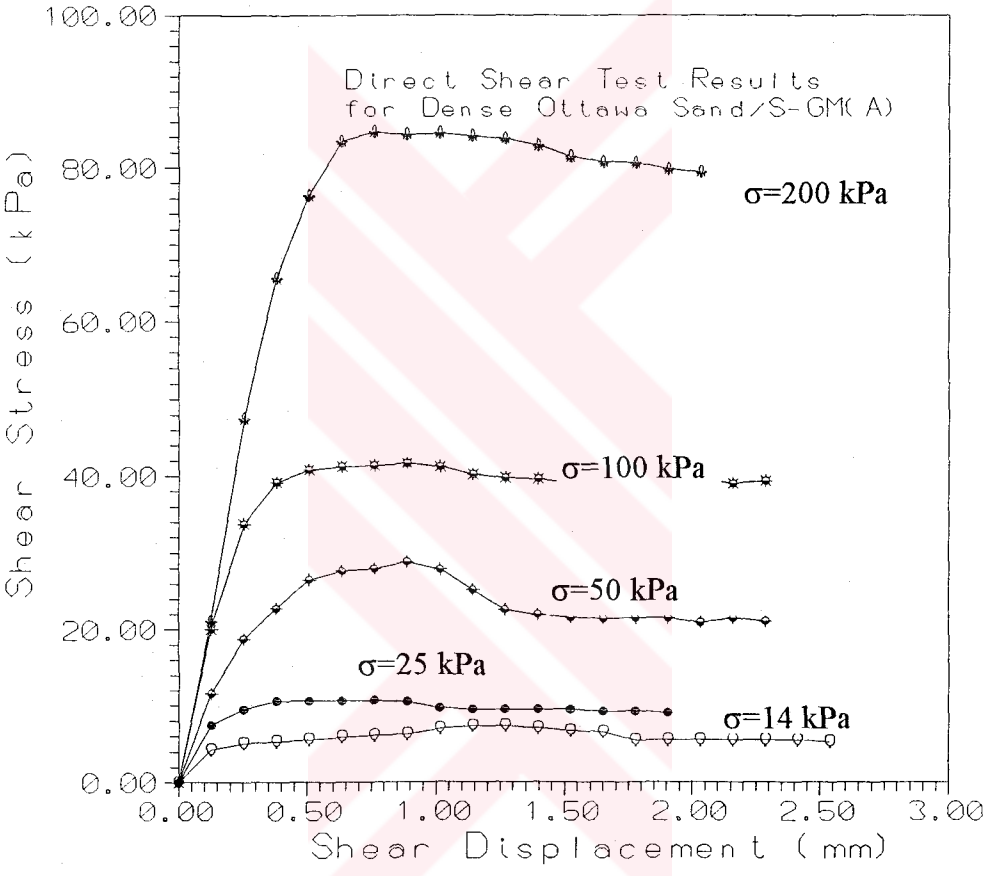

Figure C.1 Direct Shear Box Test Results for Dense Ottawa Sand/S-GM(A)

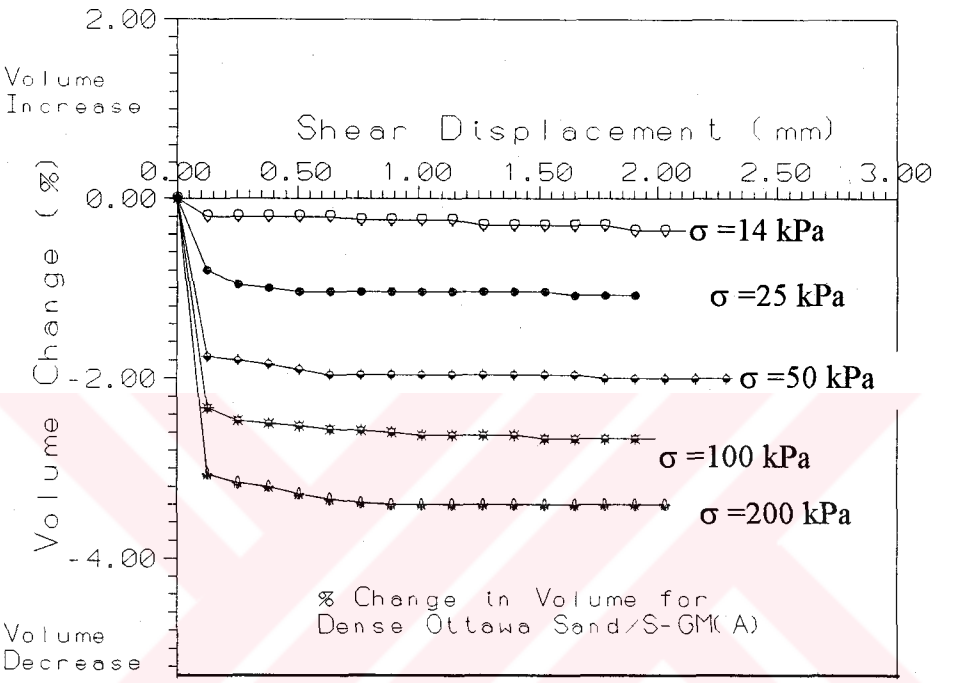

Figure C.2 Δ Volume (%) for Dense Ottawa Sand/S-GM(A)

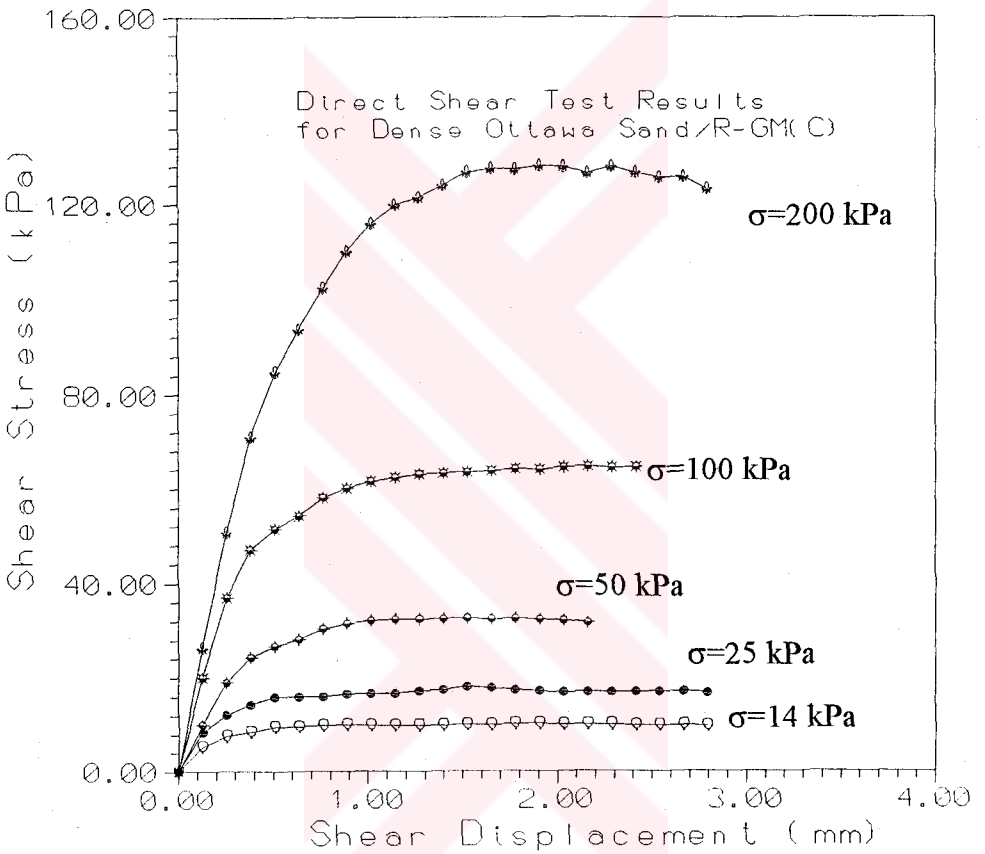

Figure C.3 Direct Shear Box Test Results for Dense Ottawa Sand/R-GM(C)

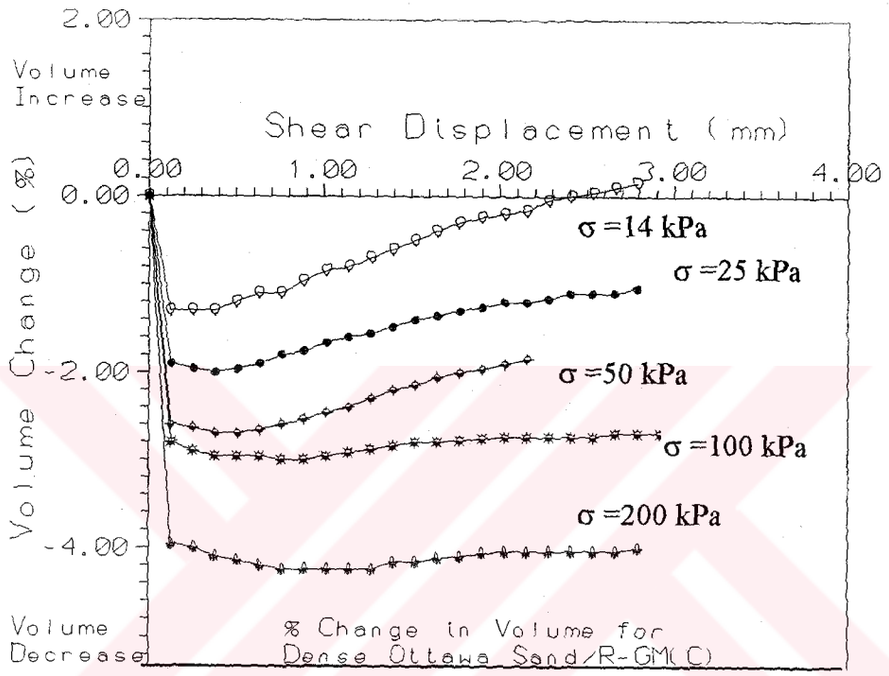

Figure C.4 Δ Volume (%) for Dense Ottawa Sand/R-GM(*C*)

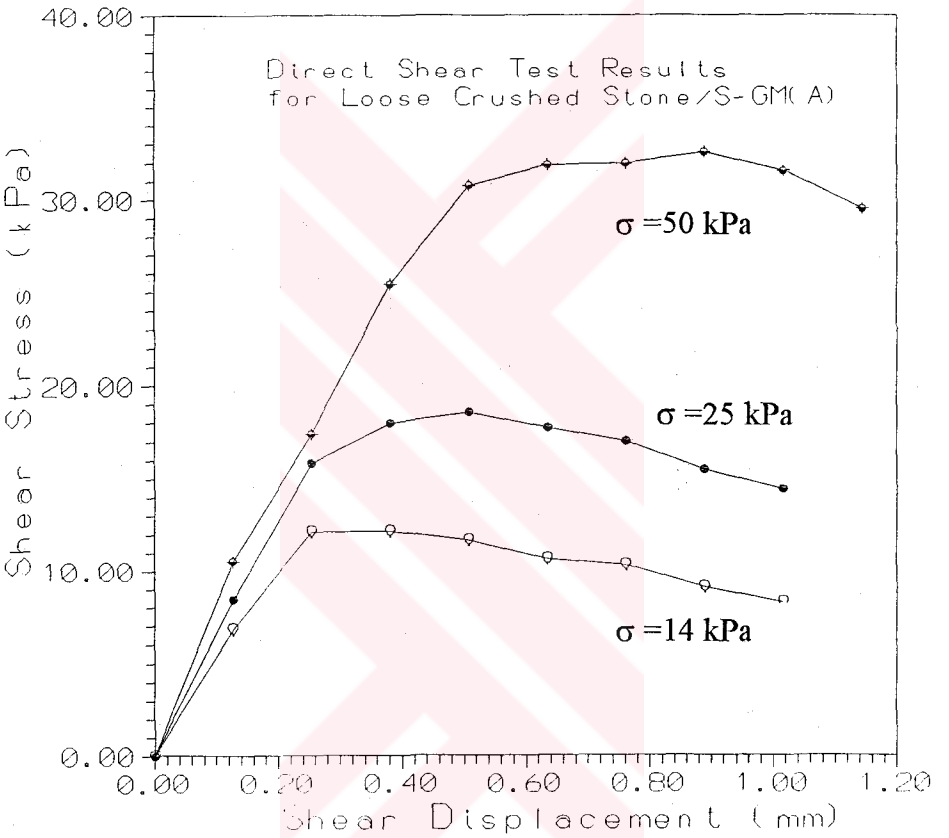

Figure C.5 Direct Shear Box Test Results for Loose Crushed Stone/S-GM(A)

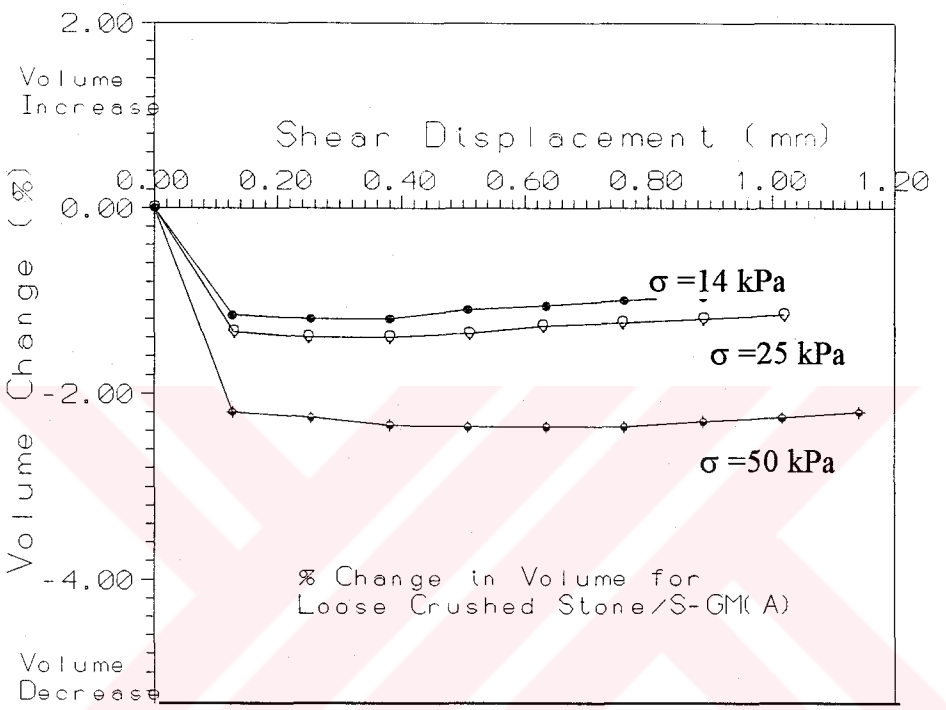

Figure C.6 Δ Volume (%) for Loose Crushed Stone/S-GM(A)

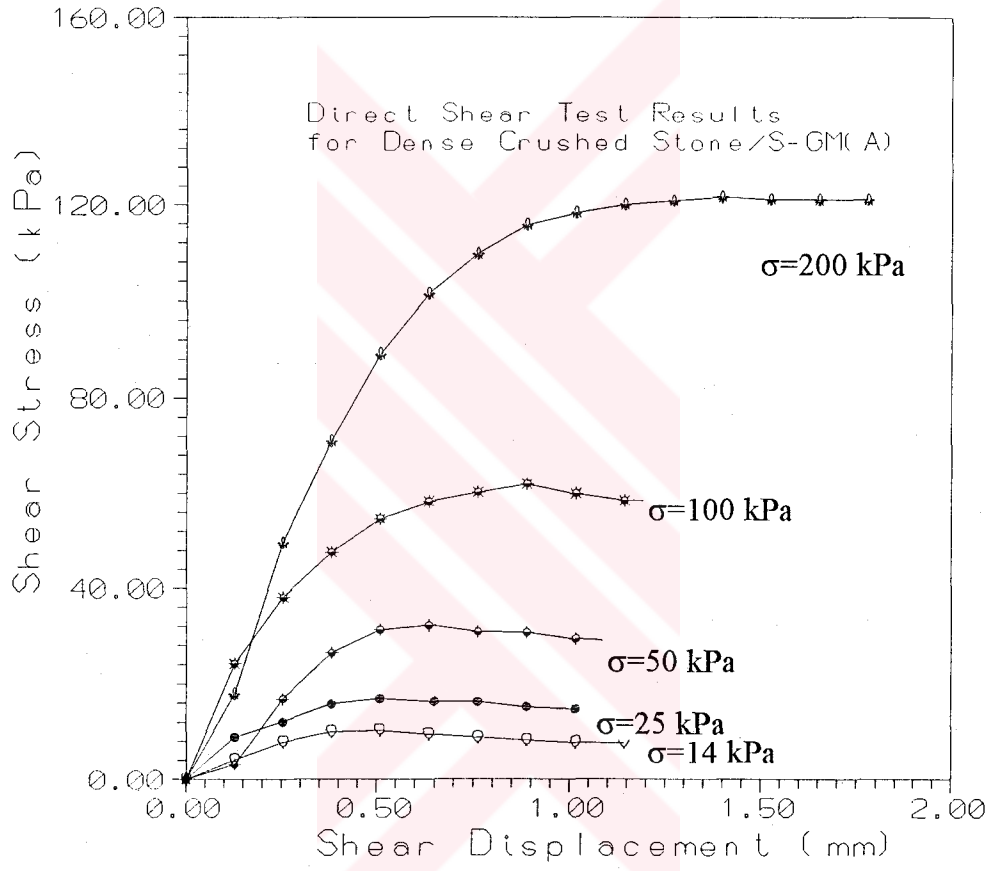

Figure C.7 Direct Shear Box Test Results for Dense Crushed Stone/S-GM(A)

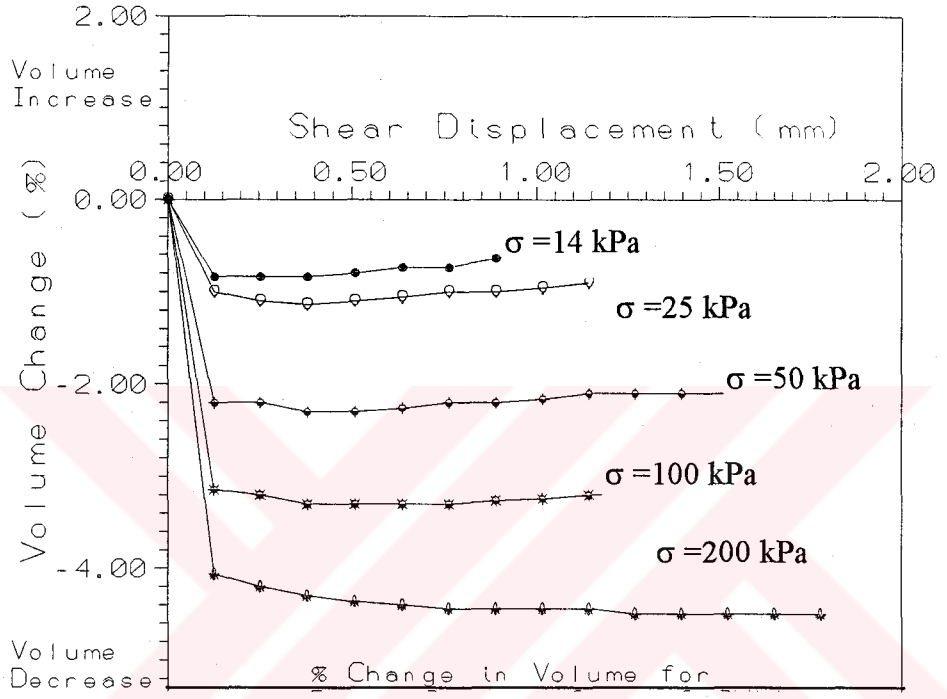

Figure C.8 Δ Volume (%) for Dense Crushed Stone/S-GM(A)

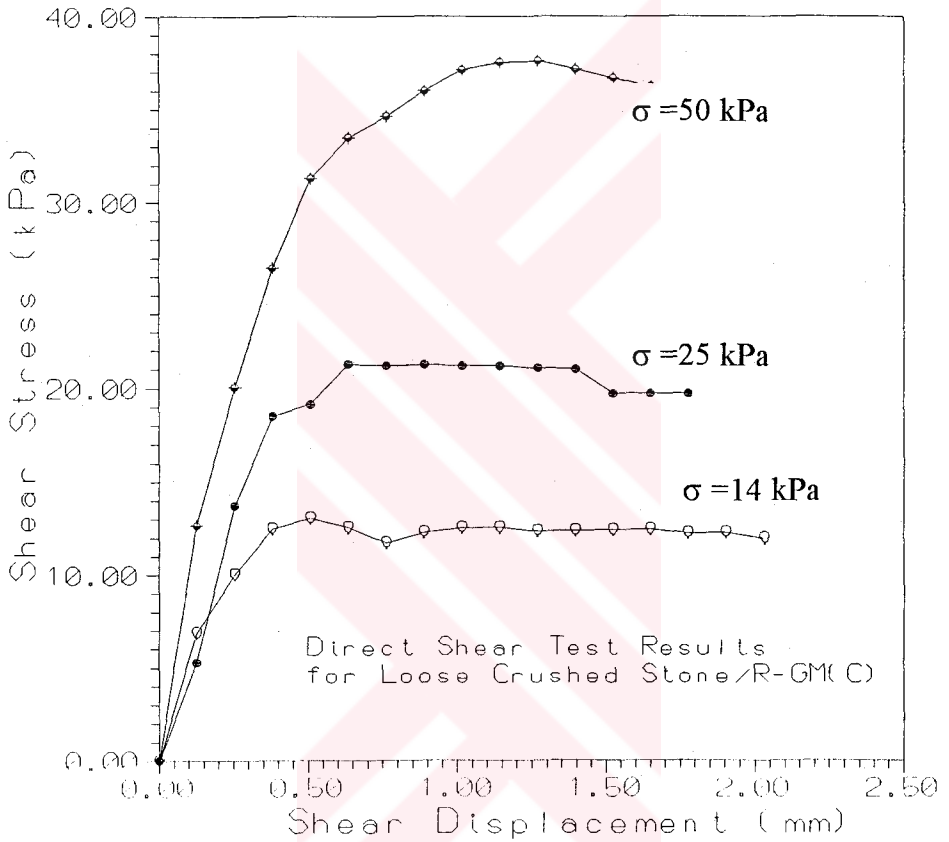

Figure C.9 Direct Shear Box Test Results for Loose Crushed Stone/R-GM(C)

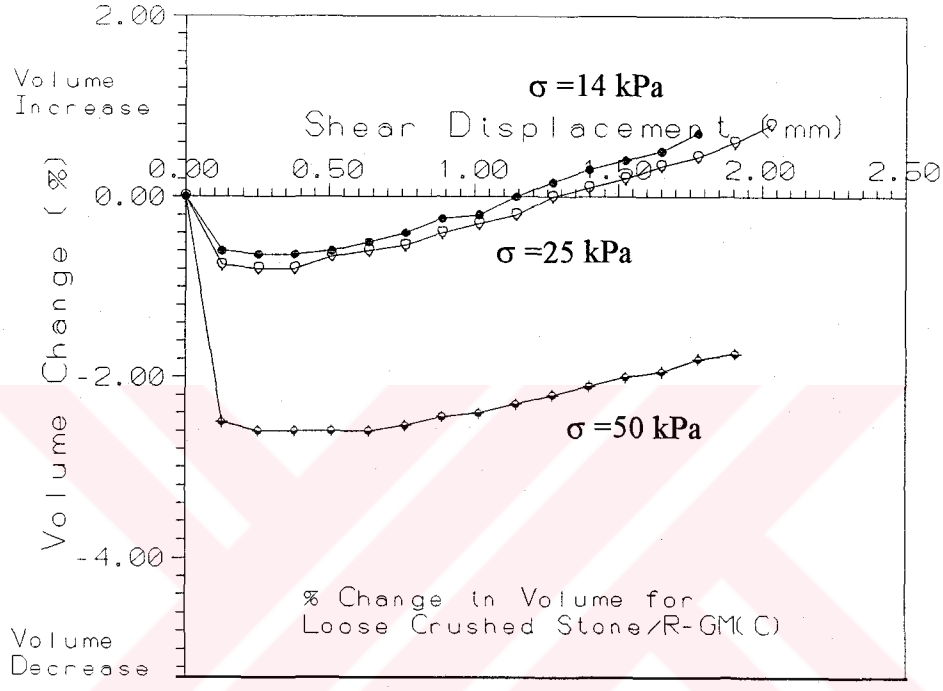

Figure C.10 Δ Volume (%) for Loose Crushed Stone/R-GM(C)

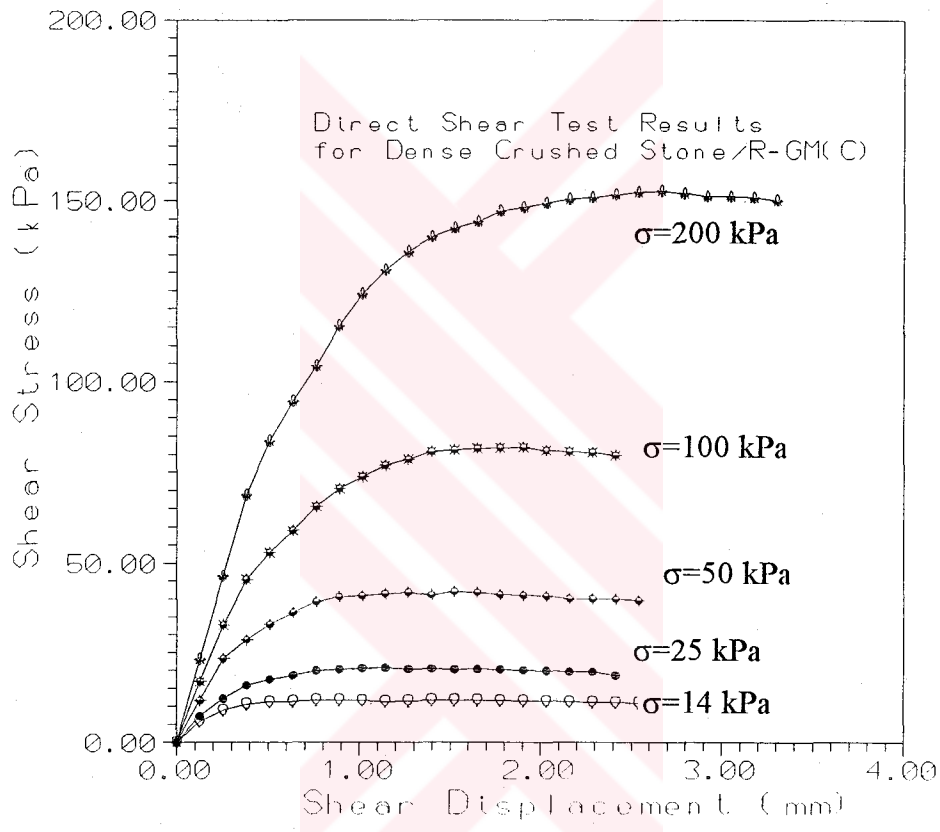

Figure C.11 Direct Shear Box Test Results for Dense Crushed Stone/R-GM(C)

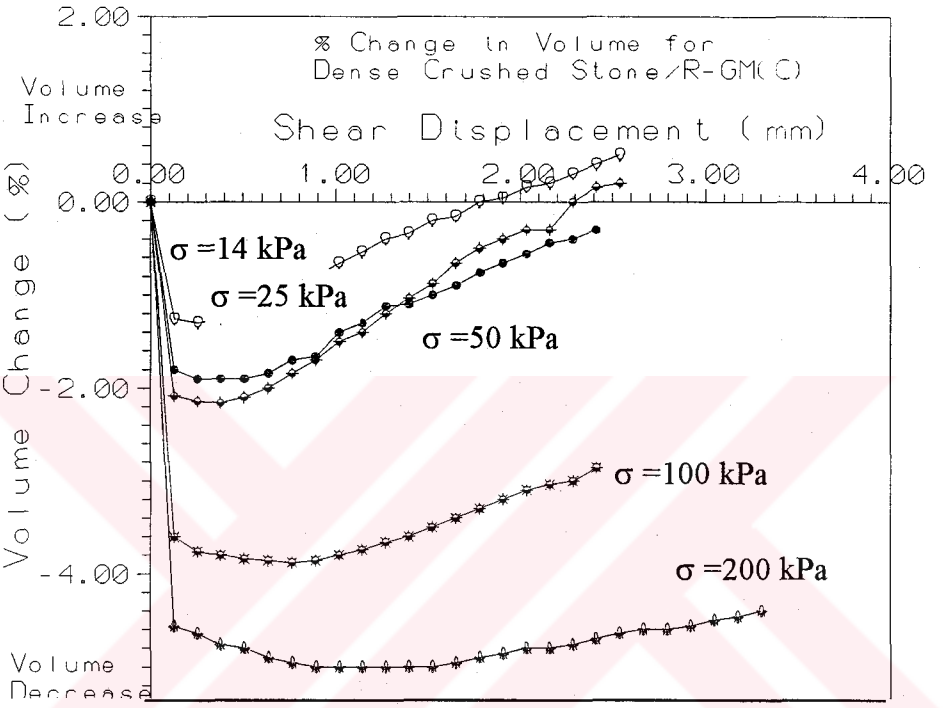

Figure C.12 Δ Volume (%) for Dense Crushed Stone/R-GM(C)

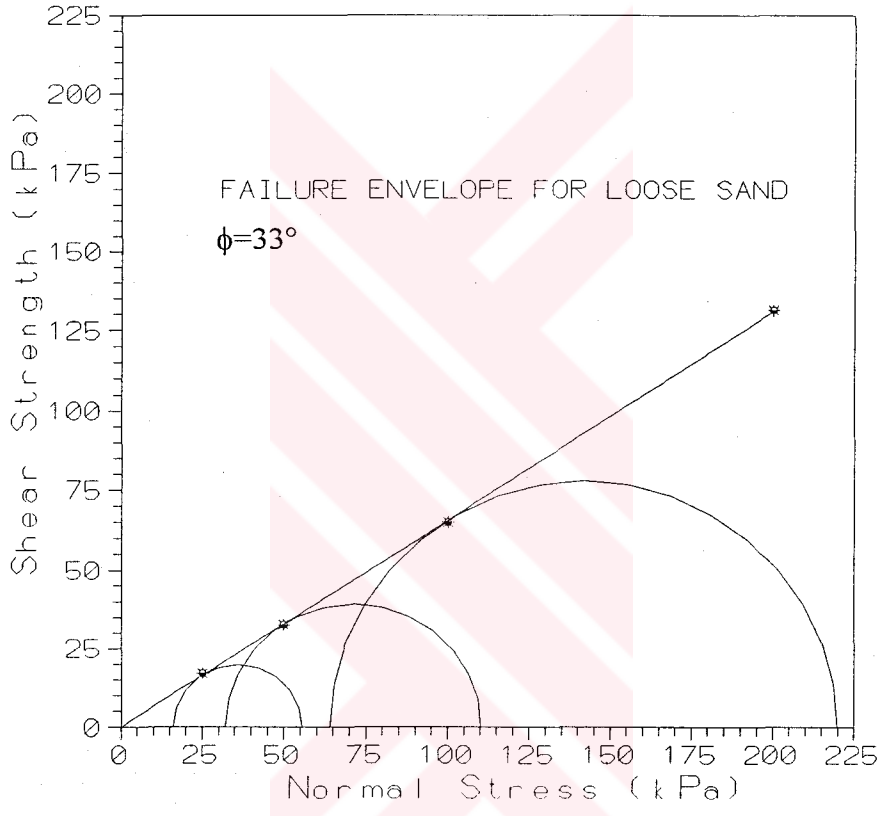

Figure C.13 Failure Envelope for Loose Ottawa Sand

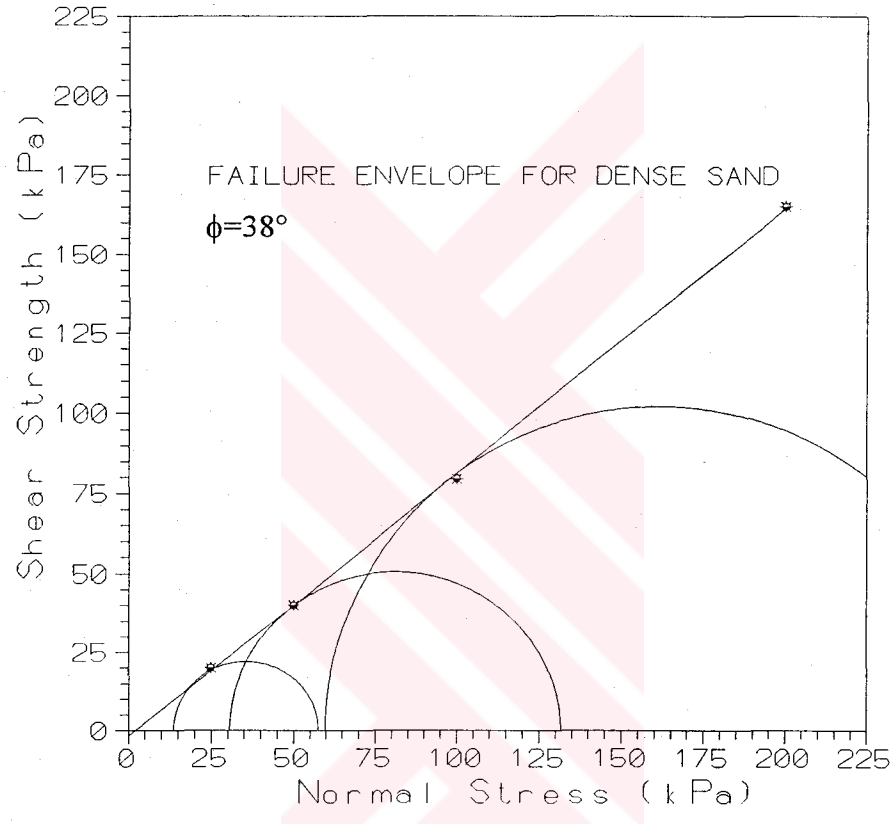

Figure C.14 Failure Envelope for Dense Ottawa Sand

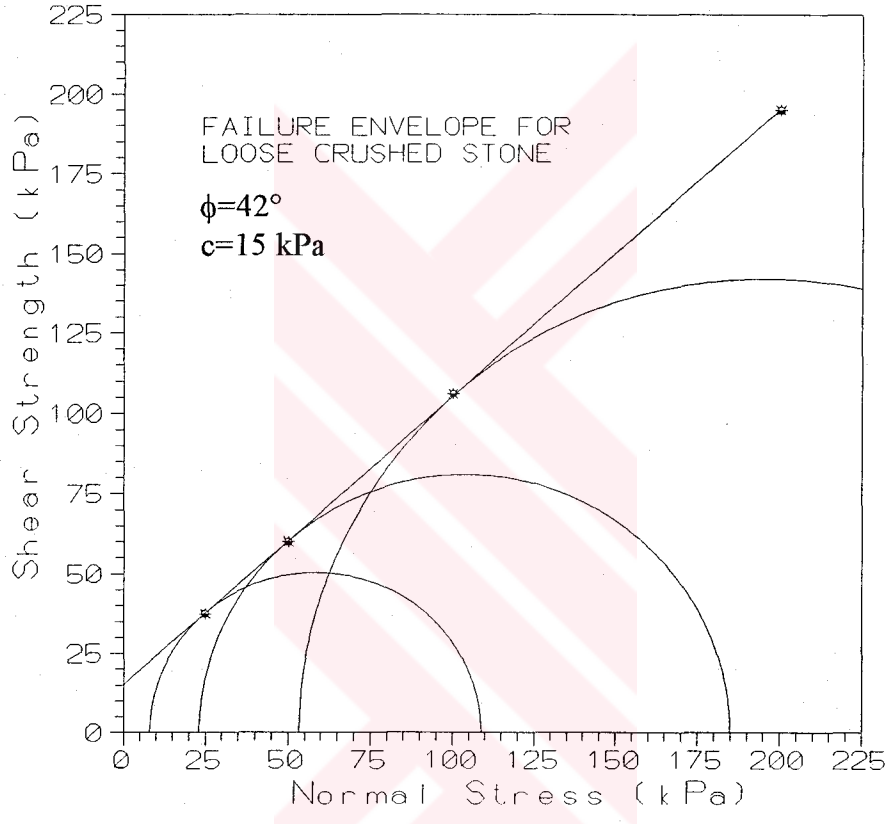

Figure C.15 Failure Envelope for Loose Crushed Stone

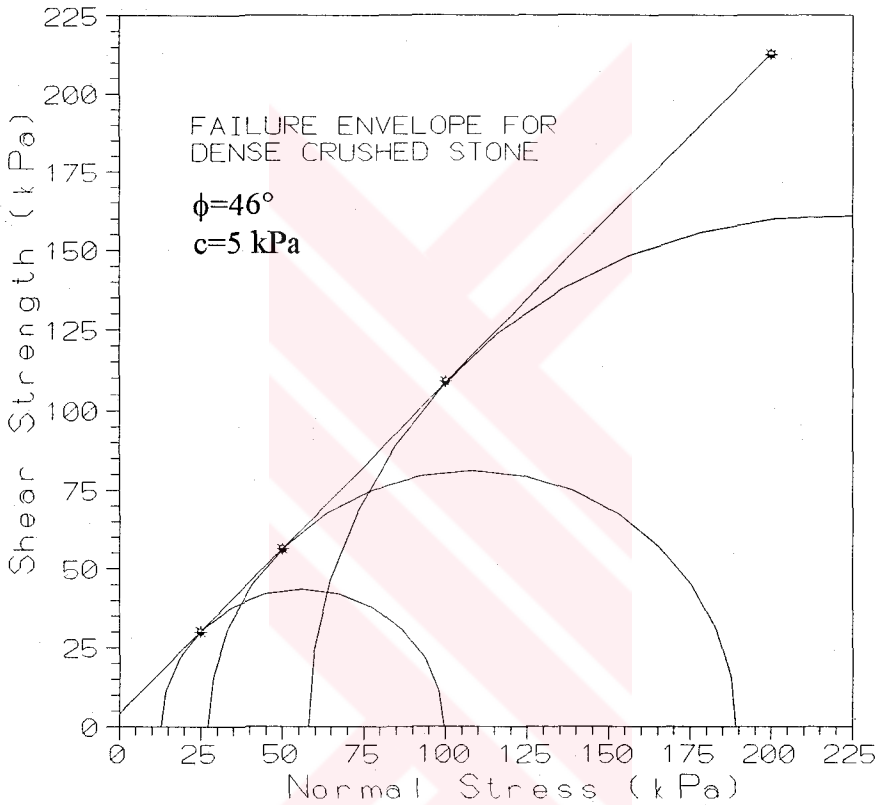

Figure C.16 Failure Envelope for Dense Crushed Stone

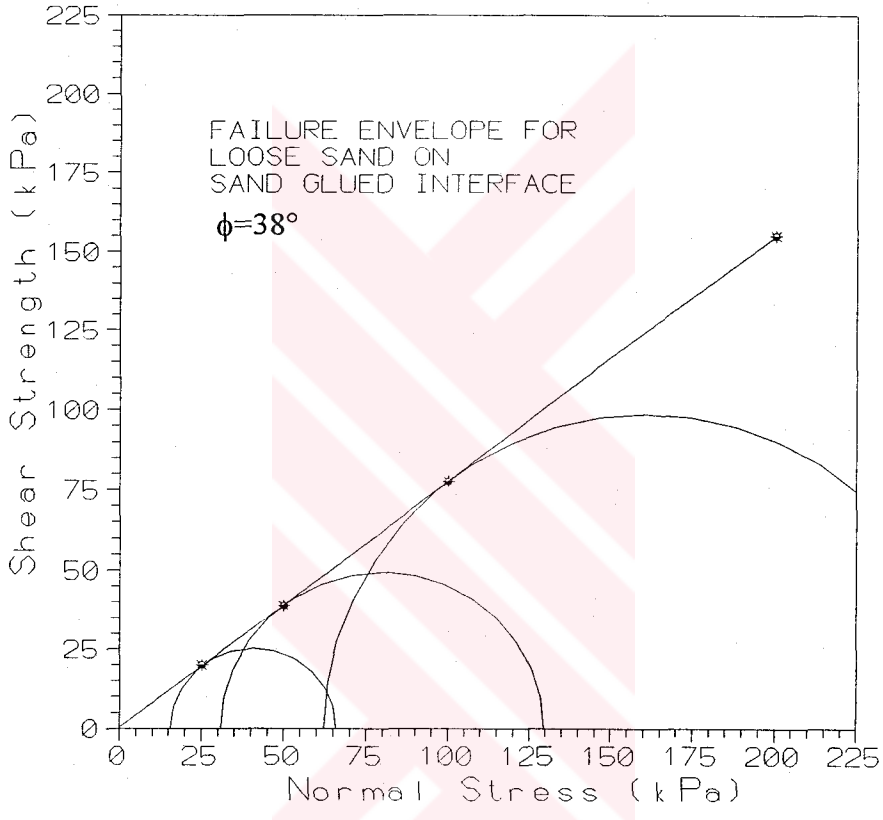

Figure C.17 Failure Envelope for Loose Sand-Sand Glued Interface

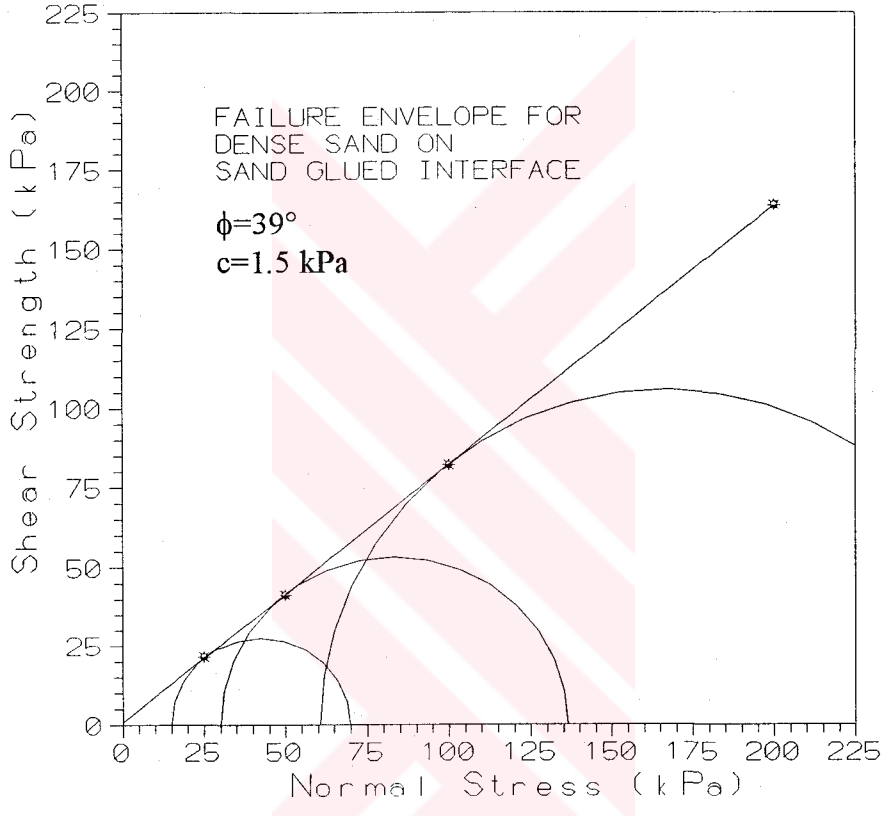

Figure C.18 Failure Envelope for Dense Sand-Sand Glued Interface

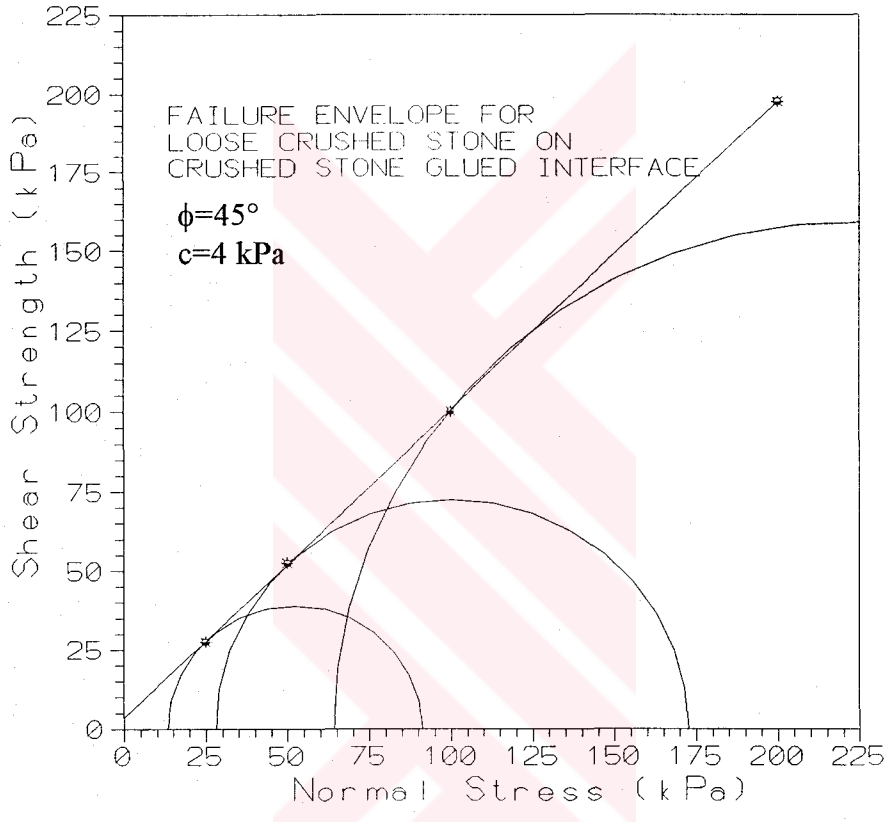

Figure C.19 Failure Envelope for Loose Crushed Stone-Crushed Stone Glued Interface

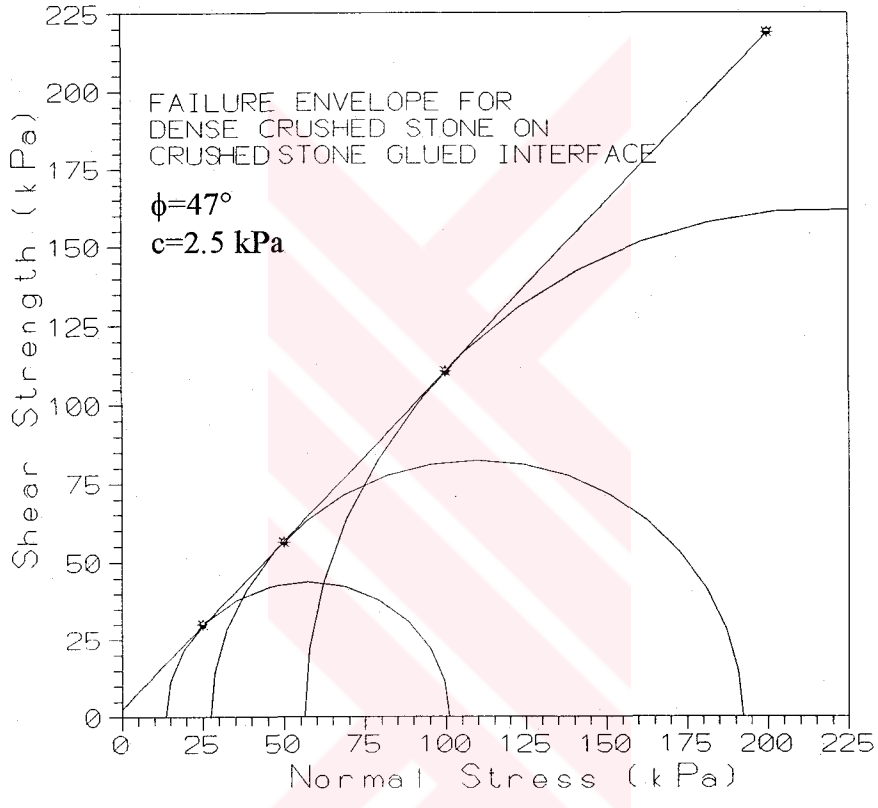

Figure C.20 Failure Envelope for Dense Crushed Stone-Crushed Stone Glued Interface

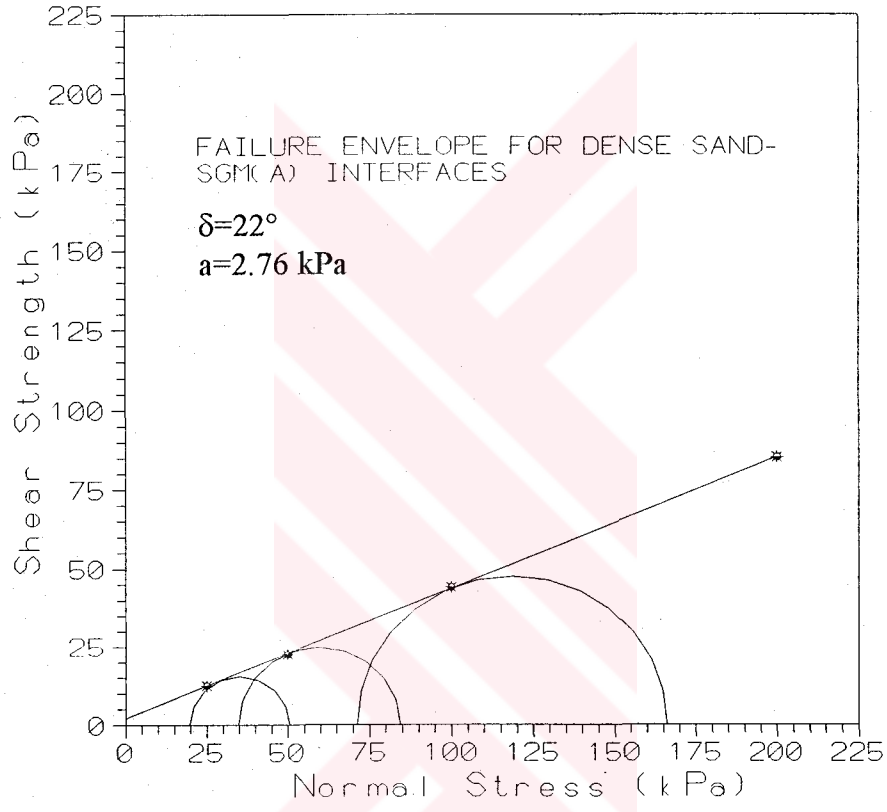

Figure C.21 Failure Envelope for Dense Ottawa Sand-SGM(A) Interface

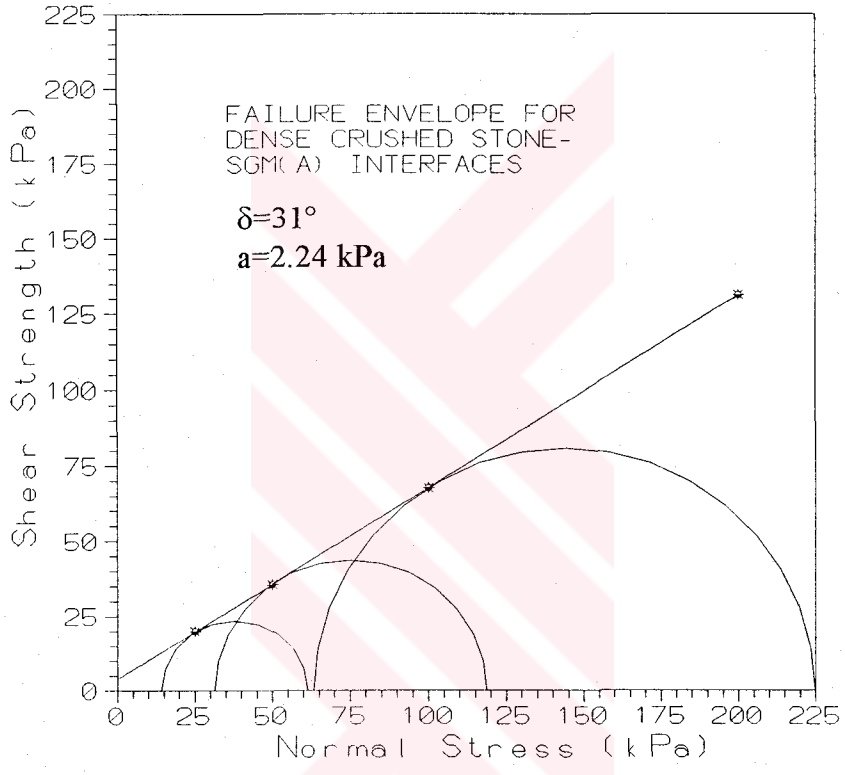

Figure C.23 Failure Envelope for Dense Crushed Stone-SGM(A) Interface

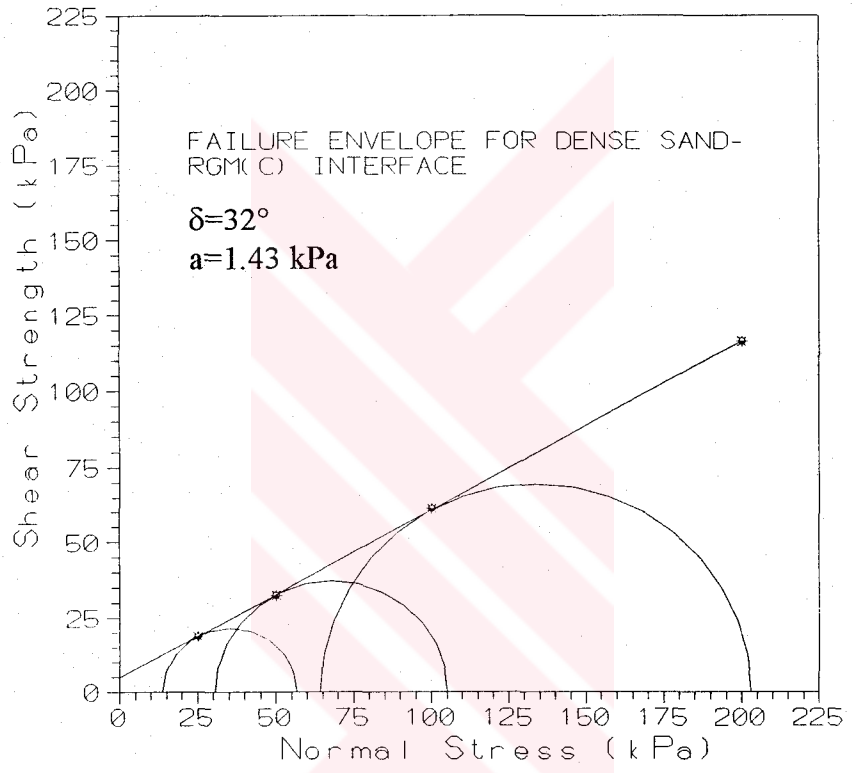

Figure C.22 Failure Envelope for Dense Ottawa Sand-RGM(C) Interface

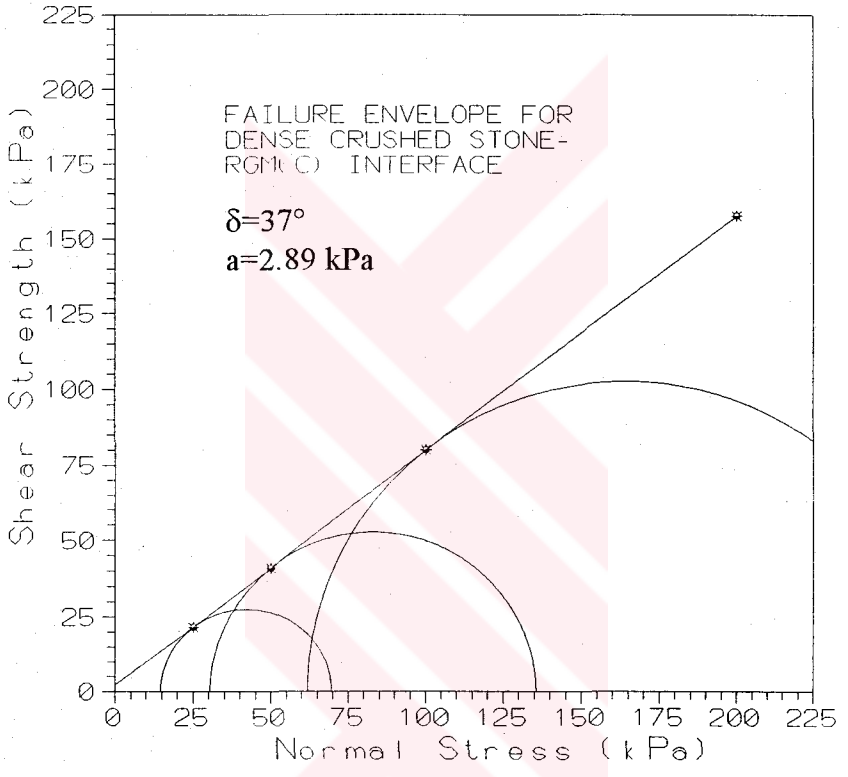

Figure C.24 Failure Envelope for Dense Crushed Stone-RGM(C) Interface